

Politecnico di Milano

School of Industrial and Information Engineering

Master of Science (MSc) in

Materials Engineering and Nanotechnology

“Perovskite Solar Cell with Reduced Graphene Oxide Integration”



Supervisor:

Professor ***Annamaria Petrozza***

Italian institute of technology (IIT), Center for Nanoscience and Technology (CNST), Perovskite group

Co-supervisor:

Dr. ***Francesco Lamberti***

Italian institute of technology (IIT), Center for Nanoscience and Technology (CNST), Perovskite group

Internal Supervisor:

Professor ***Guglielmo Lanzani***

Italian institute of technology (IIT), Center for Nanoscience and Technology (CNST)

Physics Department, Politecnico di Milano

Thesis by: ***Amir Abbas Kashi***

Student Number (Matricola): 823408

Academic Year: 2016-2017

Acknowledgment

This thesis has been conducted in Italian Institute of Technology (*IIT*), Center of Nanoscience Technology (*CNST*), Laboratory of Perovskite solar Cells (*PSC*). I would like to thank Professor Annamaria Petrozza for giving me the opportunity to work with her team. This thesis was also not possible without the daily supervision of Doctor Francesco Lamberty. In addition, I would like to express my gratitude towards Professor Guglielmo Lanzani, who acted as my internal supervisor at Polimi. Furthermore, it is necessary to thank my colleagues in Perovskite group. Especially, I acknowledge the direct contribution of Peter Topolovsek, Roberto Sorrentino, Alessandro Cito, Chen Tao, James Ball and Vijay Venugopalan. The staff of CNST Center also played a crucial role in this thesis.

Finally, I am grateful to my friends Maryam Danaei Ahmadi, Saleh Aghajani, Sina Sedaghat Nezhad, Ghobad Bagheri and Mina Farshid for providing Useful suggestions and supports during my entire Master studies.

All the rights reserved by *IIT*.



Dedicated to my greatest inspirations, my parents

And

My Love, for their endless love and efforts.

Abstract

Perovskite solar cells soon after their emerging started to grow very fast because of their spectacular properties and simplicity of their processing. These cells are able to be fabricated very cheap with wet techniques. These features caused to gain lots of attention and being one of the hot topics in the solar harvesters' field. Currently, the state of the art efficiency is greater than 25%, which is approaching the most efficient solar cells. However, there are some drawbacks which have to be addressed to make these cells commercially available. Two main problems are stability and Hysteresis. In order to overcome these problems there are ongoing researches to find a way to reduce them.

Here in this study we are focusing on finding new material for replacing currently used carrier transporting layers, in order to improve the perovskite cell performance. The material which has been studied is the reduced Graphene Oxide (rGO). Reduced Graphene Oxide has shown capability to be a good candidate for the cell performance improvement.

This thesis has two major steps, in the first step the aim was to realize a very good graphene oxide (GO) deposition on transparent conductive oxide (TCO) electrode with a good coverage, low defect, thickness controllability and reproducibility. This step have been done with different wet techniques like: Spin coating, Drop casting and Vacuum filtration. Priority was wet techniques, because of lowering the overall price and manufacturing complexity. This step also was included investigating of the prepared samples with Raman, SEM and UV-Visible Spectroscopy. Later, the best samples were subjected to be characterized by XRD, UPS and XPS.

Afterward, the optimized GO has been reduced to achieve a good conductivity. Reduction has been done chemically, electrochemically and by heat annealing.

The second step was whole cell fabrication which starts with deposition of Perovskite layer. This deposition has been done with two different techniques spin coating and vacuum evaporation.

In the end, as prepared devices have been tested and the performance was checked with solar simulator.

Results have shown using rGO as a hole transporting layer can reduce hysteresis also in the fast scan rate.

Riassunto

Poco dopo la loro apparizione le celle solari a perovskite sono divenute popolari a causa delle loro proprietà spettacolari e la semplicità del loro trattamento. Queste celle possono essere fabbricate a basso costo con tecniche "bagnate", in fase liquida. Per queste caratteristiche queste celle sono uno dei temi caldi nel campo della conversione fotovoltaica'. Attualmente lo stato dell'arte per l'efficienza è superiore al 25%, un valore che si avvicina alle celle solari più efficienti. Tuttavia, ci sono alcuni problemi che devono risolti per rendere queste cellule disponibili in commercio. Due problemi principali sono la stabilità e l'isteresi. Al fine di superare questi problemi ci sono ricerche in corso per trovare un modo per ridurli.

Questo studio riguarda la ricerca di nuovi materiali per la sostituzione di strati attualmente in uso che trasportano i portatori di carica, al fine di migliorare le prestazioni delle celle a perovskite. Il materiale studiato è ossido di grafene (RGO). L'RGO ha dimostrato la capacità di essere un buon candidato per il miglioramento delle prestazioni delle celle.

Questa tesi ha due fasi principali, nella prima fase lo scopo è realizzare un ossido di grafene di buona qualità per deposizione su un elettrodo trasparente (TCO) con una buona copertura, bassa concentrazione di difetti, controllabilità dello spessore e riproducibilità. Allo scopo sono state utilizzate diverse tecniche come: spin coating, fusione goccia e filtrazione a vuoto. I materiali prodotti sono stati caratterizzati con Raman, SEM e spettroscopia UV-Visibile. Poi i migliori campioni sono stati sottoposti a caratterizzarsi con XRD, UPS e XPS.

In seguito, il GO ottimizzato è stato ridotto per ottenere una buona conducibilità. mediante l'uso di reagenti chimici, o per via elettrochimica e ricottura di calore.

Il secondo passo è stato la fabbricazione delle celle che inizia con la deposizione di perovskite. Questo deposito è stato fatto con due diverse tecniche, spin coating o evaporazione sottovuoto.

Alla fine, i dispositivi preparati sono stati testati con un simulatore solare.

I risultati hanno dimostrato che utilizzando rGO come strato trasporto per le lacune è possibile ridurre l'isteresi anche nelle misure I-V veloci.

Contents

Table of Figures	9
1. 1. Perovskite Solar Cell [32]	15
1. 2. Synthesis of Methylammonium lead Halide Perovskite ($\text{CH}_3\text{NH}_3\text{PbX}_3$)	18
1. 3. Perovskite crystal structure and its properties	19
1. 3. 1. Electro- optical properties	22
1. 4. Perovskite solar cells different configurations.....	24
1. 5. Planar structure fabrication	26
1. 5. 1. Planar Perovskite solar cell performance	28
1. 6. Drawbacks [46].....	30
1. 6. 1. Stability.....	30
1. 6. 2. Stability of the hole transporting layer [112].....	32
1. 6. 3. Hysteretic current-voltage behavior [26, 27].....	33
1. 7. Summary	36
1. 8. Conclusion [52, 54, 57, 99, 102, 104, 118].....	37
2. Development of Reduce Graphene Oxide film	39
2. 1. Graphene.....	39
2. 1. 1. Fundamental Characteristics.....	40
2. 1. 1. 1. Electronic Properties	40
2. 1. 1. 2. Mechanical Strength	41
2. 1. 1. 3. Optical Properties.....	41
2. 2. Graphite	41
2. 3. Graphene Oxide	42
2. 4. Preparation of Graphene Oxide film.....	44
2. 4. 1. Deposition of GO solution.....	45
2. 4. 1. 1. Spin Coating.....	45
2. 4. 1. 2. Drop casting	47
2. 4. 1. 3. Vacuum Filtration [69]	48
2. 4. 2. Checking Film quality	49
2. 4. 2. 1. Drop casting Results	51
2. 4. 2. 2. Spin Coating Results	53



2. 5. Using Poly diallyl dimethylammonium chloride (PDDA) for better coverage [50]	55
2. 6. Reduction of Graphene Oxide Film [55, 59, 89, 90, 91, 92, 97, 103]	55
2. 6. 1. Thermal Annealing	56
2. 6. 2. Chemical Reduction [86]	57
2. 7. Best Reduction method selection	58
2. 7. 1. Sample 1: Drop casted 3 times on top of PDDA coated ITO – 0.33ml Go solution (1 mg/ml in water) in 0.66ml ethanol – Reduced with hydrazine.....	59
2. 7. 1. 1. SEM.....	59
2. 7. 1. 2. XPS measurement	60
2. 7. 1. 3. UPS	62
2. 7. 2. Sample 2: Drop casted 3 times on top of PDDA coated ITO -- 0.33ml Go solution (1 mg/ml in water) in 0.66ml ethanol – Reduced in glove box at 250 °C.....	63
2. 7. 2. 1. SEM.....	63
2. 7. 2. 2. XPS.....	65
2. 7. 3. Sample 3: Spin coated 4 times on top of PDDA coated ITO –1 mg/ml GO Concentration in water– reduced in glove box at 250 °C	67
2. 7. 3. 1. SEM.....	67
2. 7. 3. 2. XPS.....	68
2. 7. 3. 3. UPS	70
2. 7. 4. Comparison of the rGO deposited sample with bare ITO substrate.....	71
2. 7. 4. 1. XPS comparison	71
2. 7. 4. 2. UPS comparison	72
2. 8. Deciding to Use rGO film as a hole transporting layer or as an electron transporting layer?	73
3. 1. Perovskite layer.....	79
3. 1. 1. Two-step deposition	79
3. 1. 1. 1. SEM.....	80
3. 1. 2. Solvent Quenching	82
3. 1. 2. 1. SEM.....	83
3. 1. 3. Evaporation of PbI_2 [108]	83
3. 1. 3. 1. SEM.....	84
4. 1. Reference Cell	88
4. 1. 1. Standard structure [25, 43, 62, 63, 65, 88, 94, 107]	88
4. 1. 2. Inverted Structure [94, 95, 123].....	88

4. 2. Reference Standard Structure Cell.....	90
4. 3. Modification of the standard structure with rGO replacement	95
4. 3. 1. Solvent Quenching modified Standard Structure cell with rGO	95
4. 3. 2. Two-step deposition modified standard structure cell with rGO	96
4. 4. Reference cell without electron transport layer.....	98
4. 5. Reference Inverted Structure cell with PEDOT: PSS and PCBM.....	101
4. 6. Modification of the inverted structure with rGO replacement	103
4. 7. Control cell for using reduced Graphene Oxide (rGO) as an interlayer between TiO ₂ and Perovskite layer	105
4. 7. 1. Using Reduced Graphene Oxide (rGO) As an Interlayer between TiO ₂ and Perovskite layer.....	106
4. 7. 2. Using Reduced Graphene Oxide (rGO) deposited on top of PDDA layer As an Interlayer between TiO ₂ and Perovskite layer	107
4. 8. Using another Perovskite material.....	108
4. 8. 1. Reference Standard Structure Cell with Cs/MA PbI ₂ /FA perovskite material	109
4. 8. 2. Standard Structure Cell with Cs/MA PbI ₂ /FA perovskite material and rGO as an interlayer between TiO ₂ and perovskite layers	110
4. 8. 3. Standard Structure Cell with Cs/MA PbI ₂ /FA perovskite material and rGO as an interlayer between TiO ₂ and PCBM layers	111
4. 8. 4. Reference Standard Structure Cell with Cs/MA PbI ₂ /FA perovskite material and PCBM as an electron transport layer	112
4. 8. 5. Standard Structure Cell with Cs/MA PbI ₂ /FA perovskite material and rGO+ PCBM as an electron transport layer	113
5. Conclusion.....	115
Reference.....	117

Table of Figures

FIGURE 1- 1- BAND GAP ENGINEERING FOR $\text{CH}_3\text{NH}_3\text{PBI}_{3-x}\text{BR}_x$, ACCORDING TO BR CONTENT.....	16
FIGURE 1- 2- PEROVSKITE RESEARCH PROGRESS IN TERMS OF EFFICIENCY.	17
FIGURE 1- 3- $\text{CH}_3\text{NH}_3\text{PBI}_3$ UNIT CELL STRUCTURES. REPRINTED FROM SHIQIANG LUO AND WALID A. DAOUD [2].....	20
FIGURE 1- 4- CHEMATIC ENERGY LEVEL DIAGRAM OF MAPBBR3, MAPBI3, FAPBI3, MAPB1-XSNXI3, AND MASNI3. MA AND FA STAND FOR METHYLAMMONIUM (CH_3NH_3) AND FORMAMIDINIUM ($\text{HC}(\text{NH}_2)_2$), RESPECTIVELY. DATA FOR MAPB1-XSNXI3 ARE FOR X = 0.25, 0.5, 0.75 AND 1. REPRINTED FORM [45].....	21
FIGURE 1- 5- HIGHER CARRIER LIFE TIME IN THE MIXED HALIDE RESPECT TO TRIIODIDE PEROVSKITE. REPRINTED FROM H. SNAITH ET AL.	23
FIGURE 1- 6- (LEFT) CROSS-SECTION SEM IMAGE OF THE DEVICE. (RIGHT) ACTIVE LAYER-UNDER LAYER-FTO INTERFACIAL JUNCTION STRUCTURE. REPRINTED FROM [14]	24
FIGURE 1- 7- LEFT: SCHEMATIC REPRESENTATION OF FULL DEVICE STRUCTURE, WHERE THE MESOPOROUS OXIDE IS EITHER AL_2O_3 OR TIO_2 . RIGHT: CROSS-SECTION SEM IMAGE OF A FULL DEVICE INCORPORATING MESOPOROUS AL_2O_3 . REPRINTED FROM [15]	25
FIGURE 1- 8- STANDARD AND INVERTED CONFIGURATION OF THE PLANAR STRUCTURE.	25
FIGURE 1- 9- STRUCTURAL EVOLUTION OF PEROVSKITE SOLAR CELLS: (A) SENSITIZATION CONCEPT WITH SURFACE ADSORPTION OF NANO DOT PEROVSKITE, (B) MESO-SUPERSTRUCTURE CONCEPT WITH NON-INJECTING SCAFFOLD LAYER, (C) PILLARED STRUCTURE WITH A NANO OXIDE BUILDING BLOCK, AND (D).....	26
FIGURE 1- 10- FABRICATION STEPS OF THE STANDARD CONFIGURATION.	27
FIGURE 1- 11- PROPOSED DECOMPOSITION PATHWAY OF $\text{CH}_3\text{NH}_3\text{PBI}_3$, IN THE PRESENCE OF A WATER MOLECULE. THE MAIN PRODUCT OF THIS PATHWAY IS PBI_2 . [20]	30
FIGURE 1- 12- NORMALIZED POWER CONVERSION EFFICIENCY DEGRADATION CURVES FOR PEROVSKITE SOLAR CELLS CONTAINING TIO_2 . SHOWN ARE NON-ENCAPSULATED (BLUE OPEN CIRCLES), ENCAPSULATED (RED OPEN SQUARES), AND ENCAPSULATED WITH A 435 NM UV FILTER (BLACK CLOSED SQUARES) DEVICES. [21].....	31
FIGURE 1- 13- NORMALIZED PCE OF PEROVSKITE SOLAR CELLS BASED ON PEDOT: PSS (SQUARES) AND CU: NIOX (CIRCLES) HOLE-TRANSPORTING LAYERS AS A FUNCTION OF STORAGE TIME IN AIR. [25]	33

FIGURE 1- 14- EFFECTS OF DIFFERENT SCAN CONDITIONS ON THE I-V CURVES. (A) DIFFERENT SCAN RATES (B) DIFFERENT PRE- BIASING. (C) INFLUENCE OF THE SCANNING RANGE. (D) LIGHT SOAKING.	34
FIGURE 1- 15- ION MIGRATION EFFECT.	35
FIGURE 2- 1- GRAPHENE BOND STRUCTURE	39
FIGURE 2- 2- ENERGY VERSUS K VECTOR DIAGRAM OF GRAPHENE AT DIRAC POINT	40
FIGURE 2- 3- GRAPHITE.....	42
FIGURE 2- 4- GOING FROM GRAPHENE TO GRAPHITE	42
FIGURE 2- 5- GRAPHENE OXIDE PREPARATION	43
FIGURE 2- 6- FUNCTIONAL GROUPS ON GRAPHENE OXIDE	43
FIGURE 2- 7- GRAPHENE OXIDE BAND STRUCTURE.....	44
FIGURE 2- 8- DROP CASTING PROCESS.	48
FIGURE 2- 9- VACUUM FILTRATION SETUP (LEFT), FILTER MEMBRANE AFTER PASSING THE SOLUTION THROUGH. (RIGHT)	49
FIGURE 2- 10- RAMAN SPECTRA OF (A) GRAPHITE OXIDE (GO), (B-H) FEW LAYER WRINKLED GRAPHENE GROWN BY DIFFERENT METHODS VIZ. (B) THERMALLY EXFOLIATED GRAPHENE (TEG), (C) VACUUM EXFOLIATED GRAPHENE (VEG), (D) HYDROGEN EXFOLIATED GRAPHENE (HEG), (E) CHEMICALLY EXFOLIATED GRAPHENE (CEG), (F) MICROWAVE EXFOLIATED GRAPHENE (MEG), (G) LASER EXFOLIATED GRAPHENE (LEG), (H) SUN EXFOLIATED GRAPHENE (SEG). REPRINTED FROM [84].....	51
FIGURE 2- 11- RAMAN MEASUREMENT IN DIFFERENT LOCAL POINTS IN DROP CASTED SAMPLE.....	52
FIGURE 2- 12- RAMAN MEASUREMENT IN DIFFERENT LOCAL POINTS IN SPIN COATED SAMPLE.....	54
FIGURE 2- 13- 0.4 MG/ML GO CONCENTRATION IN MILLILITER SOLUTION (0.9 ML ETHANOL + 0.4 ML WATER)- 2500RPM- 50SECONDS- 4 TIMES (REDUCED IN GLOVEBOX AT 250 °C).....	56
FIGURE 2- 14- 1 MG/ML GO CONCENTRATION IN MILLILITER WATER- 2500RPM- 1MIN- 3 TIMES (REDUCED WITH HYDRAZINE).....	58
FIGURE 2- 15- SEM IMAGE OF THE REDUCED DROP CASTED SAMPLE. WRINKLES ARE DUE TO REDUCTION.	59

FIGURE 2- 16- XPS MEASUREMENTS IN DIFFERENT REGIONS ON SAMPLE1. C, O, N, NA, CL, S AND SI ARE STANDS FOR CARBON, OXYGEN, NITROGEN, SODIUM, CHLORIDE, SULFIDE AND SILICON RESPECTIVELY.....	60
FIGURE 2- 17- C 1S SPECTRA FOR SAMPLE 1.	61
FIGURE 2- 18- UPS MEASUREMENT ON GREEN AND BLUE MARKED REGIONS.	62
FIGURE 2- 19- SEM OF THE DROP CASTED SAMPLE REDUCED INSIDE THE GLOVEBOX.	64
FIGURE 2- 20- XPS MEASUREMENTS IN DIFFERENT REGIONS ON SAMPLE2. C, O, N, NA, CA, MN, S AND SI ARE STANDS FOR CARBON, OXYGEN, NITROGEN, SODIUM, CALCIUM, MANGANESE SULFIDE AND SILICON RESPECTIVELY.....	65
FIGURE 2- 21- C 1S SPECTRA OF THE SAMPLE2 IN MARKED REGIONS.....	66
FIGURE 2- 22- SEM MEASUREMENT ON SAMPLE 3.....	67
FIGURE 2- 23- XPS MEASUREMENT ON SAMPLE3. C, O, N, NA, CA, IN AND SN ARE STANDS FOR CARBON, OXYGEN, NITROGEN, SODIUM, CALCIUM, INDIUM AND TIN RESPECTIVELY.	68
FIGURE 2- 24- C 1S SPECTRA FOR THE SAMPLE 3.	69
FIGURE 2- 25- UPS MEASUREMENT.....	70
FIGURE 2- 26- XPS COMPARISON. SAMPLE 3 IN RED AND BARE ITO IN VIOLET.....	71
FIGURE 2- 27- UPS COMPARISON. SAMPLE 3 IN RED AND BARE ITO IN VIOLET.....	72
FIGURE 2- 28- BARE ITO TRANSMISSION.	73
FIGURE 2- 29- BEFORE REDUCTION (RESPECT TO BARE ITO). TRANSMITTANCE AT 550NM WAVE LENGTH, SOLUTION WITH 0.1MG/ML GO = 83.65 (%) (BLACK), SOLUTION WITH 0.2MG/ML GO=83.35 (%) (RED), SOLUTION WITH 1MG/ML GO=82.16 (%) (BLUE)	74
FIGURE 2- 30- AFTER REDUCTION: TRANSMITTANCE (RESPECT TO BARE ITO) AT 550NM WAVE LENGTH, SOLUTION WITH 0.2MG/ML GO= 78 (%) (RED), SOLUTION WITH 0.33MG/ML GO=72.75 (%) (BALCK), SOLUTION WITH 1MG/ML GO=65.28 (%) (BLUE)	74
FIGURE 2- 31- POSITION OF THE VALANCE AND CONDUCTION BAND OF RGO VERSUS VACUUM.	75
FIGURE 2- 32- BAND DIAGRAM ALIGNMENTS. RGO ACTING AS A HOLE TRANSPORTING LAYER.....	76
FIGURE 2- 33- BAND DIAGRAM ALIGNMENT. RGO ACTING AS AN ELECTRON TRANSPORT LAYER.....	77

FIGURE 3- 1- CLOSE LOOK ON THE GRAIN SIZE OF THE AS PREPARED PEROVSKITE LAYER ON TOP OF THE RGO.	81
FIGURE 3- 2- LARGE VIEW OF THE AS DEPOSITED PEROVSKITE FILM ON TOP OF THE RGO.	82
FIGURE 3- 3- SEM IMAGE OF THE PEROVSKITE LAYER PREPARED BY SOLVENT QUENCHING TECHNIQUE ON RGO.	83
FIGURE 3- 4- EVAPORATED PEROVSKITE LAYER UNDERNEATH OF THE TOP CARRIER TRANSPORT LAYER. NOTICE, GRAY AREAS ARE THE PEROVSKITE LAYER WITHOUT COVERAGE OF THE TOP LAYER.	85
FIGURE 3- 5- VISIBLE GRAINS OF THE PEROVSKITE LAYER UNDER THE TOP CARRIER TRANSPORT LAYER DUE TO NOT COMPLETE COVERAGE.	86
FIGURE 4- 1- STANDARD AND INVERTED PEROVSKITE CELL STRUCTURES.	89
FIGURE 4- 2- PEROVSKITE CELL WITHOUT ELECTRON TRANSPORT LAYER.	89
FIGURE 4- 3- REFERENCE SAMPLE, CELL LAYERS SEQUENCE: FTO/COMPACT TIO ₂ /PEROVSKITE/SPIRO/GOLD ELECTRODE.	92
FIGURE 4- 4- REFERENCE CELL, CELL LAYERS SEQUENCE: FTO/COMPACT TIO ₂ /PVK(LEAD ACETATE) /SPIRO/GOLD ELECTRODE.	93
FIGURE 4- 5- STANDARD STRUCTURE MODIFIED BY USING RGO AS AN ELECTRON TRANSPORT LAYER INSTEAD OF COMPACT TIO ₂ , CELL LAYERS SEQUENCE: FTO/RGO/PEROVSKITE (SOLVENT QUENCHING METHOD)/SPIRO/GOLD ELECTRODE.	95
FIGURE 4- 6- STANDARD STRUCTURE MODIFIED BY USING RGO AS AN ELECTRON TRANSPORT LAYER INSTEAD OF COMPACT TIO ₂ , CELL LAYERS SEQUENCE: FTO/RGO/PEROVSKITE (TWO-STEP METHOD)/SPIRO/GOLD ELECTRODE.	96
FIGURE 4- 7- PRE BIASING CONDITION AND SCAN RATE DEPENDENCY. CELL LAYERS SEQUENCE: FTO/RGO/PEROVSKITE (TWO-STEP METHOD)/SPIRO/GOLD ELECTRODE,	98
FIGURE 4- 8- REFERENCE CELL WITHOUT ELECTRON TRANSPORTING LAYER, CELL LAYERS SEQUENCE: FTO/PEROVSKITE (SOLVENT QUENCHING) /SPIRO/GOLD ELECTRODE, SAMPLE1.	99
FIGURE 4- 9- REFERENCE CELL WITHOUT ELECTRON TRANSPORTING LAYER, CELL LAYERS SEQUENCE: FTO/PEROVSKITE (SOLVENT QUENCHING) /SPIRO/GOLD ELECTRODE, SAMPLE2.	100
FIGURE 4- 10- REFERENCE INVERTED STRUCTURE. CELL LAYERS SEQUENCE: FTO/PEDOT : PSS/PEROVSKITE/PCBM/GOLD ELECTRODE.	101

FIGURE 4- 11- MODIFIED INVERTED STRUCTURE WITH RGO. CELL LAYERS SEQUENCE: FTO/RGO/PEROVSKITE/PCBM/GOLD ELECTRODE, (FAST SCAN)	103
FIGURE 4- 12- MODIFIED INVERTED STRUCTURE WITH RGO. CELL LAYERS SEQUENCE: FTO/RGO/PEROVSKITE/PCBM/GOLD ELECTRODE, (SLOW SCAN)	104
FIGURE 4- 13- CONTROL CELL, CELL LAYERS SEQUENCE: FTO/TIO ₂ /PEROVSKITE (SOLVENT QUENCHING)/SPIRO/GOLD ELECTRODE	106
FIGURE 4- 14- STANDARD STRUCTURE CELL WITH RGO INTERLAYER LAYER. CELL LAYERS SEQUENCE: FTO/TIO ₂ /RGO/PEROVSKITE (SOLVENT QUENCHING)/SPIRO/GOLD ELECTRODE	107
FIGURE 4- 15- STANDARD STRUCTURE CELL WITH RGO-PDDA INTERLAYER LAYER. CELL LAYERS SEQUENCE: FTO/TIO ₂ /RGO ON TOP OF PDDA MONO LAYER/PEROVSKITE LAYER (SOLVENT QUENCHING)/SPIRO/GOLD ELECTRODE	108
FIGURE 4- 16- REFERENCE SAMPLE, CELL LAYERS SEQUENCE: FTO/COMPACT TIO ₂ /PEROVSKITE(SOLVENT QUENCHING)/SPIRO/GOLD ELECTRODE	109
FIGURE 4- 17- CELL LAYERS SEQUENCE: FTO/COMPACT TIO ₂ /RGO/PEROVSKITE(SOLVENT QUENCHING)/SPIRO/GOLD ELECTRODE	110
FIGURE 4- 18- CELL LAYERS SEQUENCE: FTO/COMPACT TIO ₂ /RGO/PCBM/PEROVSKITE(SOLVENT QUENCHING)/SPIRO/GOLD ELECTRODE	111
FIGURE 4- 19- CELL LAYERS SEQUENCE: FTO/PCBM/PEROVSKITE(SOLVENT QUENCHING)/SPIRO/GOLD ELECTRODE.....	112
FIGURE 4- 20- CELL LAYERS SEQUENCE: FTO/RGO/PCBM/PEROVSKITE(SOLVENT QUENCHING)/SPIRO/GOLD ELECTRODE	113



Chapter 1

Introduction

1. 1. Perovskite Solar Cell [32]

Perovskite materials have got their names after the Russian mineralogist L.A. Perovski. Perovskite, is a crystal structure with the ABX_3 formula. X is a halogen or Oxygen. A and B are both cations. A is a cation which is stabilized in a cubo-octahedral cage composed from 12 nearest X atoms. The B cations are coordinated with the six nearest X anions in order to form octahedral geometry.

Since, it is possible to make perovskite structure with different sets of the atoms, the stability of the different perovskite crystal structure is compared by the Madelung electrostatic potential. In Table 1-1, a range of ABX_3 perovskite structure has been listed with corresponding lattice energies.

Stoichiometry	E_{lattice} (eV/cell)	V_A (v)	V_B (v)	V_X (v)
I-V-VI₃	-140.48	-8.04	-34.59	16.66
II-IV-VI₃	-118.82	-12.93	-29.71	15.49
III-III-VI₃	-106.92	-17.81	-24.82	14.33
I-II-VII₃	-29.71	-6.46	-14.85	7.75

Table 1- 1- Electrostatic lattice energy and site Madelung potentials for a range of ABX_3 perovskite structures (cubic lattice, $a = 6.00 \text{ \AA}$) assuming the formal oxidation state of each species

In the beginning Oxide perovskite received lots of attention for its interesting physical properties like superconductivity [35, 36] and ferroelectricity [32- 34]. Halide perovskite in contrary to oxide perovskite has gained not so much attention for their not unique physical properties.

Later, inorganic element was replaced in A site instead of the previously organic molecule. This new molecule also had a perovskite structure.

Gradually, inorganic halide compounds which featured layered structure became more popular because of their ability to convert from semiconductor to metal and the following superconductivity. [37] One of the early organic- inorganic perovskite structures which have been discovered was methylammonium lead halide ($CH_3NH_3PbX_3$). This crystalline compound featured the molecular motion of the methylammonium ion. [38, 39] however,

this compound could not initially gain the attentions because of not fully discovered the interesting electronic and Opto- electronic properties. However, in 2009, Miyasaka et al. were the leading researchers who found that $\text{CH}_3\text{NH}_3\text{PbX}_3$ has light harvesting properties when they are under illumination. They have used this material in a dye-sensitized solar cell. [40]

In this work $\text{CH}_3\text{NH}_3\text{PbBr}_3$ deposited on a nanocrystalline TiO_2 layer had a power conversion efficiency (PCE) of 3.1% and $\text{CH}_3\text{NH}_3\text{PbI}_3$ showed slightly higher efficiency around 3.8%. This improvement in the efficiency came from this fact that iodide perovskite has a narrower band gap respect to bromide one. (Fig.1.1) [40]

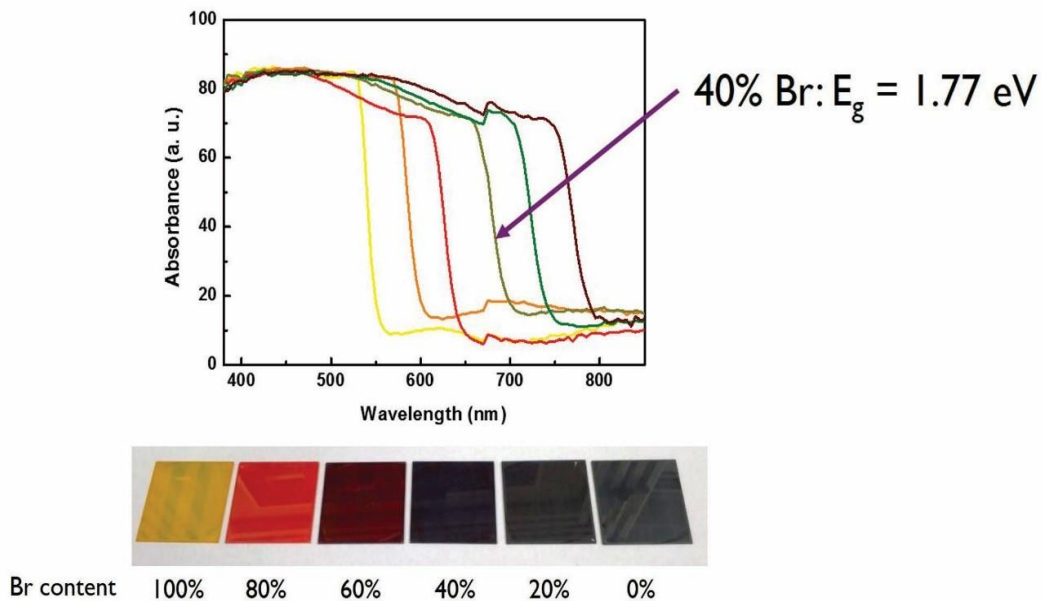


Figure 1- 1- Band gap engineering for $\text{CH}_3\text{NH}_3\text{PbI}_{3-x}\text{Br}_x$, according to Br content.

In the following years, on 2011, a higher PCE (6.5%) has been reported for the iodide perovskite ($\text{CH}_3\text{NH}_3\text{PbI}_3$). In this work dye molecule of the dye sensitized solar cell has been replaced by nanocrystals of the $\text{CH}_3\text{NH}_3\text{PbI}_3$ which had a higher absorption coefficient. [41] This new discovery attracted the attention of the researchers to employ

perovskite halide material in the thin film solar cells. In 2012, an all solid state solar cell based on perovskite iodide has been developed. This cell shown a PCE around 10%. This cell was produced by deposition of the perovskite layer on top of the 600nm thick TiO₂ layer. [14] Following this trend, a non-sensitized cell by using a mixed halide perovskite CH₃NH₃PbI_{3-x}Cl_x was produced and deposited on top of Al₂O₃ surface which a 10.9% efficiency was reported for this structure. [15]

This new emerging solar cell, started to grow very fast and soon after the introduction efficiency of this so called perovskite solar cells approached to the state of the art efficiency for solar energy harvesters. In 2013, modification of the depositing methods or junction structures resulted in the improving efficiency (PCE) to higher than 15%. In Figure 1.2 a brief summary of the growth trend of the perovskite solar cells in terms of the efficiency, has been depicted. As it is clear, just in a few years, they have grown very rapidly.

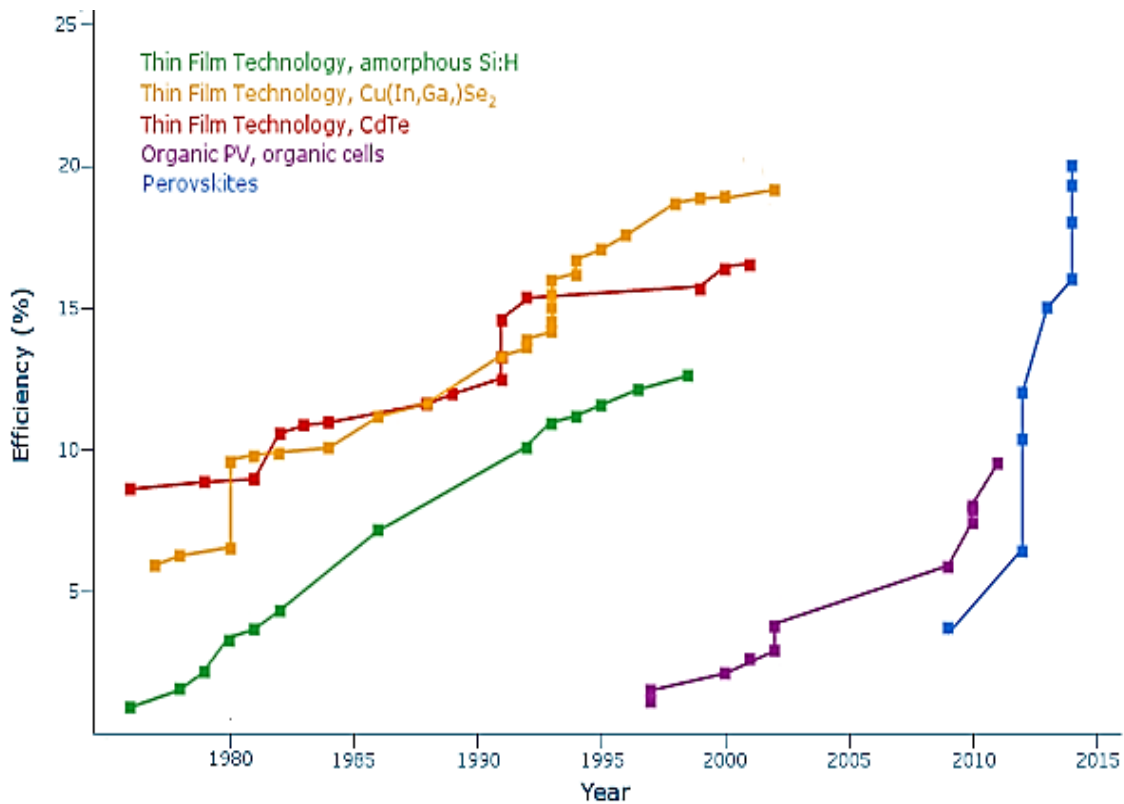


Figure 1- 2- Perovskite research progress in terms of efficiency.

1. 2. Synthesis of Methylammonium lead Halide Perovskite ($\text{CH}_3\text{NH}_3\text{PbX}_3$)

Synthesis of the $\text{CH}_3\text{NH}_3\text{PbX}_3$ (X can be Cl, Br, I or a mixture of them) can be done by reacting $\text{CH}_3\text{NH}_3\text{X}$ with PbX_2 . For instance, $\text{CH}_3\text{NH}_3\text{PbI}_3$ case, have to be started with the preparation of the $\text{CH}_3\text{NH}_3\text{I}$ which is obtained by reacting methylamine (CH_3NH_2) and Hydro iodide acid (HI) at a temperature equal to 0°C . Next, Product have to be rinsed with diethyl ether in order to eliminate unreacted chemical species. In the end, the final product can be obtained by heating the washed powder to the 60°C for 12 hours. Additionally, there are also commercial $\text{CH}_3\text{NH}_3\text{I}$ which can be bought and use as it is.

To reach the final solution of the $\text{CH}_3\text{NH}_3\text{PbI}_3$, as prepared $\text{CH}_3\text{NH}_3\text{I}$ and PbI_2 Powder have to be dissolved in an aprotic polar solvent in the 1:1 molar ratio. The best solvent is Dimethylformamide (DMF). In the other solvents PbI_2 has a very subtle solubility and they are not as good as DMF.

Evaporation of the solvent leads to the formation of the $\text{CH}_3\text{NH}_3\text{PbI}_3$ from the solution. In order to form a thin film, the solution is spin coated on the sample (sample can be a bare ITO / FTO or it can be pre deposited with an oxide film). Then, sample has to be dried out to evaporate the solvent and perovskite crystals start to form. The detailed process can be found elsewhere. [41] Perovskite film can be prepared with two-step process or one step process, which will be explained in the following chapters in details. In two-step method, the mechanism is based on an intercalation (diffusion) reaction. PbI_2 is a layered structure and methylammonium iodide ($\text{CH}_3\text{NH}_3\text{I}$) can be intercalated into the interlayer of the PbI_2 layers. By using this method, it is possible to create thick films. Additionally, it is suitable for filling the pores in the mesoporous films. [42- 44]

On the other hand, synthesis of $\text{CH}_3\text{NH}_3\text{PbI}_{3-x}\text{Cl}_x$ is reaction between $\text{CH}_3\text{NH}_3\text{I}$ and PbCl_2 instead of reaction with PbI_2 . In order to have a similar structure like $\text{CH}_3\text{NH}_3\text{PbI}_3$, it is advised to consider 3:1 molar ratio between $\text{CH}_3\text{NH}_3\text{I}$ and PbCl_2 . [15]

1. 3. Perovskite crystal structure and its properties

Perovskite materials have a structure with the general formula ABX_3 . A and B are both cations and X is an anion which is usually Oxygen or a halogen. The Cation A normally is larger than B. In fact, A is a very large atom which can occupy the bulky cubo-octahedral site in the structure. In the case which X atom is a halide such as Cl, Br or I, B atom is a divalent and the cation A is a monovalent ion in order to satisfy charge neutrality.

Determination of the crystal stability of the perovskite materials, normally can be estimated from Goldschmidt tolerance factor (t), [1]

$$t = (r_A + r_X) / (\sqrt{2}(r_B + r_X))$$

Where, r_A , r_B and r_X are the ionic radiuses.

One of the most used perovskite structures is $CH_3NH_3PbX_3$. This perovskite based on the tolerance factor (t), has a similar value of t factor of the cubic structure, so it is predicted to have a cubic structure in terms of the stability. [24] Moreover, according to the crystal phase and temperature- dependent phase transitions, for X=I cubic phase was detected for temperature (T) greater than 327.4 °K, for X=Cl, $T > 178.8$ °K and for X=Br, $T > 236.9$ °K. [4]. So, $CH_3NH_3PbI_3$ perovskite, has a tetragonal structure at ambient temperature with lattice parameters of $a=8.855$ Å and $C= 12.659$ Å. In the Figure 1-3, unit cell for the $CH_3NH_3PbI_3$ has been depicted.

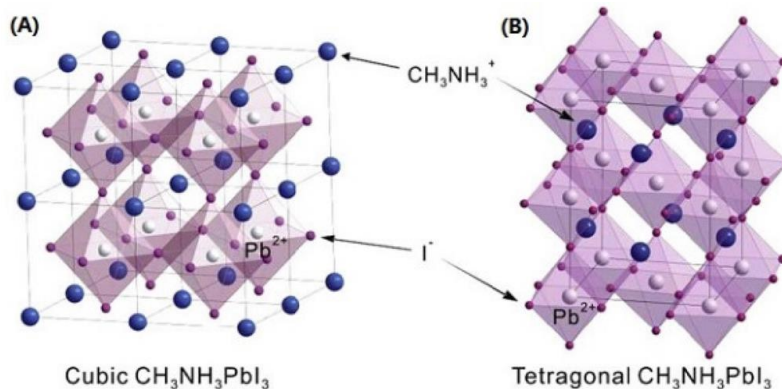


Figure 1- 3- $\text{CH}_3\text{NH}_3\text{PbI}_3$ unit cell structures. Reprinted from Shiqiang Luo and Walid A. Daoud [2]

The basic physical properties of the $\text{CH}_3\text{NH}_3\text{PbX}_3$ are listed in the Table 1- 2. [3]

Physical property	X= Cl	X= Br	X= I
Dielectric Constant	23.9	25.5	28.8
Dipole Moment (C m)	0.85	0.77	0.85
Energy Band Gap (Theoretical) (eV)	2.34	1.8	1.57
Energy Band Gap (Experimental) (eV)	3.1	2.3	1.5

Table 1- 2- physical properties of the $\text{CH}_3\text{NH}_3\text{PbX}_3$. [3]

As it is shown, band gap energies increase as halogen size decreases from I to Cl. All the reported data are calculated for the cubic structures of $\text{CH}_3\text{NH}_3\text{PbX}_3$. The experimentally observed data also has shown similar trends. [4]

In General, physical properties are tunable by the right choice of the atoms. For example, methylammonium which is placed at A site can be replaced with ethylammonium ($\text{CH}_3\text{CH}_2\text{NH}_3^+$), [6] or Formamidinium ($\text{HC}(\text{NH}_2)_2^+$), [5]. These modifications cause change in the band gap energy as it is shown in the Table 1- 3, mainly because of the structural modification.

	Band Gap Energy (eV)	Crystal Structure
Methylammonium (CH ₃ NH ₃) ⁺	1.52	Cubic
Formamidinium (HC(NH ₂) ₂) ⁺	1.45	Hexagonal Prism
ethylammonium (CH ₃ CH ₂ NH ₃) ⁺	2.2	orthorhombic

Table 1- 3- band gap modification by atom replacements and corresponding structures.

Furthermore, it is also possible to replace Pb²⁺ in B site with other divalent atom such as Sn²⁺. This change, modify the band gap energy from 1.5 eV for Pb²⁺ to 1.2 eV for Sn²⁺. [5]

So, according to kind of application and required range of the response, it is possible to use proper elements. (Figure 1-4)

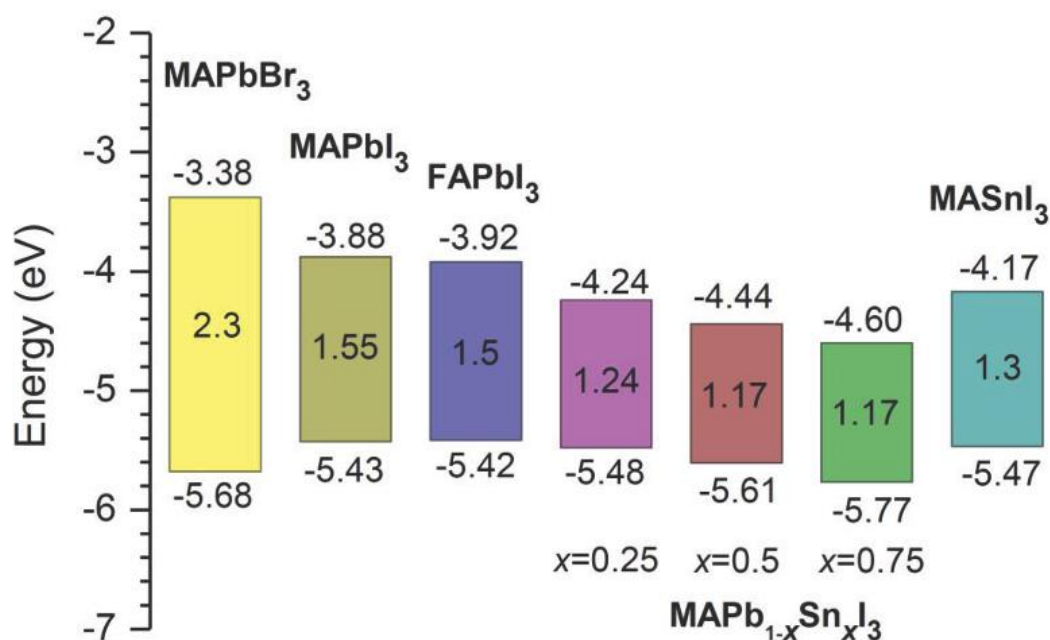


Figure 1- 4- schematic energy level diagram of MAPbBr₃, MAPbI₃, FAPbI₃, MAPb_{1-x}Sn_xI₃, and MASnI₃. MA and FA stand for methylammonium (CH₃NH₃) and formamidinium (HC(NH₂)₂), respectively. Data for MAPb_{1-x}Sn_xI₃ are for x = 0.25, 0.5, 0.75 and 1. Reprinted from [45]

1. 3. 1. Electro- optical properties

Opto- electronic properties of the perovskite materials are closely related to the structural dimensionality.

Perovskite materials are semiconductor materials with low band gap energy. Organometal halide perovskite composes both organic and inorganic parts. Under illumination, they are able to form two different kinds of the excitons. One is Frenkel-type exciton which has high binding energy and small Bohr radius. The other form is Wannier type exciton which in contrary has a low exciton binding energy and large Bohr radius. Frankel excitons originate from the organic part and the Wannier ones arise from the inorganic part. [7] Values of Bohr radius, binding energy and the reduced mass for the lowest-energy excitons in $\text{CH}_3\text{NH}_3\text{PbX}_3$ has been reported in the Table 1- 4. [8]

	Exciton Bohr radius (\AA)	Exciton Binding Energy (m eV)	Exciton Reduced mass
CH₃NH₃PbI₃	22	50	0.15 m_0
CH₃NH₃PbBr₃	20	76	0.13 m_0

Table 1- 4- Values of Bohr radius, binding energy and reduced mass for the lowest-energy excitons in $\text{CH}_3\text{NH}_3\text{PbX}_3$. [8]

As it is clear from Table 1- 4 exciton Bohr radiuses are relatively large and binding energies are small, so, excitons can be classified as a 3D Wannier ones. [9-12]

Perovskite materials have a good charge mobility and life time for both electrons and holes. Moreover, diffusion length extracted from Photoluminescence quenching measurement (PL) for the carriers, revealed that mixed halide perovskite has a very high diffusion length for both electrons and holes in the order of 1000 nm. [13] Besides, low absorption depth (100-200 nm) made them superior to the other kind of the perovskites such as $\text{CH}_3\text{NH}_3\text{PbI}_3$ which has a diffusion length around 100 nm for both holes and electrons. (Figure 1- 5)

The recombination time constant can be defined roughly by:

$$\tau_R = L_e^2 / D_e$$

Where Le and De are diffusion length and diffusion coefficient for the electron respectively. By considering measured data in the Table 1- 5, recombination time constant can be calculated. The calculated values are considerably higher for the mixed halide perovskite respect to the trihalide perovskite, which proved superiority of the mixed halide perovskite versus trihalide one, in the charge carriers extraction.

Perovskite Material	Carrier	D (cm ² s ⁻¹)	L (nm)	Recombination time constant (n S)
CH ₃ NH ₃ PbI _{3-x} Cl _x	electron	0.042±0.016	1069±204	272
	hole	0.054±0.022	1213±243	272
CH ₃ NH ₃ PbI ₃	electron	0.017±0.011	129±41	9.8
	hole	0.011±0.007	105±32	10

Table 1- 5- Measured data for diffusion length and coefficient and calculated recombination constant, for different perovskite materials.

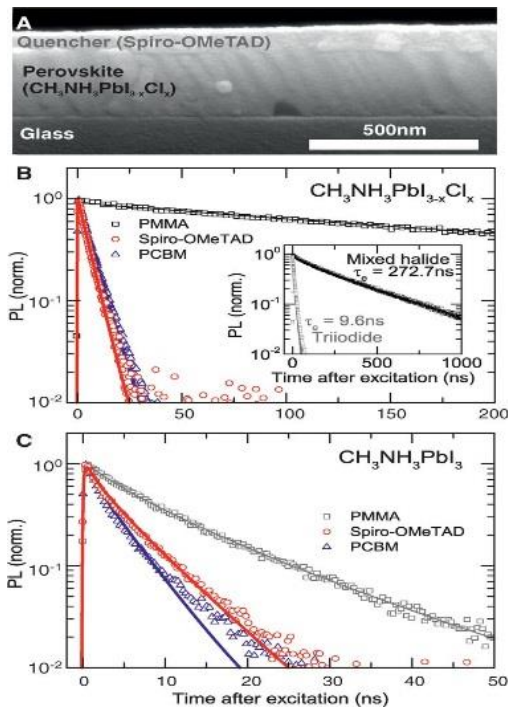


Figure 1- 5- higher carrier life time in the mixed halide respect to triiodide perovskite. Reprinted from H. Snaith et al.

1. 4. Perovskite solar cells different configurations

In general perovskite solar cells are divided into three categories:

1. Sensitized structure
2. Meso-superstructure
3. Planar structure.

In the sensitized configuration (Figure 1- 6), the only difference with dye sensitized cells, is the replacement of the dye molecules by perovskite. In fact, this configuration was the first generation of the perovskite solar cells in which $\text{CH}_3\text{NH}_3\text{PbI}_3$ perovskite dots formed on the nanocrystalline TiO_2 surface and then Spiro-OMeTAD was infiltrated on top of the perovskite coated mesoporous TiO_2 film. [14]

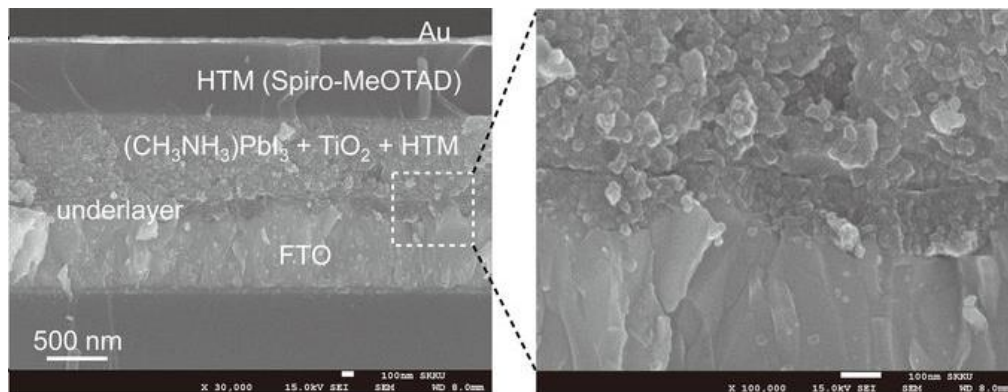


Figure 1- 6- (left) Cross-section SEM image of the device. (right) Active layer-under layer-FTO interfacial junction structure. Reprinted from [14]

In meso- superstructure, perovskite layer infiltrates in a scaffold of the Al_2O_3 or TiO_2 . In this case a thin layer of the perovskite material is formed on top of the scaffold and in contrary to the previous case it is a continuous film and not dots. [15] (Figure 1- 7)

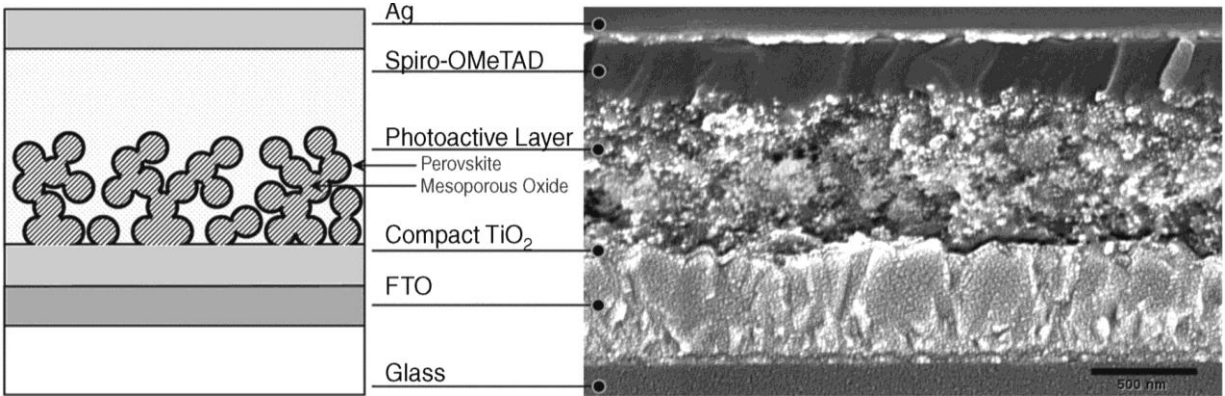


Figure 1- 7- Left: Schematic representation of full device structure, where the mesoporous oxide is either Al₂O₃ or TiO₂. Right: Cross-section SEM image of a full device incorporating mesoporous Al₂O₃. Reprinted from [15]

In a planar structure, there is no mesoporous layer and all the layers are compact layers and they form junctions at the boundaries of the each layer. In general, there are two different types of the planar structure, which are called standard and inverted configuration. (Figure 1- 8) [94]

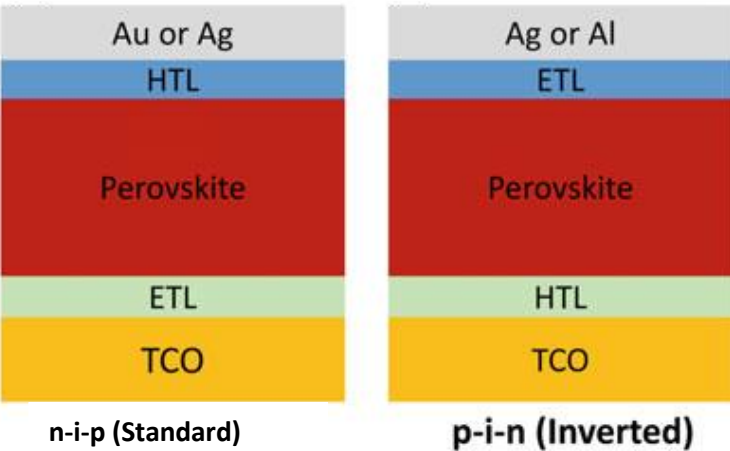


Figure 1- 8- standard and inverted configuration of the planar structure.

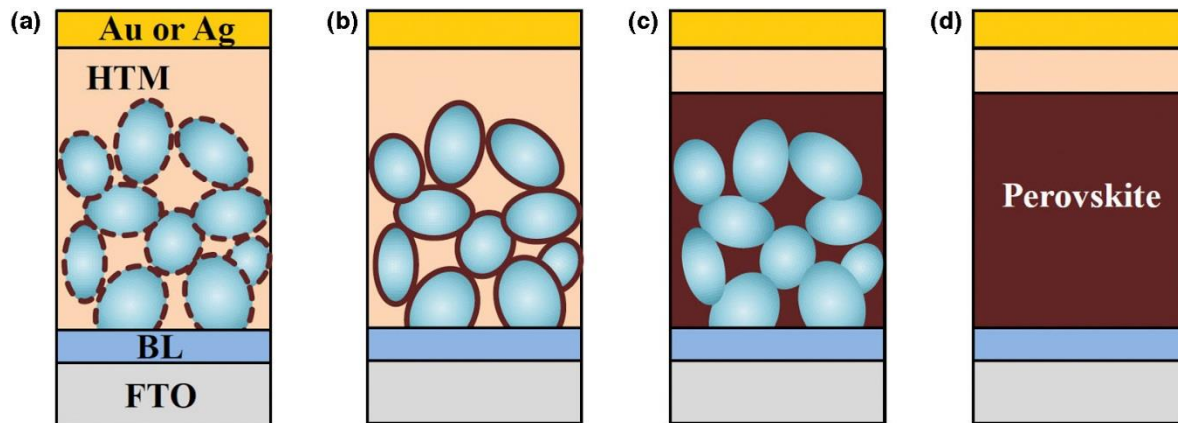


Figure 1- 9- Structural evolution of perovskite solar cells: (a) sensitization concept with surface adsorption of Nano dot perovskite, (b) meso-superstructure concept with non-injecting scaffold layer, (c) pillared structure with a Nano oxide building block, and (d)

1. 5. Planar structure fabrication

Following, the laboratory base instruction to form a planar perovskite structure, is presented.

First, a transparent conductive oxide (TCO) substrate has to be patterned by etching or laser ablation. Then electron transport compact layer (ETL) forms on top of the TCO. Material for this layer recommended to be an oxide with proper electron transport and good hole blocking property, in order to have a high efficiency electron extraction layer. This layer has to be well covered the TCO since there should not be any direct contact between hole transporting layer and TCO. Thickness of this layer is suggested to be less than 100nm. Next, it is time to deposit perovskite layer either with already mentioned one step or two-step method. Thickness of this layer is recommended to be between 200 to 400 nm. Later, hole transporting layer (HTM) has to be deposited on top of the perovskite layer. Material for this layer should have a high hole transporting behavior and good electron blocking property. Thickness of this layer also has to be enough thin in order to have a good hole extraction efficiency. Finally, the last layer is a metal contact electrode. Candidates for this electrode have to fulfill some criteria such as inertness and matching work function with the valence band of the HTM. Au is commonly used metal for this purpose. (Figure 1- 10)

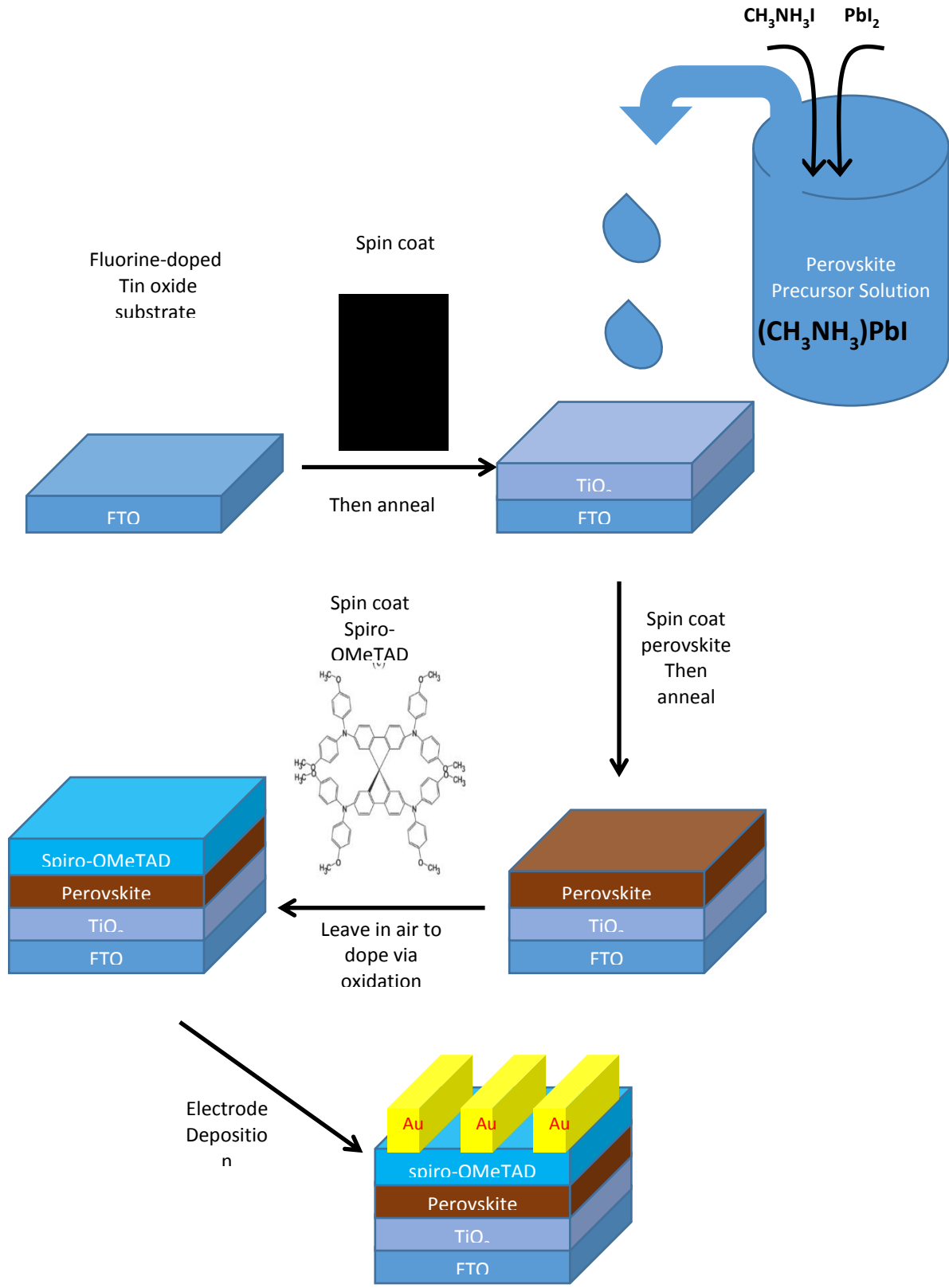


Figure 1- 10- Fabrication steps of the standard configuration.

1. 5. 1. Planar Perovskite solar cell performance

Because the structure which have been used in this thesis is a planar structure, here you can find the state of the art of this structure. [108]

Planar perovskite is a very popular structure and there are a lot of researchers and groups who are working on this structure. Below in the table 5 it is possible to find the recent progress reported in this field. In this table, layer stacks, processing methods and power conversion efficiencies are reported. [16]

Device structure	Additives/treatment	Processing method	PCE (%)	Processing temperature	Reference
FTO/bl-TiO ₂ /MAPbBr ₃ /PIF8-TAA/Au	HBr	SC	10.4	100°C	Heo et al. (2014)
FTO/c-TiO ₂ /MAI ₃ -XCIX/spiro-OMeTAD/Ag	–	DSVD	15.4	120–325°C	Liu et al. (2013)
FTO/bl-TiO ₂ /MAPbI ₃ /spiro-OMeTAD/Au	Gass-assisted crystallization	SC	17.1	35–100°C	Huang et al. (2014)
FTO/bl-TiO ₂ /MAPbI ₃ /spiro-OMeTAD/Au	Electrospun nanofibers	SD	9.82	70°C	Dharani et al. (2014)
FTO/bl-TiO ₂ /TiO ₂ :MAPbI ₃ /Au	No hole transporter	SD	12.22	450°C	Xiao et al. (2015)
ITO/PEDOT:PSS/MAPbI ₃ /PC61BM/Al	N-cyclohexyl-2-pyrrolidone	SC	10	100°C	Jeon et al. (2014a)
FTO/bTiO ₂ /mpTiO ₂ :(5AVA)x(MA) _{1-x} PbI ₃ /ZrO ₂ :(5AVA)x(MA) _{1-x} PbI ₃ /Graphite	5-ammonium valeric acid	SC	12.8	50°C	Mei et al. (2014)
FTO/TiO ₂ /CsSnI ₃ -xFx/N719/H2PtCl6/FTO	Lead-free absorber	DC	9.28	400°C	Chung et al. (2012a)
FTO/c-TiO ₂ /Al ₂ O ₃ :MAPbI ₃ /spiro-OMeTAD/Ag	Al ₂ O ₃ scaffold	SC	10.9	100°C	Lee et al. (2012)
ITO/PEDOT:PSS/MAPbI ₃ -xClx/PC61BM/Bis-C60/Ag	1<comma>4-Diiodobutane	SC	13.09	90°C	Chueh et al. (2015)
FTO/c-TiO ₂ /MAPbI ₃ /spiro-OMeTAD/Ag	Non-halide lead source	SC	14	150°C	Zhang et al. (2015b)
FTO/bl-TiO ₂ /MAPbI ₃ -xClx/spiro-OMeTAD/Ag	Vapor-assisted crystallization	VASP	12.1	110–150°C	Chen et al. (2014)
FTO/c-TiO ₂ /TiO ₂ :MAPbI ₃ /spiro-OMeTAD/Au	Mesoscopic composite	SD	12.6	70°C	Burschka et al. (2013)
FTO/NiO/MAPbI ₃ -xClx/PC60BM/Ag	–	DSVD	7.26	120–325°C	Subbiah et al. (2014)
FTO/c-TiO ₂ /Al ₂ O ₃ :MAPbI ₃ /SWNT:P3HT/Ag	Carbon nanotube/PMMA	SC	15.4	100°C	Habisreutinger et al. (2014)
ITO/PEDOT:PSS/PolyTPD/MAPbI ₃ /PCBM/Au	PolyTPD	DSVD	12.04	70–250°C	Malinkiewicz et al. (2014)

FTO/TiO ₂ /MAPbI ₃ -xClx/spiro-OMeTAD/Au	–	SC	11.4	90–170°C	Eperon et al. (2014a)
PET/AZO/PEDOT:PSS/MAPbI ₃ /PCBM/Au	Silver	DSVD	7	70–200°C	Roldán-Carmona et al. (2014)
FTO/c-TiO ₂ /MA3PbI ₃ /spiro-OMeTAD/Ag	Solvent–solvent extraction	SD	15.2	Room temp.	Zhou et al. (2015)
FTO/TiO ₂ /MAPbI ₃ /spiro-OMeTAD/Au	TiO ₂ nanobeads	SC	7.7	70°C	Tathavadekar et al. (2015)
FTO/bi-TiO ₂ /MAPbI ₃ /Spiro-OMeTAD/Au	Fast-crystallization deposition	SC	13.8	100°C	Xiao et al. (2014)
ITO/PEDOT:PSS/MAPbI ₃ /PC61BM/Al	Poly(2-ethyl-2-oxazoline)	SC	6.35	100°C	Xue et al. (2015)
FTO/TiO ₂ /MAPbI ₃ -xClx/spiro-OMeTAD/Au	PEG	SC	13.2	100°C	Chang et al. (2015)
FTO/TiO ₂ /MAPb(I<comma>Cl) ₃ /spiro-OMeTAD/Au	Mixed halide source	SD	10.49	100°C	Jiang et al. (2015)
ITO/PEDOT:PSS/CsxMA1–xPbI ₃ /PCBM/Al	Caesium	SC	7.68	110°C	Choi et al. (2014)
ITO/PEDOT:PSS/MAPbI ₃ /PC61BM/Bis-C60/Ag	1<comma>8-Diiodooctane	SC	11.8	90°C	Liang et al. (2014)
ITO/PEDOT:PSS/MAPbI ₃ /PCBM/C60/BCP/Al	Gass-assisted crystallization	SC	13.6	70°C	Lian et al. (2015)
ITO/PEDOT:PSS/MAPbI ₃ -xClx/PCBM/Al	1-Chloro-naphthalene	SC	9.46	100°C	Song et al. (2015)
FTO/mp-TiO ₂ /MAPbI ₃ /electrolyte/Pt/FTO	–	SC	3.81	40–70°C	Kojima et al. (2009)
ITO/PEDOT:PSS/MAI ₃ -xClx/PC61BM/TPPI/Al	Tetraphenyl phosphonium iodide	SC	13	100°C	Sun et al. (2015)
FTO/c-TiO ₂ /mp-TiO ₂ :MAPbI ₃ /spiro-OMeTAD/Au	High humidity	SC	15.76	50–100°C	Ko et al. (2015)
ITO/PEIE/Y:TiO ₂ /MAPbI ₃ -xClx/spiro-OMeTAD/Au	Ethoxylated poly-ethyleneimine <comma> yttrium	SC	19.3	100°C	Zhou et al. (2014)
FTO/PEDOT:PSS/MAPbI ₃ /PCBM/Al	Hot-casting crystallization	SC	18	170–190°C	Nie et al. (2015)
FTO/TiO ₂ /MAPbI ₃ /electrolyte/Pt/FTO	Quantum-dot sensitized	DC	6.5	40–160°C	Im et al. (2011)
FTO/TiO ₂ :SiO ₂ /MAPbI ₃ -xClx/spiro-OMeTAD/Au	SiO ₂ scaffold	SC	8.8	100°C	Zhang et al. (2015a)
FTO/NiO NC's/MAPbI ₃ -xClx/PC61BM:PS/Al	Polystyrene	SC	10.68	100°C	Bai et al. (2015)

Table 1- 6 - Various structure of organic–inorganic perovskite solar cells, processing approach, additional treatment deposition technique and reported efficiencies; (SC: spin-coating; DSVD: dual source vapor deposition; SD: sequential deposition; VASP: vapor assisted. Reprinted from [16]

1. 6. Drawbacks [46]

1. 6. 1. Stability

Short and long term stability of the perovskite solar cells (PSCs), is one of the biggest issues that researchers are trying to find a way to overcome. Instability roots in several factors which are mainly environmental impacts like moisture and oxygen, thermal impacts (temperature variation due to internal heating under applied voltage) and degradation caused by radiation. [17] Currently, there are a lot of researchers who are trying to investigate this problem and finding a way to improve it. However, still stability remained as an unsolved problem. [93]

The organic constituents of the PSCs are mainly water soluble and prone to dissolve in the water present in the air and cause major damages to the device. So, humidity in the air is one of the main agents which has to be avoided. [18] Moisture degradation can be reduced by being careful in the material selection, architecture of the cell and control over environmental conditions. Encapsulation is the other effective way to prevent direct contact of the PSCs with the air. For instance encapsulation with a polymer composite has been reported to be a successful solution to overcome the problem related to being exposed to the air at elevated temperature. [18, 19]

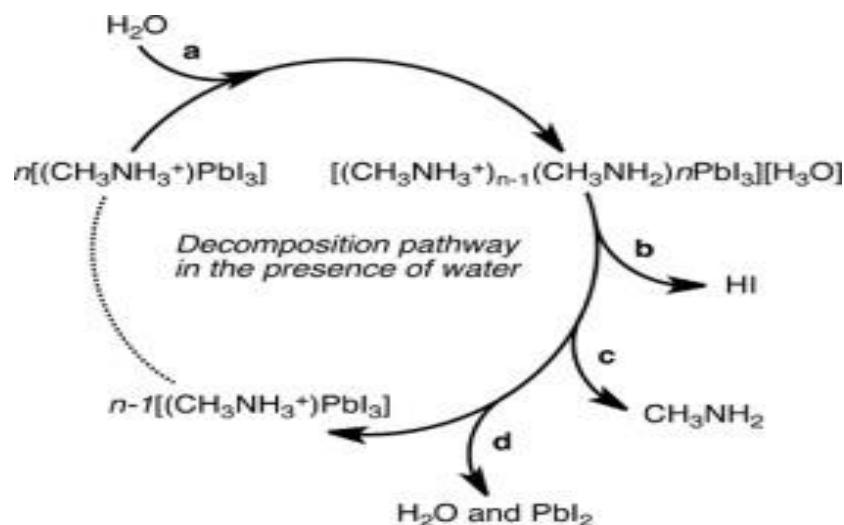


Figure 1- 11- Proposed decomposition pathway of $\text{CH}_3\text{NH}_3\text{PbI}_3$, in the presence of a water molecule. The main product of this pathway is PbI_2 . [20]

Moreover, UV light instability is another major degradation mechanism which is presented specially in the mesoporous structures. It is mainly due to the interaction between photo induced holes inside TiO₂ layer and oxygen radicals placed on the TiO₂ surface. [21]

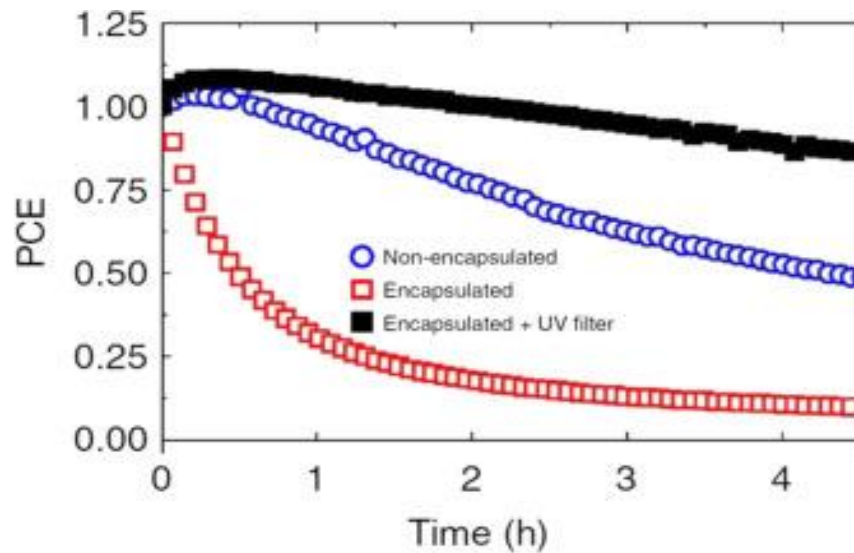


Figure 1- 12- Normalized power conversion efficiency degradation curves for perovskite solar cells containing TiO₂. Shown are non-encapsulated (blue open circles), encapsulated (red open squares), and encapsulated with a 435 nm UV filter (black closed squares) devices. [21]

Thermal conductivity of the CH₃NH₃PbI₃ is very low, around 0.5 W/(K m) at room temperature. This low thermal conductivity prevents fast propagation of the heat over the sample, so it may cause internal thermal stress which reduces its lifetime. [22]

1. 6. 2. Stability of the hole transporting layer [112]

Spiro-OMeTAD is the most commonly used material as a hole transporting layer (HTL). In the preparation of the solution of the Spiro, it is necessary to use two additives, 4-*tert*-butylpyridine (TBP) and bis (trifluoromethane) sulfonimide lithium salt (Li-TFSI), in order to intensify the conductivity. But, these materials are harmful to the perovskite layer and reducing the stability of the device. [23]

Degradation mechanism which is induced by Spiro leads to increase in the series resistance (R_s) when cells were tested at RH of 50% and constant temperature at 55 °C. [24] SEM images showed formation of voids on the Spiro layer which can be formed by the gaseous by-products from the degradation of the perovskite layer which went through the Spiro layer. Spiro is a very soft and permeable layer and it is a very good pass way to let gaseous species to escape. [20]

Another equally important material which is commonly used as a HTL in the inverted configuration is PEDOT: PSS. This layer also undergoes rapid degradation and leads to lowering the performance of the cell. Like Spiro this material also let moisture to infiltrate and cause decomposition of the perovskite layer.

For elimination of the instability problem related to the HTL, researchers proposed some other materials like Cu: NiO_x. Figure1- 13 showed the comparison of their performances. [25]

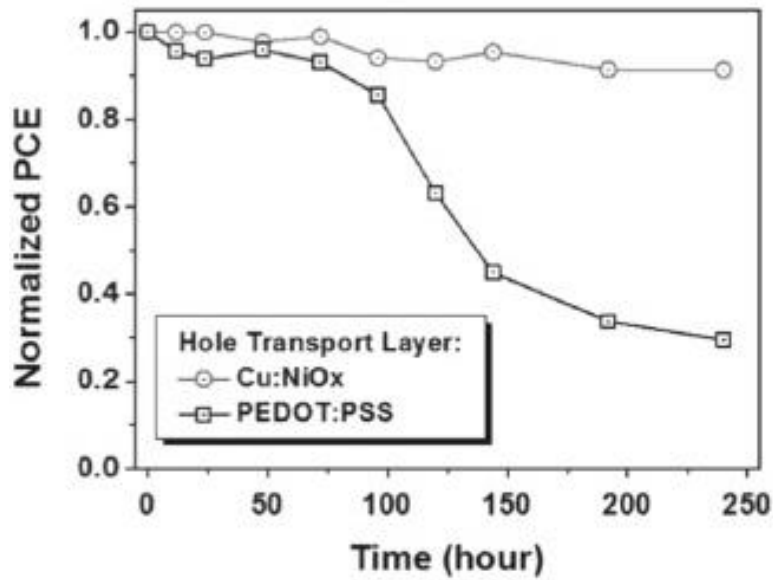


Figure 1- 13- Normalized PCE of perovskite solar cells based on PEDOT: PSS (squares) and Cu: NiOx (circles) hole-transporting layers as a function of storage time in air. [25]

1. 6. 3. Hysteretic current-voltage behavior [26, 27]

Another important matter in the perovskite solar cells is the dependency of the Current-Voltage (IV) curves to the scan conditions. The power conversion efficiency (PCE) of a perovskite solar cell is obtained via characterizing its IV behavior under simulated solar emission. The dependency of the IV behavior to the scan conditions called hysteresis behavior. It means according to different scan conditions like scan direction, scan rate, light soaking and biasing, behavior of the IV curve can be different. It means curve obtained in the scan from forward bias to short circuit (FB-SC) and the scan from short circuit to forward bias (SC-FB) have different behavior, in contrary to the other solar cells. (Figure 1- 14) [96]

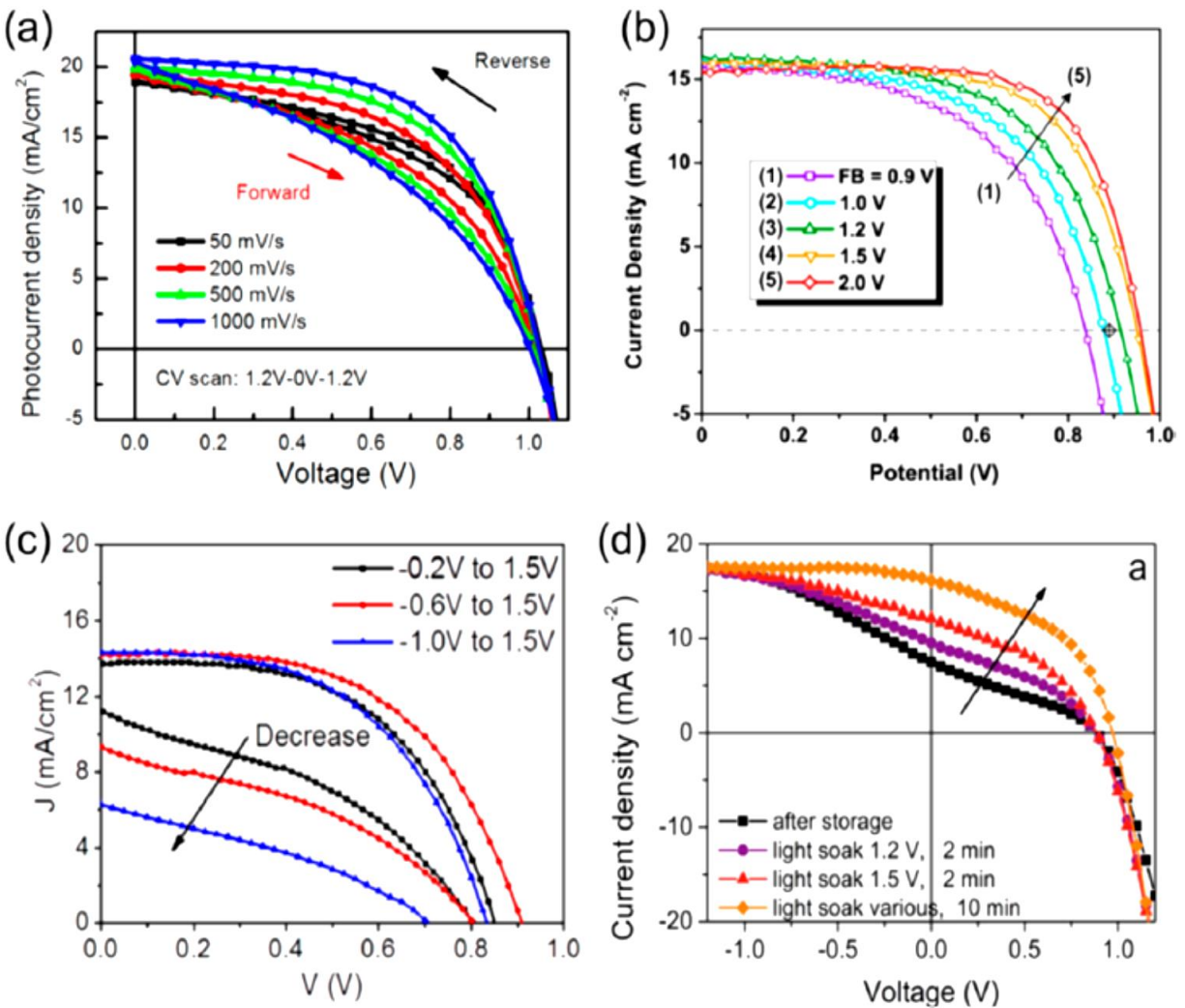


Figure 1- 14- effects of different scan conditions on the I-V curves. (a) Different scan rates (b) Different pre- biasing. (c) Influence of the scanning range. (d) Light soaking.

The reason for this discrepancy have been proposed to be ion movement, ferroelectric effects, polarization and trap states. However, it is a very controversial topic and there are lots of ongoing projects to understand this phenomena better. (Figure 1- 15) This phenomena imposes the risk of producing wrong numbers for the PCE which can be misleading. This phenomena shows that perovskite solar cell does not work in the electronic steady state condition. There are two possible solutions, Unger et al. suggested to perform very slow scan rate, which keep cell working in the steady state condition. [27]

The second solution proposed by Henry Snaith et al. which called stabilized power output. This value is obtained by testing the sample at constant voltage (voltage corresponds to the maximum product of the voltage and current, which is called maximum power) and reading the power output until reaching its constant value. Both solutions have been demonstrated to produce PCE values lower than what obtained by fast scans. [26, 27] Nevertheless, it has been shown that surface passivation of the perovskite layer would result in less hysteresis and efficiencies near to the stabilized one also with fast scan. [28, 29, 94, 95]

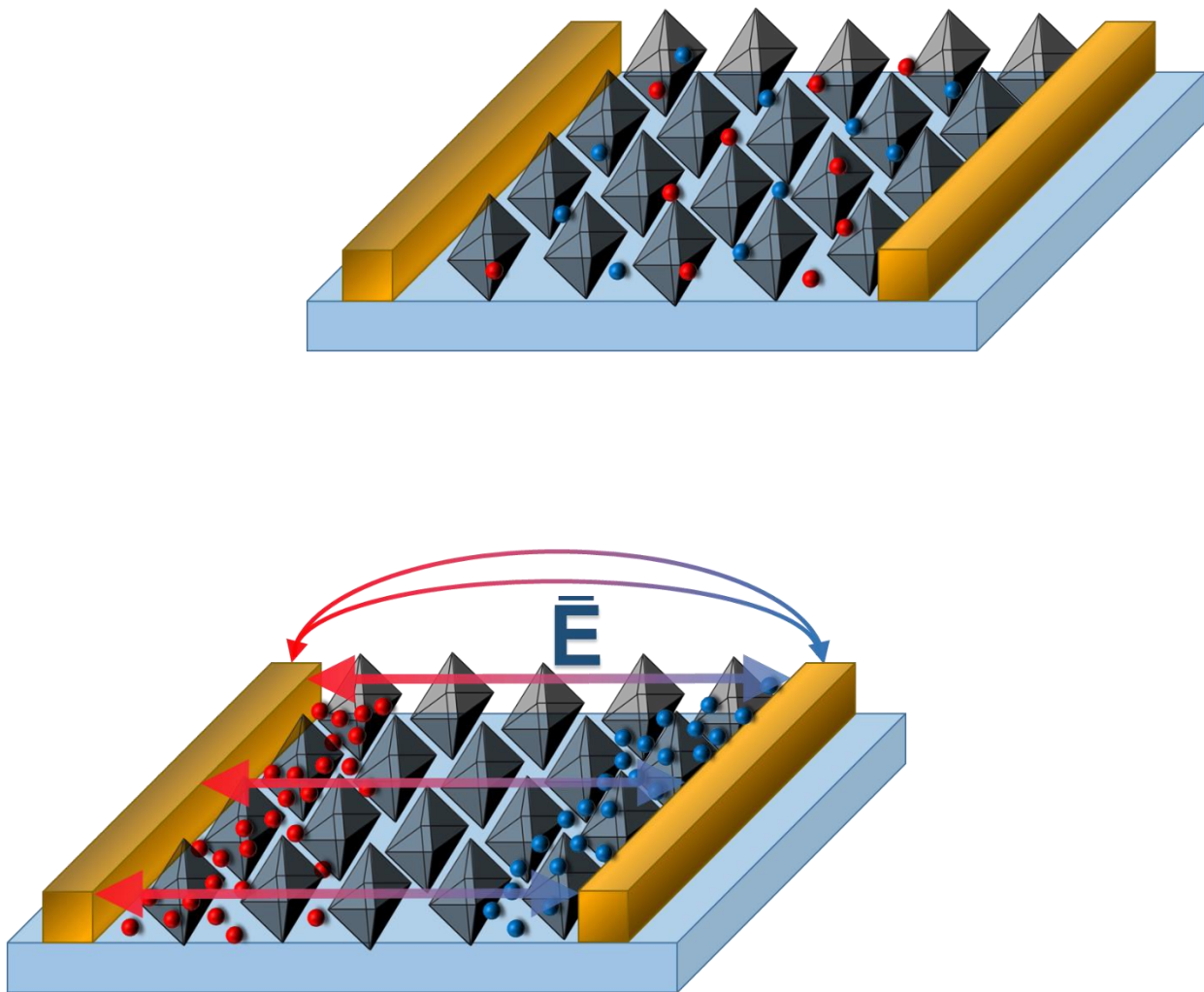


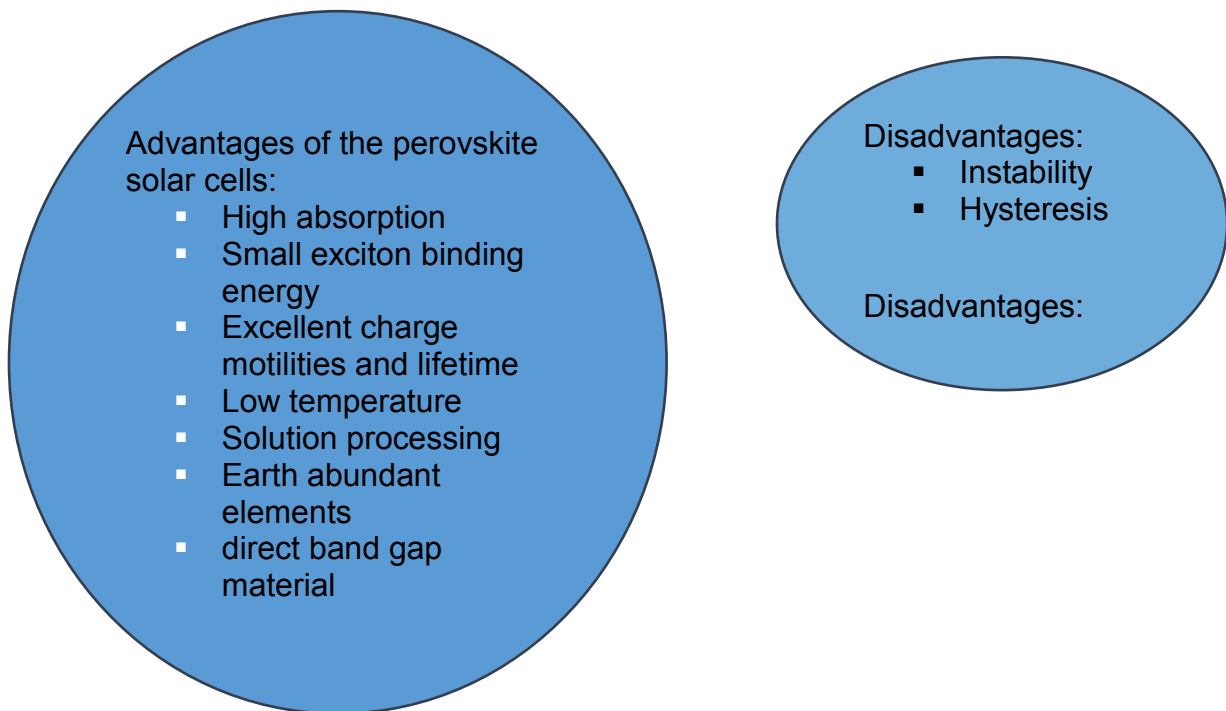
Figure 1- 15- Ion migration effect.

It has been noted that in the inverted structure, there is a little to no hysteresis behavior. [30] This could be an indication of the crucial role of the interface [116] in the hysteretic IV behavior. Since the only difference of the inverted structure respect to the standard structure is the replacement of the n-type metal oxide with an organic n-type material (Phenyl-C61-butyric acid methyl ester (PCBM)).

Unfortunately, usually hysteresis behavior is neglected or ignored by the majority of the publications and data is reported by the fast rate IV curves which is not reliable results for the evaluation of the cell performance.

This ambiguity caused to establish a standard method for the cell certification by accredited laboratories such as NREL. [31] So just certified cells counted as the state of the progress of the perovskite solar cells field.

1. 7. Summary



1. 8. Conclusion [52, 54, 57, 99, 102, 104, 118]

The aim of this thesis is to make a perovskite solar cell with better performance In terms of stability and hysteresis.

This goal can be reached by replacing the materials of different layers. So, as a candidate for this replacement, it has been suggested to use reduced Graphene Oxide (rGO).

rGO is a good candidate for the carriers transport layers since it has all the required properties of these layers.

rGO, is a semiconductor with a band gap which can be tuned by the degree of the reduction. Additionally, it has a fabulous mobility and diffusion length for both electrons and holes. Moreover, it is possible to use rGO as an interlayer between already existing layers to improve the interfaces.

At the moment of starting this thesis there were just a few papers with using rGO in the perovskite solar cells. Therefore, there were lots of undiscovered issues to obtain a proper procedure for this aim.

Details of this work will be presented in the following chapters.



Chapter 2

Reduced Graphene Oxide

This project is divided in two major steps:

First step is aimed to develop a good reduce Graphene Oxide film and the second step realization of whole perovskite solar cell.

2. Development of Reduce Graphene Oxide film

2. 1. Graphene

Graphene is an allotrope of carbon in a 2-dimensional form and it is a one-atom thick layer. It has a honey-comb lattice in which one atom forms each vertex. From Bond Energy Diagram point of view, this structure has a special feature which is touching of Conduction and Valence bands on special points. (Figure 2- 1)

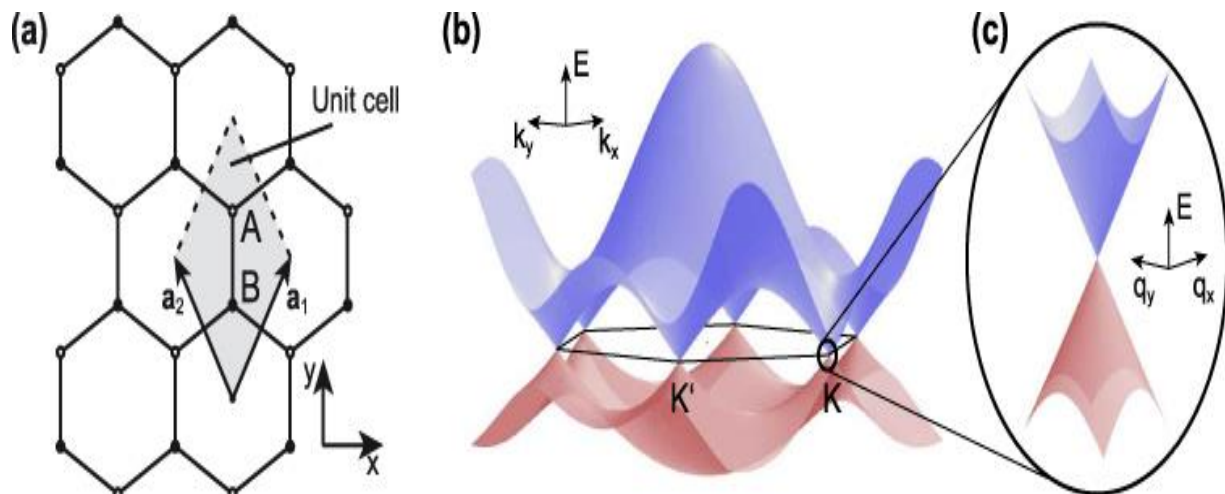


Figure 2- 1- Graphene Bond Structure

This Structure provides a metal like behavior for the Graphene. In a way that a small amount of energy gives electrons inside the valence band enough energy to be promoted to the Conduction band and act as free carriers.

2. 1. 1. Fundamental Characteristics

2. 1. 1. 1. Electronic Properties

Graphene as a one-layer material has a zero band gap energy in certain points. This zero band gap gives graphene metal like behavior which cause very high conductivity.

High conductivity of the graphene comes from the less localized pi (π) electrons. These electrons are located on the planes parallel to the graphene sheet on above and below. Fundamentally, bonding and anti-bonding (the valence and conduction bands) electrons of the π orbitals, are ruling the electronic properties of the graphene.

From the theoretical model and experimental data, it is proven electron and holes have a zero mass at the Dirac points (K points in the Figure 2- 1). This is coming from linear relation of the energy versus k vector at Dirac points. (Figure 2- 2) Dirac points are located at the 6 corners of the Brillouin zone. Although, density of states is quite low at Dirac points which leads to low conductivity, Fermi energy can be changed by doping to have a material with conductivity even higher than copper at room temperature.

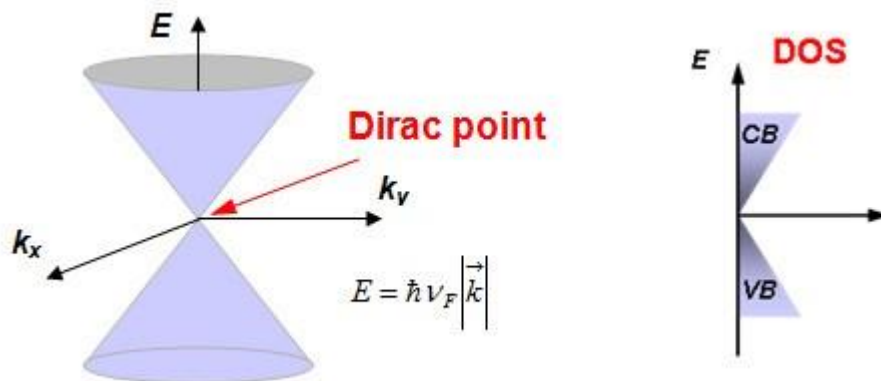



Figure 2- 2- Energy versus K vector diagram of Graphene at Dirac point

Moreover, other property which makes the graphene very interesting material, is a high electron mobility. Since electrons have zero mass, it is said that they behave very similar



to the photons. Electrons operate on the ballistic transport regime and are able to travel sub-micron distances without scattering. Nevertheless, the quality of the graphene film has to be taken into account, in fact, all the above mentioned properties are applicable just for the defect less graphene layer.

2. 1. 1. 2. Mechanical Strength

Other outstanding property of the graphene is its inherent strength. Actually, graphene is the strongest material which have ever been discovered. Ultimate tensile strength of graphene is about 130 GPa. Not only graphene is interestingly strong, it is also very light weighted. Its weight is about 0.77 milligrams per square meter.

Another feature of the graphene is its high strain strength. They can stand high elongations with their elastic behavior and retain their initial size after strain.

2. 1. 1. 3. Optical Properties

High absorption coefficient of the graphene is the other stand out property which makes it very unique. It can absorb near 2.3 % of white light only within one-layer thick layer.

2. 2. Graphite

Graphite is stacked of Graphene layers over each other. In contrary to Graphene, Graphite is an insulating material and it has a band gap. (Figure 2- 4)

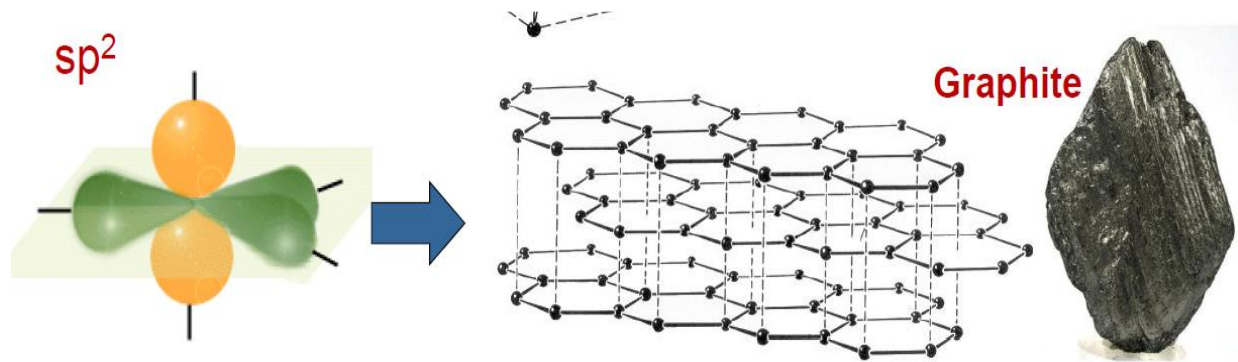


Figure 2- 3- Graphite

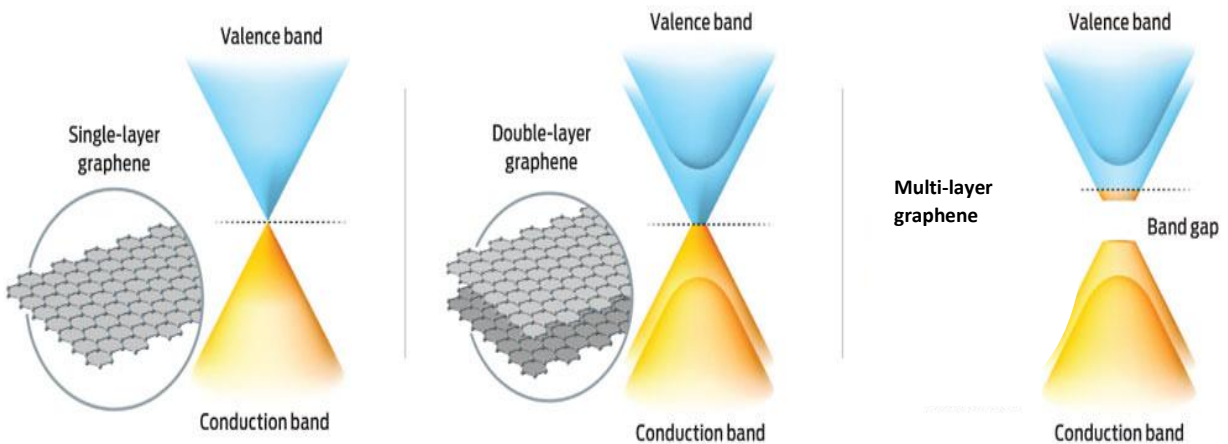


Figure 2- 4- Going from Graphene to Graphite

2. 3. Graphene Oxide

Graphene oxide usually is obtained by oxidizing the graphite and then exfoliating graphite oxide by ultrasonic. Figure 2- 5, illustrates briefly the process of graphene oxide preparation. After sonication and exfoliating graphene oxide flakes which are sheets of functionalized graphene will be formed.

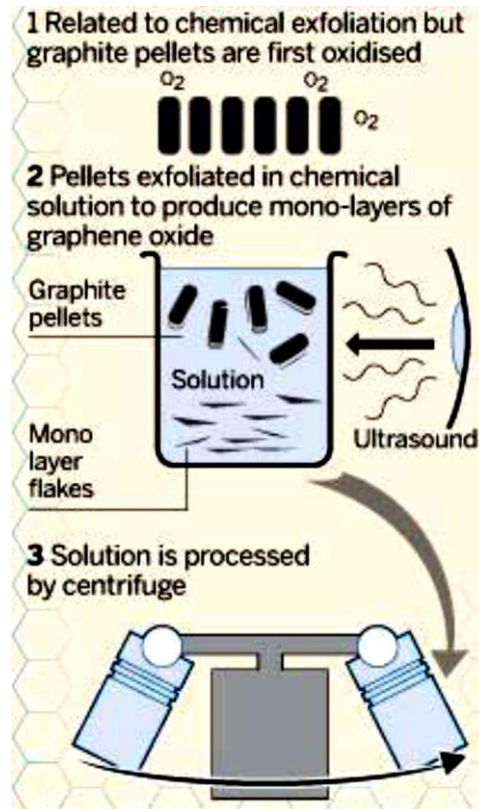


Figure 2- 5- Graphene Oxide Preparation

Functional groups which are normally can be found on the carbon back bone of graphene oxide are usually carboxyl groups, epoxy groups, carbonyl and hydroxyl groups. [103]

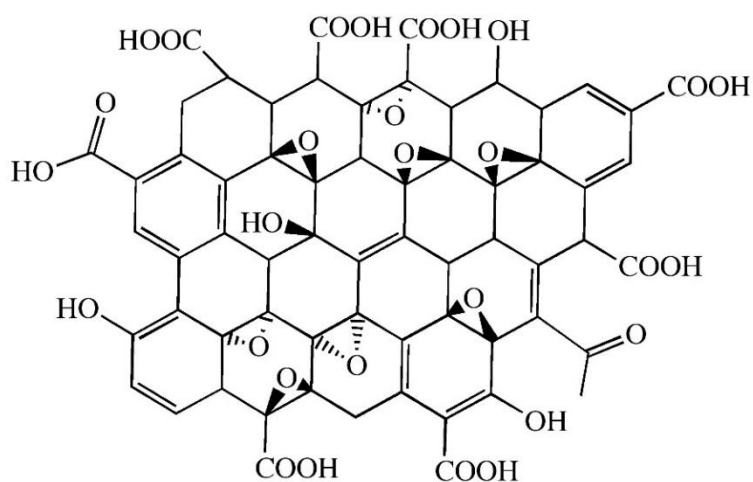


Figure 2- 6- Functional groups on Graphene Oxide

As mentioned previously, adding new layers, introduction of the functional groups and doping to the graphene will open up a gap between conduction and valence band. So, Graphene Oxide itself is an insulator which the amount of the gap can be controlled by controlling the number of layers and amount of introduction of the functional groups. (Figure 2- 7)

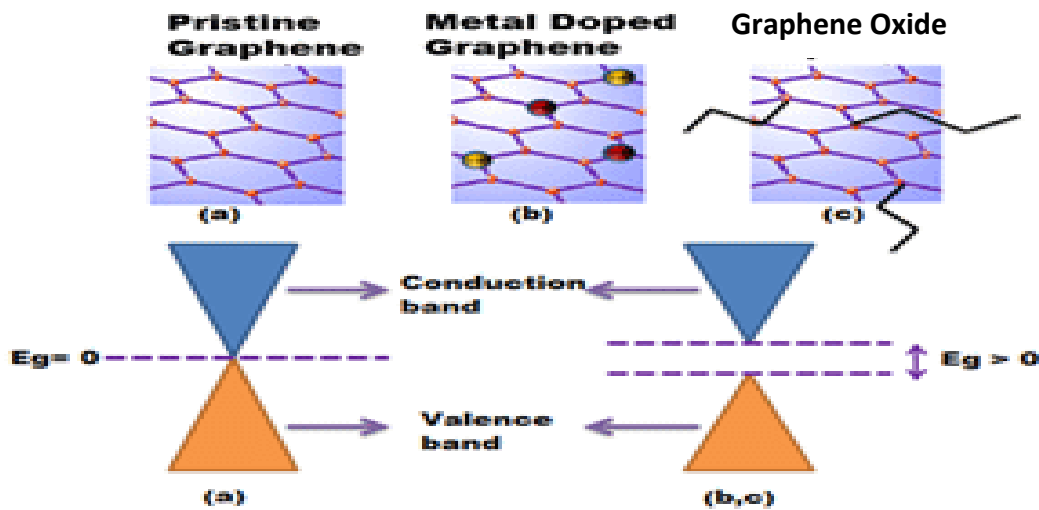



Figure 2- 7- Graphene Oxide Band Structure

2. 4. Preparation of Graphene Oxide film

The Graphene Oxide (GO) flakes usually is provided by modified hammer method, which you can find the procedure for the production elsewhere. [103, 55, 47]

GO was provided by our colleagues in Padua University. For preparation of the GO solution, GO powder is weighted precisely and water added to the solution in the exact amount to get a solution with a particular concentration. Then, as prepared solution is subjected to the bath sonication for 2 hours to initially disperse the powder in water. After first step, then the solution is subjected for the tip sonication for 2 hours in a pulsed



condition with 40 seconds “on” and 20 seconds “off” mode and power equal to 25 percent of the maximum power.

After this long sonication the solution visually has been checked to be sure about well dispersion of the powder. Afterward, the sonicated solution was subjected to centrifugation to remove the big flakes and having high quality and well dispersed solution of GO in water. The centrifugation has been done with rotation speed equal to 5000rpm and for 30 minutes. In the end of centrifugation the flakes with bigger size precipitate on the bottom of the vial and smaller sized flakes floating on the top of the solution. As reported in the literatures, [47] For having a high quality deposited film it is better to remove the flakes with big size. So, after centrifugation the supernatant of the solution pipetted and collected and preserved as a stock of GO solution for the film deposition. Remaining sediments dried and added to the stock of the GO powder for the next time. Finally, as prepared solution was placed in the bath sonication for extra 2 hours sonication.

2. 4. 1. Deposition of GO solution

For this purpose three different techniques have been used:

1. Spin coating
2. Drop casting
3. Vacuum filtration

2. 4. 1. 1. Spin Coating

For having the best spin coated film, there are a lot of parameters which have to be optimized. For this purpose all the parameters varied to obtain the best condition. Parameters which are involved in the variation of the film are:

Solution concentration

Spinning Speed

Duration of spinning

Acceleration of spinning

Times of spin coating

All of the above mentioned parameters have to be examined and get to the best combination.

For simplicity of the work acceleration set as half of the spinning speed so in this way one parameter will be omitted.

Solution concentration:

After initial measurements it is shown if ethanol will be added to the solution of the GO in water, film with better quality can be produce so for the dilution and getting the best solution a lot different solutions have been prepared and tested to realize the best condition. In the Table 2-1 there is a list of the used solutions.

GO concentration in water	Percentage of Ethanol addition
0.01 mg/ml	80%, 85%, 90%, without
0.02 mg/ml	80%, 85%, 90%, without
0.05 mg/ml	80%, 85%, 90%, without
0.1 mg/ml	80%, 85%, 90%, without
0.2 mg/ml	80%, without
0.33 mg/ml	66%
0.4 mg/ml	60%
0.5 mg/ml	50%
1 mg/ml	0%


Table 2- 1- list of the used solutions

Spinning speed has been set to the following values:

Start from 1500 to 5000 rpm with 500 rpm incremental steps. (1500, 2000, 2500.....)

Duration has been set to two values, 1 minute and the other 1.5 minutes.

Some of the samples also prepared with several times of spinning in such a way that after each spinning sample has been dried on a hot plate at 110 °C for 10 minutes and then spin coated for other times. In some cases to have a perfect film it is repeated up to 5 times.



GO have been deposited on ITO (Indium Thin Oxide) and FTO (Fluorine Doped Thin Oxide) substrates. Before starting the deposition, substrate should be cleaned to remove the possible contaminations to get a good film. Cleaning of the samples is done with 10 minutes bath sonication in the Helmanex solution, 10 minutes bath sonication in Milli-Q water (Deionized water), afterward changing the Milli-Q water and sonicating for an extra 10 minutes in Milli-Q water. Subsequently, bath sonication in the clean IPA (Isopropyl Alcohol) for 10 minutes, 10 minutes bath sonication in Acetone and Finally 10 minutes bath sonication in IPA again. After all, the cleaned samples were placed in the Plasma Asher for 10 minutes with 100% power to increase wettability of the surface and removing high resistant contamination exactly before spin coating of the samples. Notice Plasma treatment has to be done exactly before spin coating since after few minutes it is not effective anymore and wettability decreases drastically.

After preparation of the substrates it is time to spin coat the samples with GO solution. Spin coating has been done with setting all the parameters fixed except one parameter. In this regard the best combination is obtained by checking the film quality with optical microscope and then with Raman measurement. The best film is a film with a good coverage and uniformity on the substrate.

2. 4. 1. 2. Drop casting

Drop casting is another technique for deposition of the thin films. In this technique precise amount, depends on the size of the substrate, of the desired solution, pipette on top of the cleaned substrate. Then substrate left to be dry in the saturated or unsaturated atmosphere for the proper time. Substrate have to be placed over a very flat surface to guarantee the uniformity of the deposition.

In this work also drop casting have been used. ITO substrates first were cleaned with the already mentioned procedure and plasma treated to increase the wettability. Next, GO solution which was sonicated for near one hour pipetted over the clean substrate which was placed over an optical table to ensure flatness of the surface. Immediately after dispersing the solution a petri dish was placed over the sample to maintain the saturated

atmosphere near the samples. Samples have been left for near 12 hours to be dried. In this technique solutions were same as the solutions for the spin coating.

In some of the cases drop casting repeated for several times to guarantee complete coverage of the surface.

Problems of this method are, not being reproducible and being highly dependent on the environmental condition like the flatness of the surface and temperature.

Another problem which is very problematic is a coffee ring effect which is unavoidable and create inhomogeneous deposition. For these problems it has been decided to not use this method further.

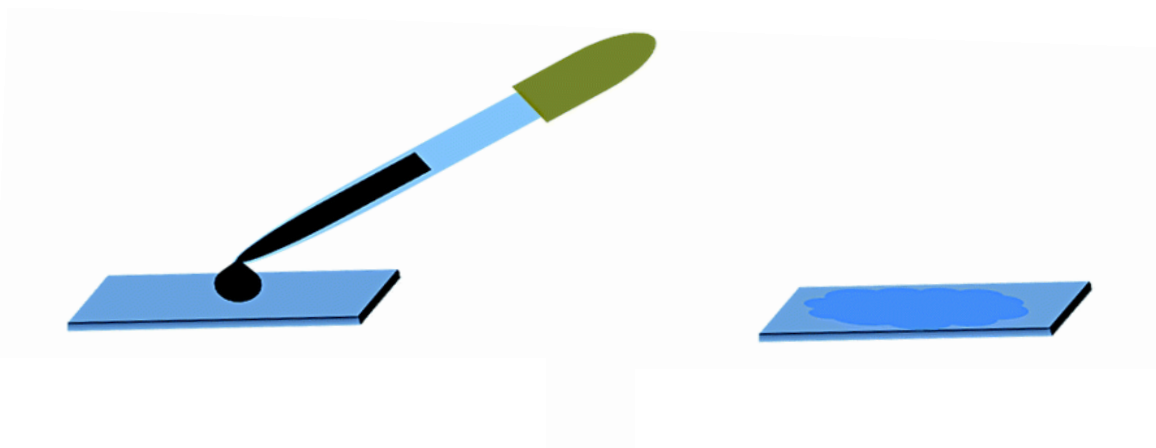


Figure 2- 8- Drop casting process.

4. 4. 1. 3. Vacuum Filtration [69]

This technique is another simple wet technique for film deposition. In this technique a diluted solution of the desired film composition is forced to pass through a very fine filter. Particles or flakes greater than the size of the filter pore cannot pass through the filter and remain at the surface of the filter. Then the film (Figure 2- 9 (right)) on the filter have to be transferred to the substrate by leaving the filter on top of the clean and slightly wet substrate, under a heavy mass.

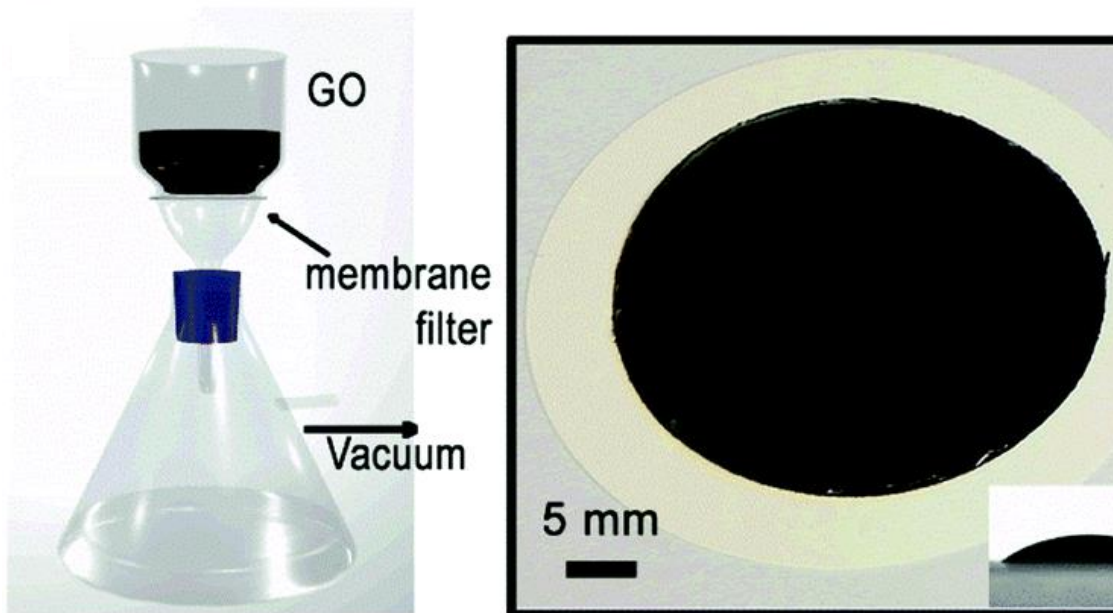


Figure 2- 9- Vacuum filtration setup (left), Filter membrane after passing the solution through. (right)

This method has been done in this study but did not result in a good film deposition. The complete coverage was not achieved and have been decided to not continue with this technique.


2. 4. 2. Checking Film quality

Film Quality has been checked initially in three ways:

1. Optical Microscope Check

As prepared films are checked with an optical microscope to realize complete coverage.

2. Raman measurement [81-85]



Samples have been subjected to the local Raman measurement in order to identify peaks of the GO which are G and D peaks. In order to be sure all over the sample was covered with GO, different points all over the surface have been selected and measured.

3. UV-Vis Spectroscopy

This measurement has been done to measure the transparency of the samples and estimate the thickness of the film.

As prepared samples first have been checked with the optical microscope to see the first estimation of the quality of the films.

Afterward Raman measurement is conducted to get better insight about the film quality, uniformity, homogeneity and coverage of the deposited films. There are three distinctive peaks for the GO which is named G, D and 2D peaks. G peak is due to the presence of the sp^2 carbon rings. D peak is due to the presence of the defects. 2D Peak is formally present in Graphene and as we increase the number of layers, it starts to decrease. It is reported numerously as the number of layers increase, the intensity of the G band increases significantly, while that of the 2D band decreases. Additionally the shape of the 2D band has a two peak profile rather than a single Lorentzian as in Single layer Graphene. [84]

Generally, as the ratio of I_G/I_D will be greater, the film quality is better and it is more near Graphene structure. [84]

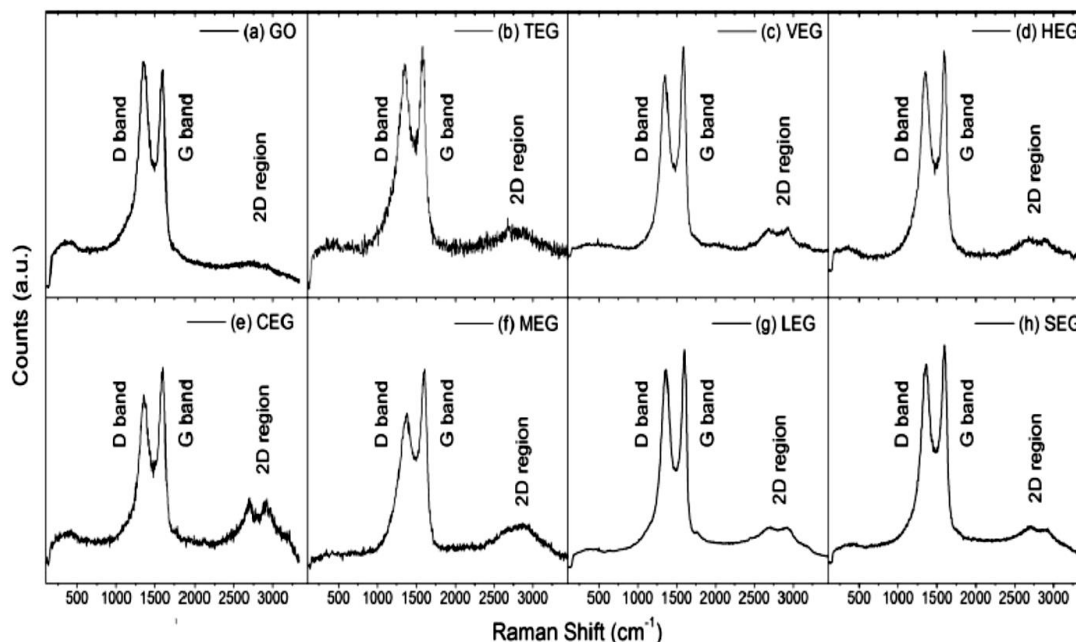


Figure 2- 10- Raman spectra of (a) graphite oxide (GO), (b-h) few layer wrinkled graphene grown by different methods viz. (b) thermally exfoliated graphene (TEG), (c) vacuum exfoliated graphene (VEG), (d) hydrogen exfoliated graphene (HEG), (e) chemically exfoliated graphene (CEG), (f) microwave exfoliated graphene (MEG), (g) laser exfoliated graphene (LEG), (h) sun exfoliated graphene (SEG). Reprinted from [84]

In this technique different points all over the samples have been checked. A lot of data were obtained and compared to get to the best film deposition. The following table is a summary of the best results.

2. 4. 2. 1. Drop casting Results

Drop Casting			
Sample	normalized G ratio	normalized D ratio	G/D ratio
0.01mg/ml GO concentration in milliliter solution (0.8 ml Ethanol+ 0.2 ml water)	0.11	0.09	1.15
0.01mg/ml GO concentration in milliliter solution (0.95 ml Ethanol+ 0.05 ml water) _double drop casting	0.17	0.15	1.11
0.05mg/ml GO concentration in milliliter solution (0.8 ml Ethanol+ 0.2 ml water)	0.21	0.19	1.11



0.01mg/ml GO concentration in milliliter solution (0.85 ml Ethanol+ 0.15 ml water)	0.15	0.14	1.10
0.2mg/ml GO concentration in milliliter solution (0.9 ml Ethanol+ 0.2 ml water)	0.79	0.73	1.08
0.01mg/ml GO concentration in milliliter solution (0.9 ml Ethanol+ 0.1 ml water)_ double drop casting	0.13	0.12	1.07
0.2 mg/ml GO concentration in milliliter solution (0.8 ml Ethanol+ 0.2 ml water)	0.24	0.23	1.07

Table 2- 2- Drop Casting best films according to the Raman Measurements

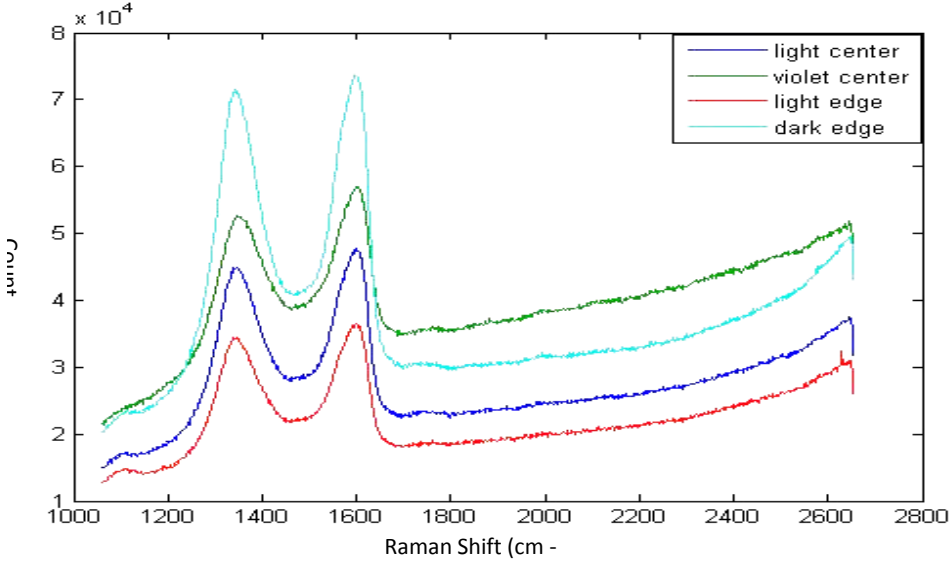


Figure 2- 11- Raman measurement in different local points in drop casted sample.

2. 4. 2. 2. Spin Coating Results

Spin Coating			
Sample	Normalized G ratio	normalized D ratio	G/D ratio
1 mg/ml GO concentration in milliliter water _2000rpm_1min	0.15	0.04	3.70
1 mg/ml GO concentration in milliliter water _3500rpm_1min	0.08	0.02	3.67
1 mg/ml GO concentration in milliliter water _5000rpm_1min	0.16	0.07	2.42
0.1 mg/ml GO concentration in milliliter solution (0.9 ml ethanol + 0.1 ml water) _1000rpm_1min	0.18	0.09	1.90
1 mg/ml GO concentration in milliliter water _1500rpm_1.5min	0.03	0.02	1.86
1 mg/ml GO concentration in milliliter water _4000rpm_1min	0.13	0.07	1.81
0.2 mg/ml GO concentration in milliliter solution (0.8 ml ethanol + 0.2 ml water) _1500rpm_1.5min	0.03	0.01	1.79
1 mg/ml GO concentration in milliliter water _3000rpm_1min_3times	0.21	0.12	1.78
0.1 mg/ml GO concentration in milliliter solution (0.9 ml ethanol + 0.1 ml water) _2000rpm_1.5min	0.02	0.01	1.60
0.2 mg/ml GO concentration in milliliter solution (0.8 ml ethanol + 0.2 ml water) _2000rpm_1.5min	0.08	0.05	1.59
1 mg/ml GO concentration in milliliter water _3000rpm_1min	0.28	0.18	1.56
1 mg/ml GO concentration in milliliter water _2000rpm_1.5min	0.03	0.02	1.51
1 mg/ml GO concentration in milliliter water _3500rpm_1min_5times	0.64	0.46	1.39
1 mg/ml GO concentration in milliliter water _2500rpm_1min	0.29	0.21	1.37

1 mg/ml GO concentration in milliliter water _2500rpm_1min_5times	0.58	0.43	1.36
1 mg/ml GO concentration in milliliter water _3500rpm_1min_3times	0.58	0.43	1.34
0.2 mg/ml GO concentration in milliliter solution (0.8 ml ethanol + 0.2 ml water) _1000rpm_1min	0.73	0.55	1.34
1 mg/ml GO concentration in milliliter water _2000rpm_1min_3times	0.43	0.33	1.32
1 mg/ml GO concentration in milliliter water _4000rpm_1min_3times	0.18	0.14	1.27
0.1 mg/ml GO concentration in milliliter solution (0.9 ml ethanol + 0.1 ml water) _1500rpm_1.5min	0.04	0.03	1.19
1 mg/ml GO concentration in milliliter water _4500rpm_1min	0.28	0.24	1.14

Table 2- 3- Spin Coating best films according to the Raman Measurements.

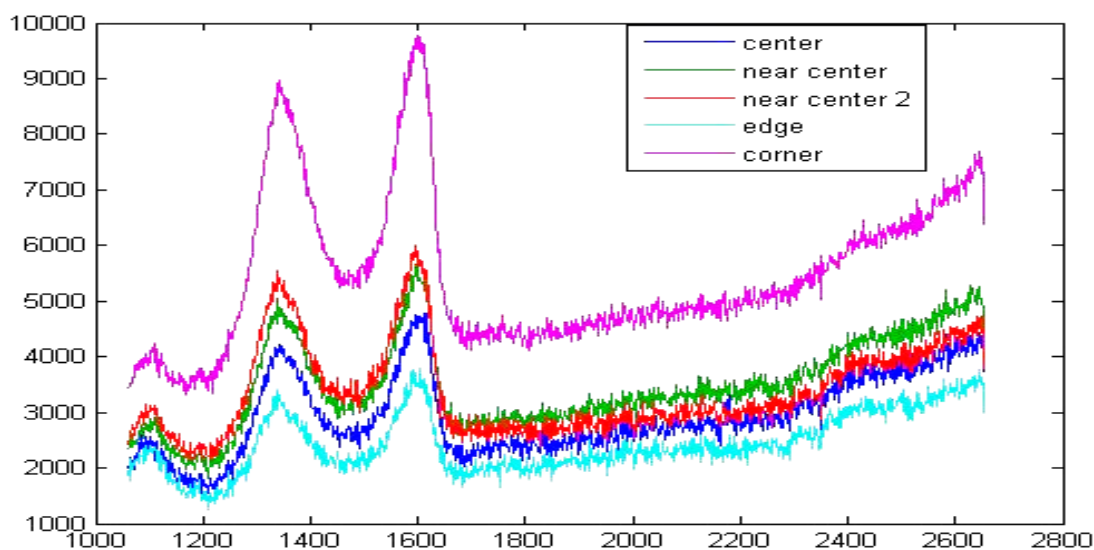



Figure 2- 12- Raman measurement in different local points in spin coated sample.



As it is clear from the tables the one with the highest G/D ratio is the best sample. So, the best deposition condition was selected as spin coating 1mg/ml Graphene Oxide solution in Water with rotation speed 2000rpm for 1 minute.

Later on, the above mentioned conditions were used to deposit Graphene Oxide layer.

2. 5. Using Poly diallyl dimethylammonium chloride (PDDA) for better coverage [50]

For increasing the uniformity of the coverage, a positively charged polymer (PDDA) was used to increase the uniformity of the deposition of the negatively charged graphene oxide flakes. After cleaning the substrates (ITO or FTO), they have been immersed in PDDA solution (0.2 wt%) containing of 0.5 wt% NaCl for 15 min, then substrate with mono layer PDDA on top was rinsed with deionized water and dried with nitrogen stream, then exfoliated GO solution have been spin coated on top. This procedure gave one deposition cycle. The cycle was then repeated as many as it is desired to obtain the composite of GO and PDDA.

This pre layer was used frequently for the sample preparation, but gradually in the end of the work, this mono layer has been ignored since there was no significant effect on the cell performance.

2. 6. Reduction of Graphene Oxide Film [55, 59, 89, 90, 91, 92, 97, 103]

Reduction means removing the functional groups on the graphene backbone, in order to reduce the band gap of GO film and increasing conductivity.

For this purpose there are two major ways:

1. Thermal annealing
2. Chemical reduction

2. 6. 1. Thermal Annealing

In this method by increasing temperature to over 1000 °C, all the functional groups will be removed. However, for our purpose the required temperature is lower than this, since reduction should not be complete and presence of the band gap, which makes the film semiconductor, is a major requirement of the materials in solar cell application. Band gap is needed in order to have a band alignment in different layers.

The most effective temperature has to be selected by considering the best alignment of different layers in different structures.

The best temperature was 250 °C. Annealing in this temperature gave the reduced film desired properties which were required.

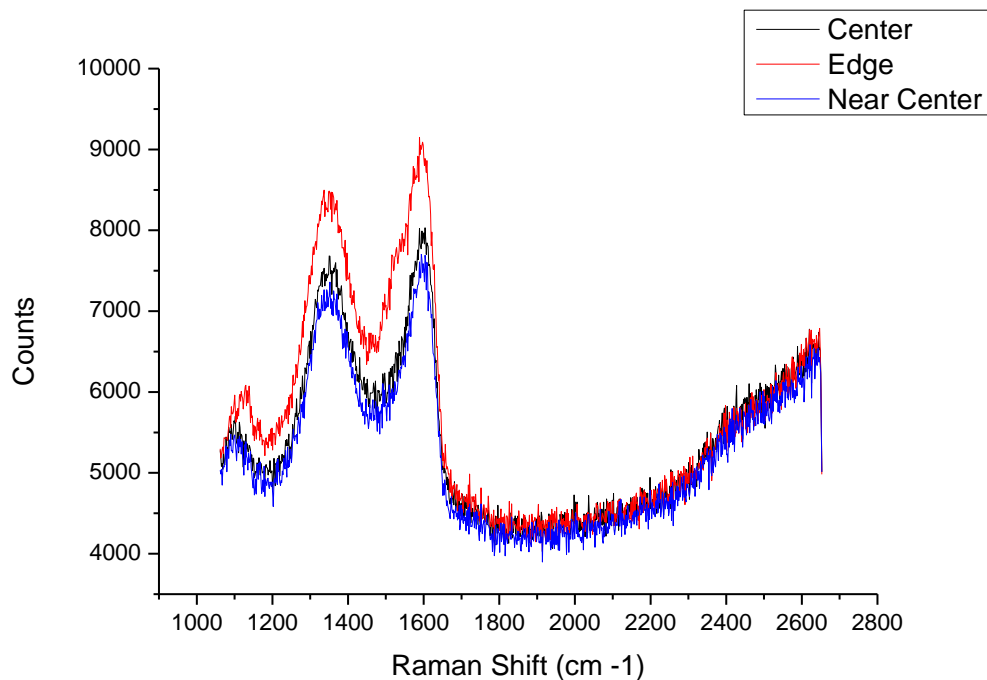


Figure 2- 13- 0.4 mg/ml GO concentration in milliliter solution (0.9 ml ethanol + 0.4 ml water)- 2500rpm- 50seconds- 4 times (reduced in glovebox at 250 °C)

2. 6. 2. Chemical Reduction [86]

There are generally two approaches in chemical reduction, one before deposition of the film and by adding chemicals to the GO solution, and the other one is using chemicals for reduction after deposition of the film.

There are several chemical agents which can reduce GO. The most common ones are, hydrazine, hydroxylamine, hydro iodoc acid, iron (II) and tin (II) ions.

In this regard, in this project, Hydrazine, Hydro Iodic Acid and Hydro Bromic Acid solutions diluted in water were used. For Hydrazine a spin coated GO sample was placed in the chamber with hydrazine atmosphere to be reduced. Temperature of the chamber was set to 80 °C. The detailed procedure is reported in the reference work. [48, 103]

Hydro iodoc and Bromic Acid were diluted in water then the diluted solution immersed in a silicon oil bath to be heated up. The solution temperature set to 100 °C and then GO samples immersed in the solution for 2 minutes. Detailed process is reported in. [47, 103]

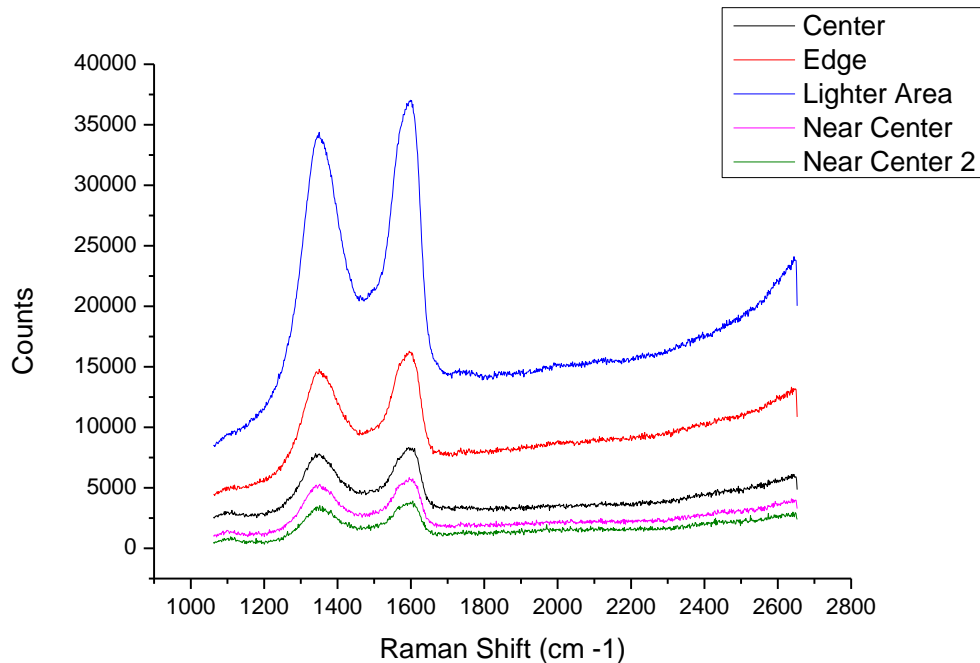


Figure 2- 14- 1 mg/ml GO concentration in milliliter water- 2500rpm- 1min- 3 times (Reduced with Hydrazine)

2. 7. Best Reduction method selection

The best sample recipes with thermal annealing and chemical reduction have been selected and was sent to Genoa (**IIT center**) to be subjected to complete investigation in order to select the best recipe for the preparation of the Reduced Graphene Oxide film. In Genoa, samples subjected to FESEM, UPS and XPS measurement by our colleague Dr. Mirko. Below there is a summary of the measurements.

2. 7. 1. Sample 1: Drop casted 3 times on top of PDDA coated ITO – 0.33ml Go solution (1 mg/ml in water) in 0.66ml ethanol – Reduced with hydrazine

2. 7. 1. 1. SEM

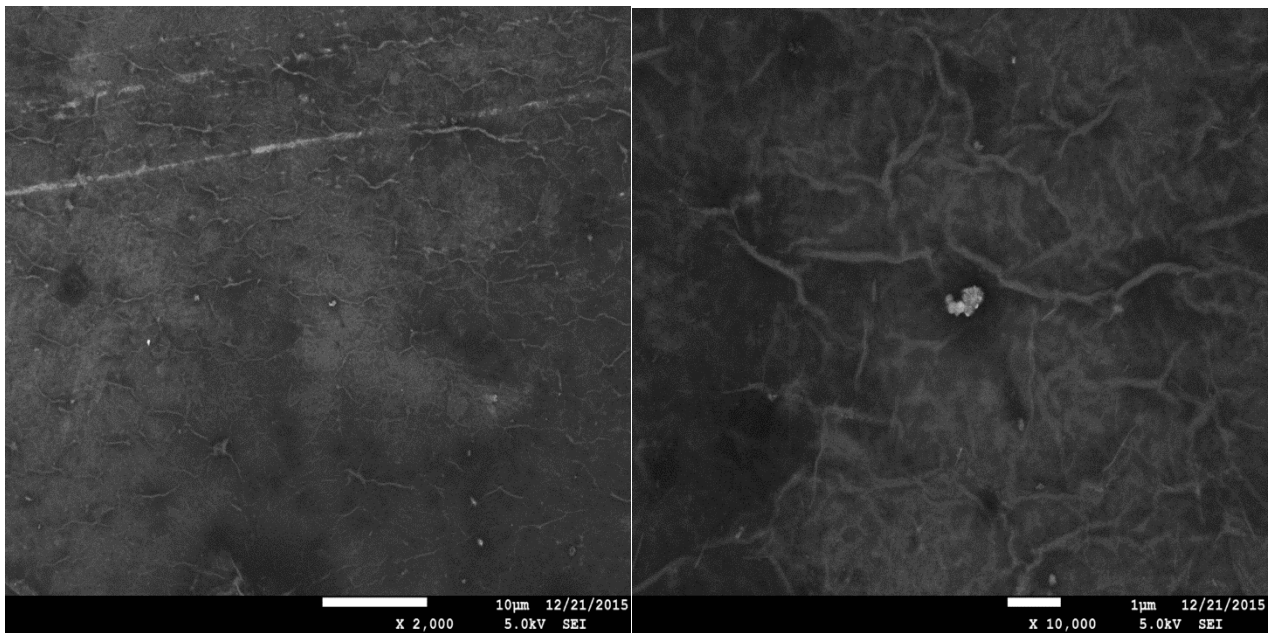


Figure 2- 15- SEM image of the reduced drop casted sample. Wrinkles are due to reduction.

The sample coverage seems to be not homogeneous. XPS check on 4 areas. As shown in Figure 2- 16 chemical composition of the surface depends on the position.

2. 7. 1. 2. XPS measurement

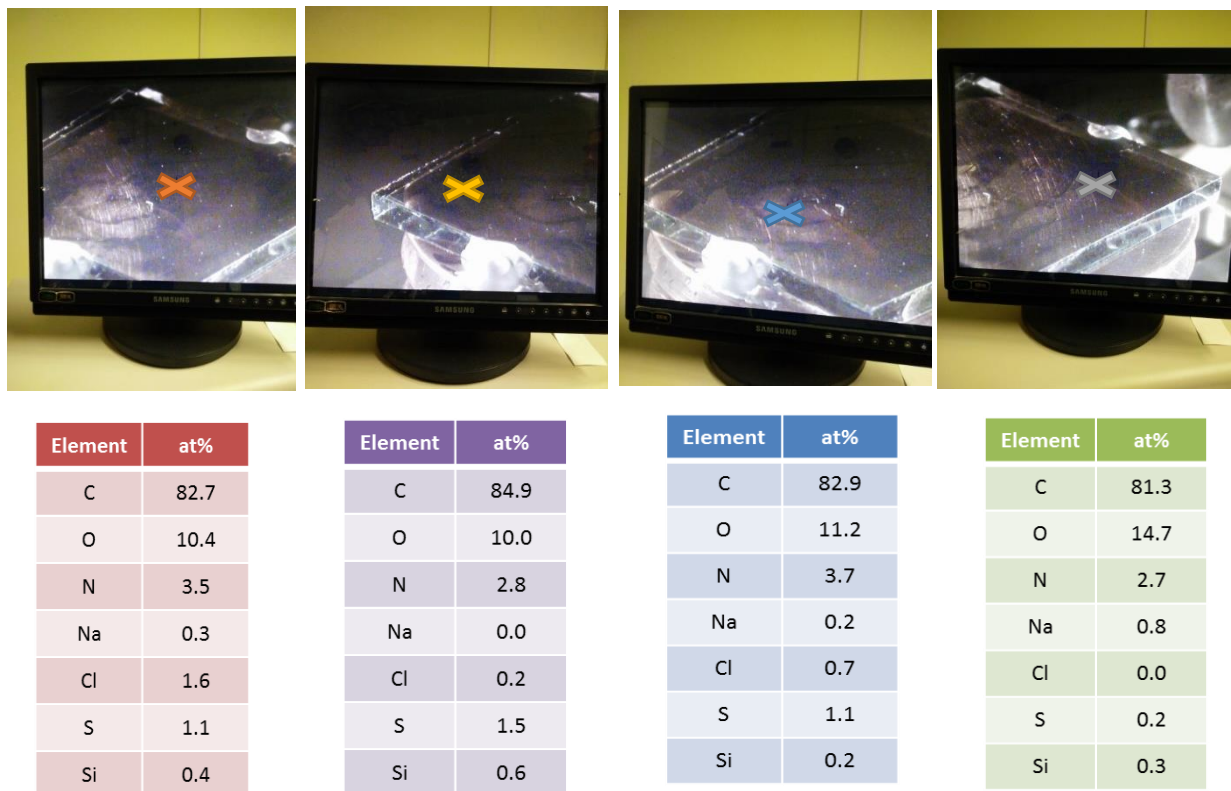


Figure 2- 16- XPS measurements in different regions on sample1. C, O, N, Na, Cl, S and Si are stands for Carbon, Oxygen, Nitrogen, Sodium, Chloride, Sulfide and Silicon respectively.

As it is clear from XPS data, sample contains elements like Carbon, Oxygen, Nitrogen, Sodium, Chloride, Sulfide and Silicon. Na and Cl come from the PDDA solution as mentioned previously. Si and S came from an unknown source.

The most important data is the percentage of the Oxygen and Carbon contents. As a general rule for the reduction of GO, as low as possible Oxygen content, more complete the reduction. So, from data, sample reduced up to a reasonable amount.

Additionally, inhomogeneity in the reduction is obvious, as Oxygen content varies region by region.

Moreover, the other interesting point is that, there was a considerable amount of Nitrogen in the sample which suggests sample was nitrogen doped. [58]

Chemical inhomogeneity can be observed on C 1s spectrum as well.

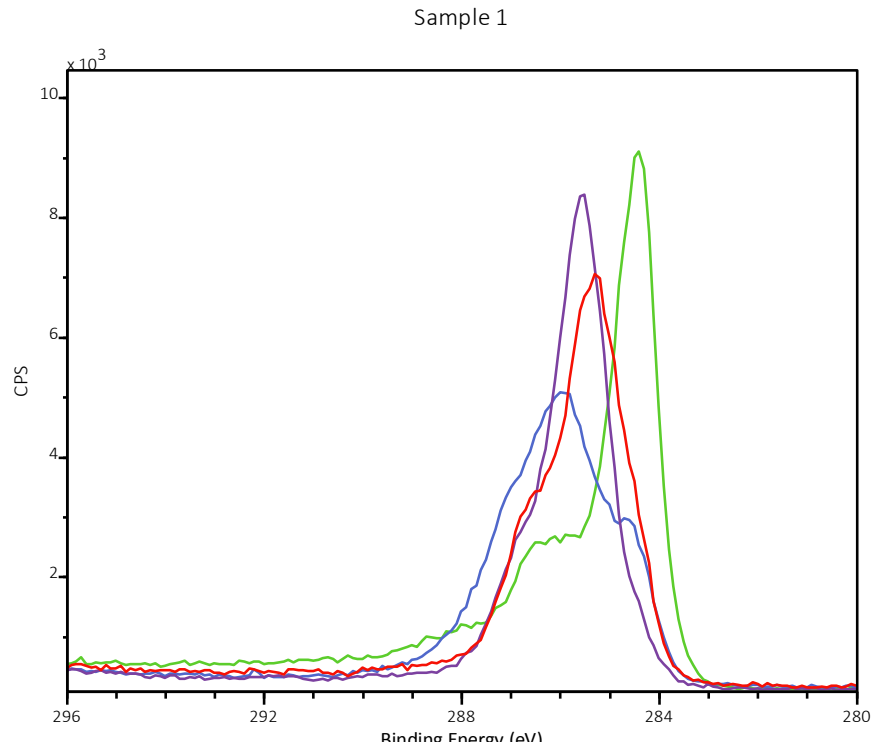


Figure 2- 17- C 1s spectra for sample 1.

Colors in Figure 2- 17 refer to the different acquisition positions, as defined in the Figure 2- 16.

Reduction by hydrazine was not homogeneous on the surface of the sample.

The “green” position is the more reduced one, while the “blue” one shows a still high concentration of oxidized C components.

Then UPS was acquired on these two regions only, chosen as extremes.

2. 7. 1. 3. UPS

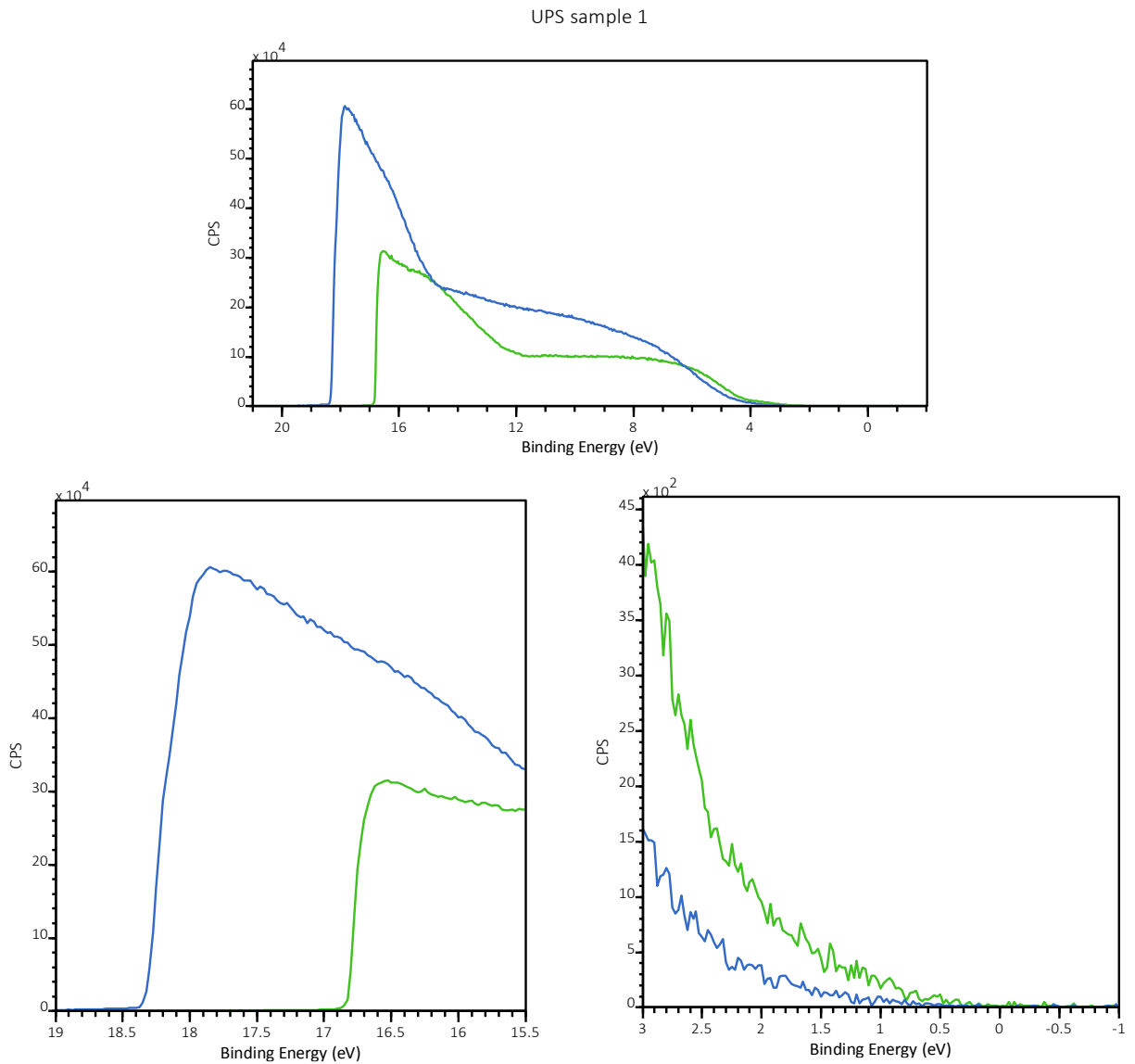


Figure 2- 18- UPS measurement on green and blue marked regions.

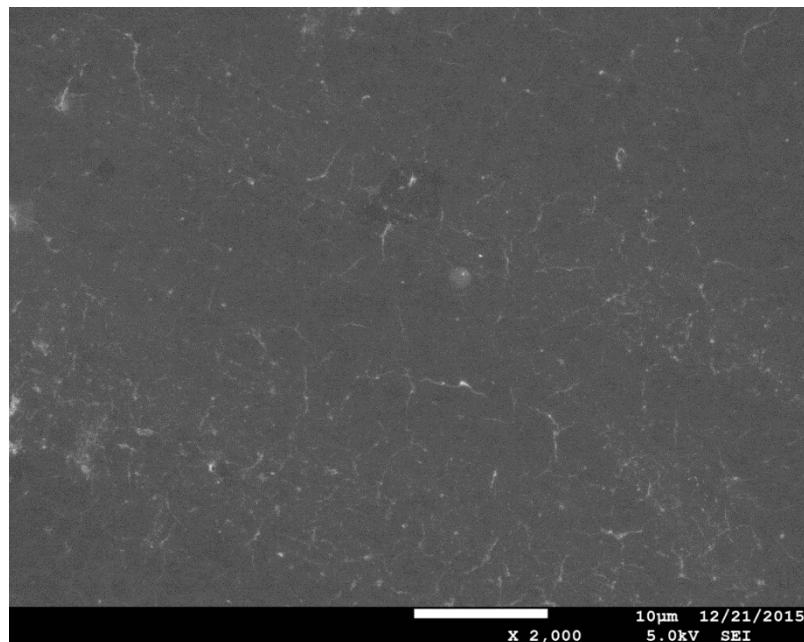
Oxidation has a large effect on the UPS spectra. While at low binding energy the two spectra show a similar onset, on the high binding side there is a difference of about 1.5 eV.

The “green” region (reduced more) shows work function of 4.4 eV and Valance Band Maximum (VBM) at -4.9 eV versus vacuum level.

The “blue” one (reduced less) instead has a work function of approximately 3 eV and VBM at -3.5 eV versus vacuum.

2. 7. 2. Sample 2: Drop casted 3 times on top of PDDA coated ITO --
0.33ml Go solution (1 mg/ml in water) in 0.66ml ethanol – Reduced in
glove box at 250 °C

2. 7. 2. 1. SEM



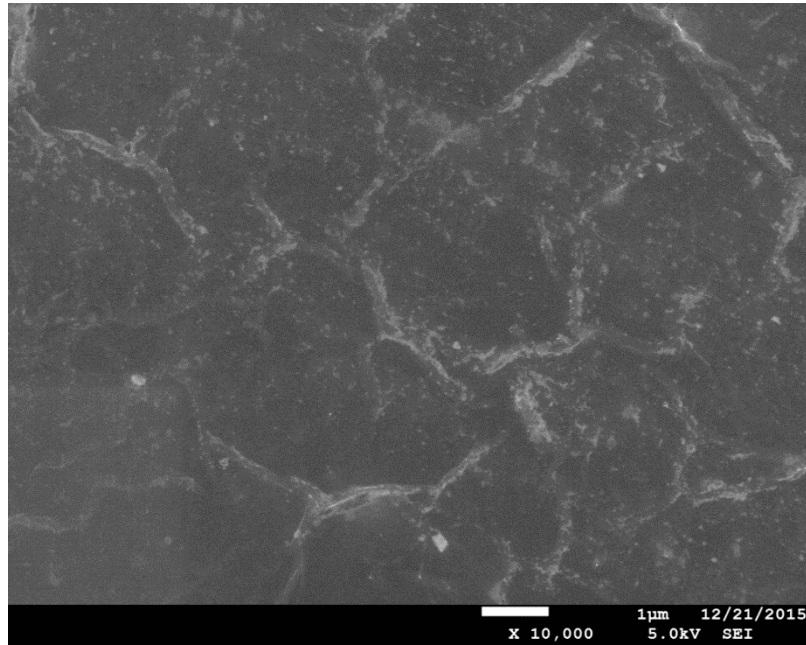


Figure 2- 19- SEM of the drop casted sample reduced inside the glovebox.

The sample coverage seems to be quite homogeneous. XPS check on 2 areas of apparently different thickness (the first is darker).

Some wrinkles are visible on the SEM images which are a common sign of the reduction of the GO with Annealing. [89]

2. 7. 2. 2. XPS



Element	at%
C	83.8
O	14.7
N	0.5
Na	0.7
Ca(?)	0.1
S	0.2
Si	0.0

Element	at%
C	83.3
O	14.9
N	0.5
Na	0.8
Mn (?)	0.1
S	0.4
Si	0.0

Figure 2- 20- XPS measurements in different regions on sample2. C, O, N, Na, Ca, Mn, S and Si are stands for Carbon, Oxygen, Nitrogen, Sodium, Calcium, Manganese Sulfide and Silicon respectively.

Here, again as it is clear from XPS data, sample contains elements like Carbon, Oxygen, Nitrogen, Sodium, Calcium, Manganese Sulfide and Silicon. Na and Cl come from the PDDA solution as mentioned previously. Ca, Mn and S came from an unknown source.

From data, sample reduced up to a reasonable amount.

Additionally, reduction all over the sample is very homogenous, as Oxygen content is approximately fixed.

Moreover, there was a subtle amount of Nitrogen in the sample which suggests sample was slightly nitrogen doped.

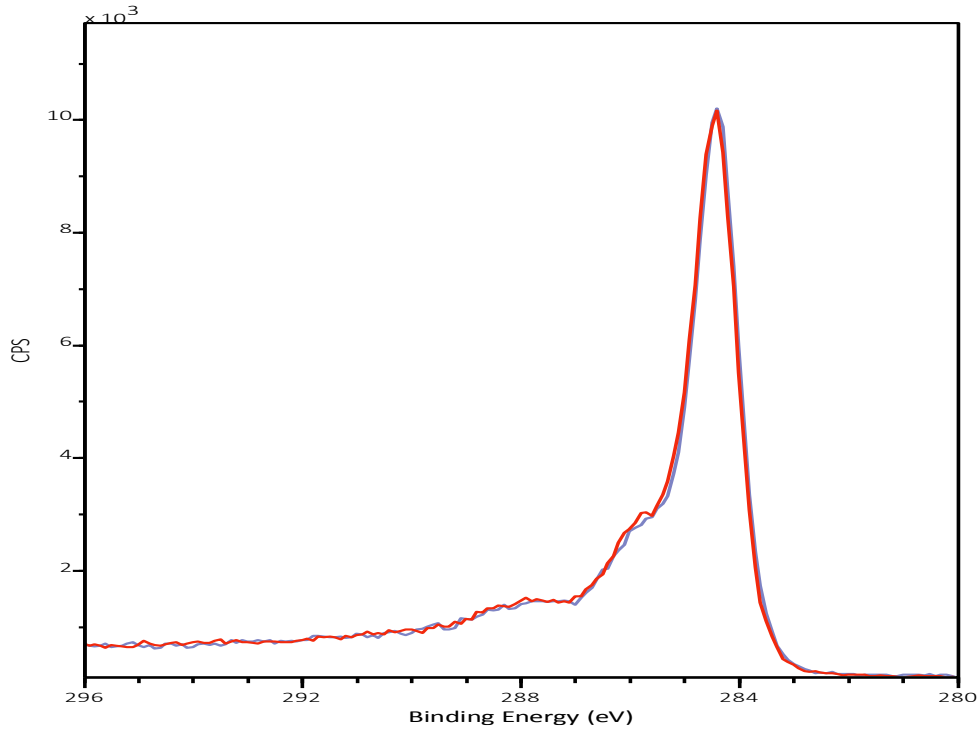


Figure 2- 21- C 1s spectra of the sample2 in marked regions.

This was so far the most chemically uniform and reduced sample. This strongly suggests that reduction in Glove Box is performing better than reduction with hydrazine.

2. 7. 3. Sample 3: Spin coated 4 times on top of PDDA coated ITO –1 mg/ml GO Concentration in water– reduced in glove box at 250 °C

2. 7. 3. 1. SEM

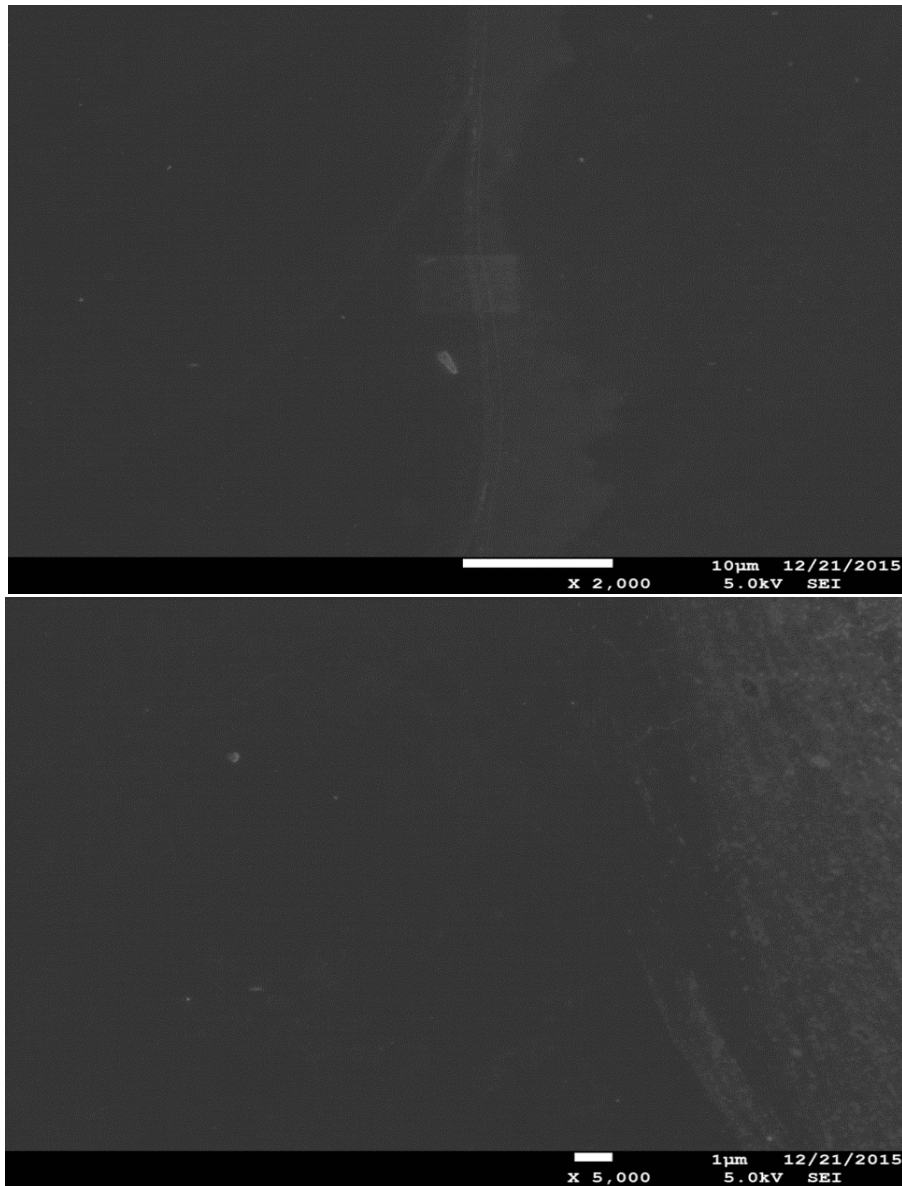


Figure 2- 22- SEM measurement on sample 3.

The sample seemed really uniform. The analysis was run on one region in the center of the sample.

2.7.3.2. XPS

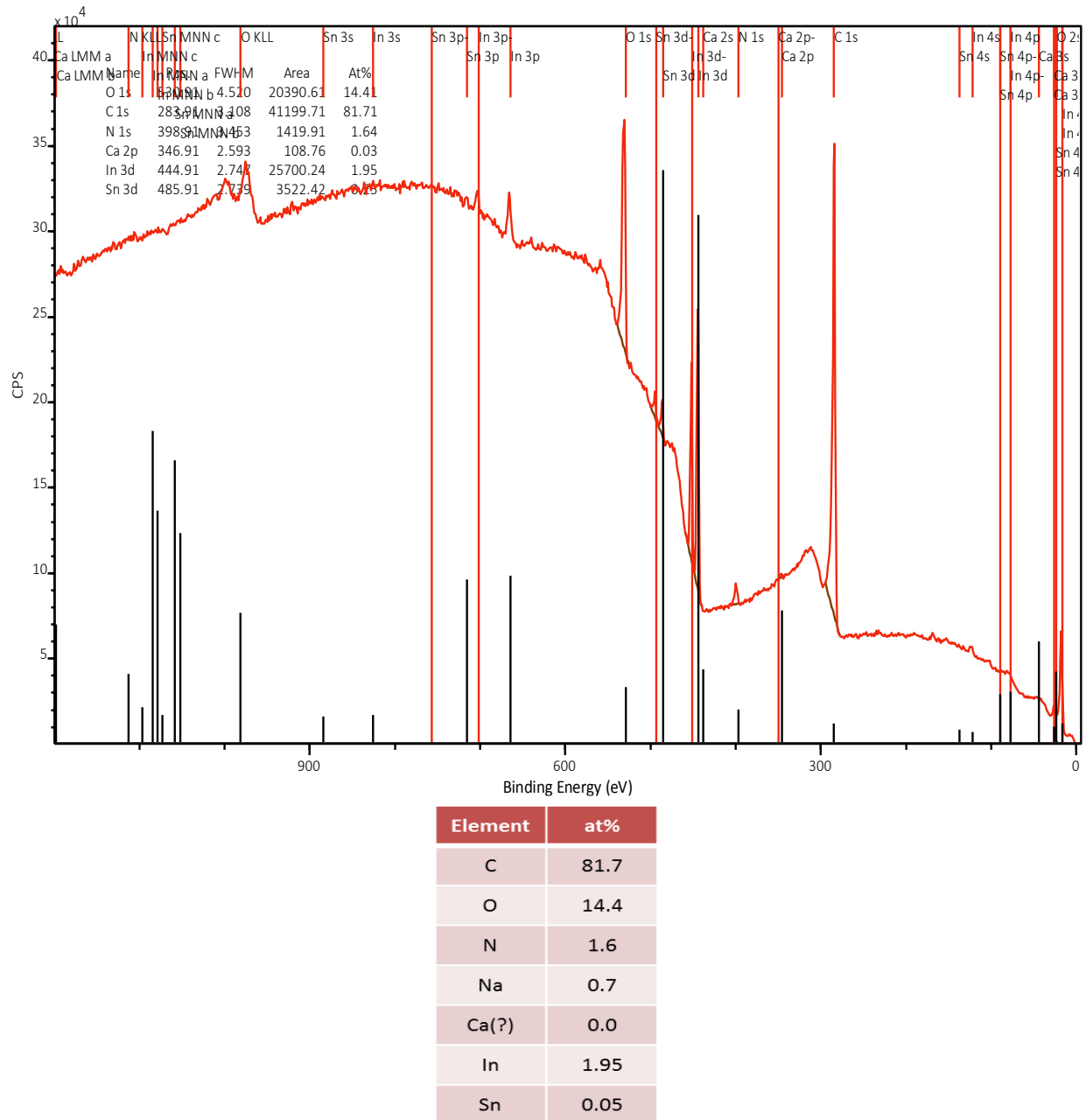


Figure 2- 23- XPS measurement on sample3. C, O, N, Na, Ca, In and Sn are stands for Carbon, Oxygen, Nitrogen, Sodium, Calcium, Indium and Tin respectively.

This data suggests that the sample was reduced well enough for our application.

However, it contained In and Sn elements, which can be sign of the not complete coverage or very thin layer of rGO. But, with regards to SEM image it was concluded that these signals were due to the thin layer which let the X-ray radiation go through the rGO layer and reaching ITO substrate.

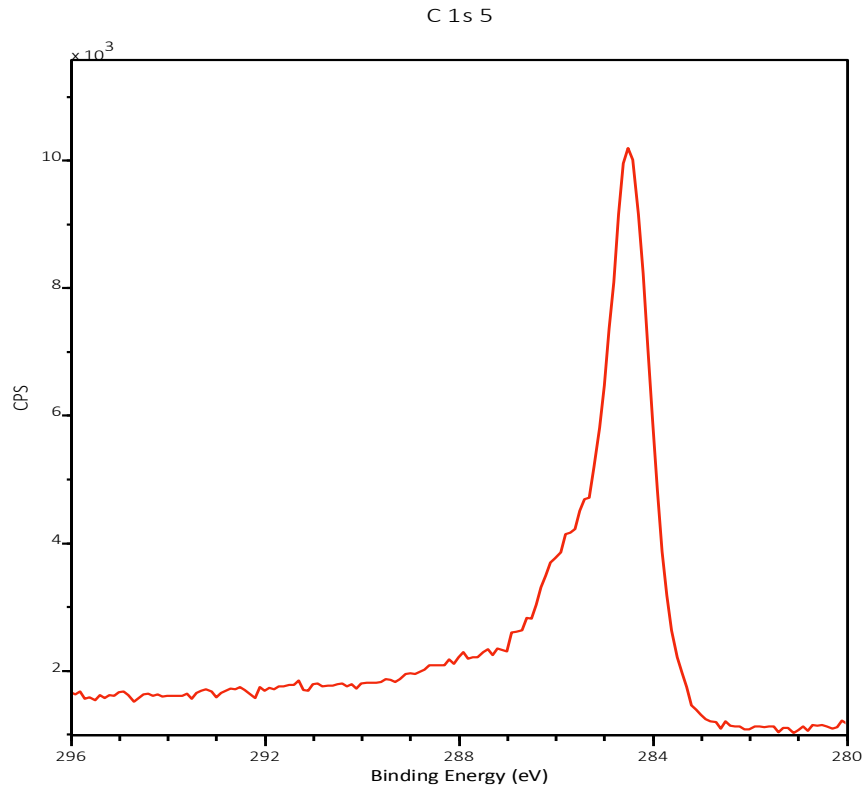


Figure 2- 24- C 1s spectra for the sample 3.

2. 7. 3. 3. UPS

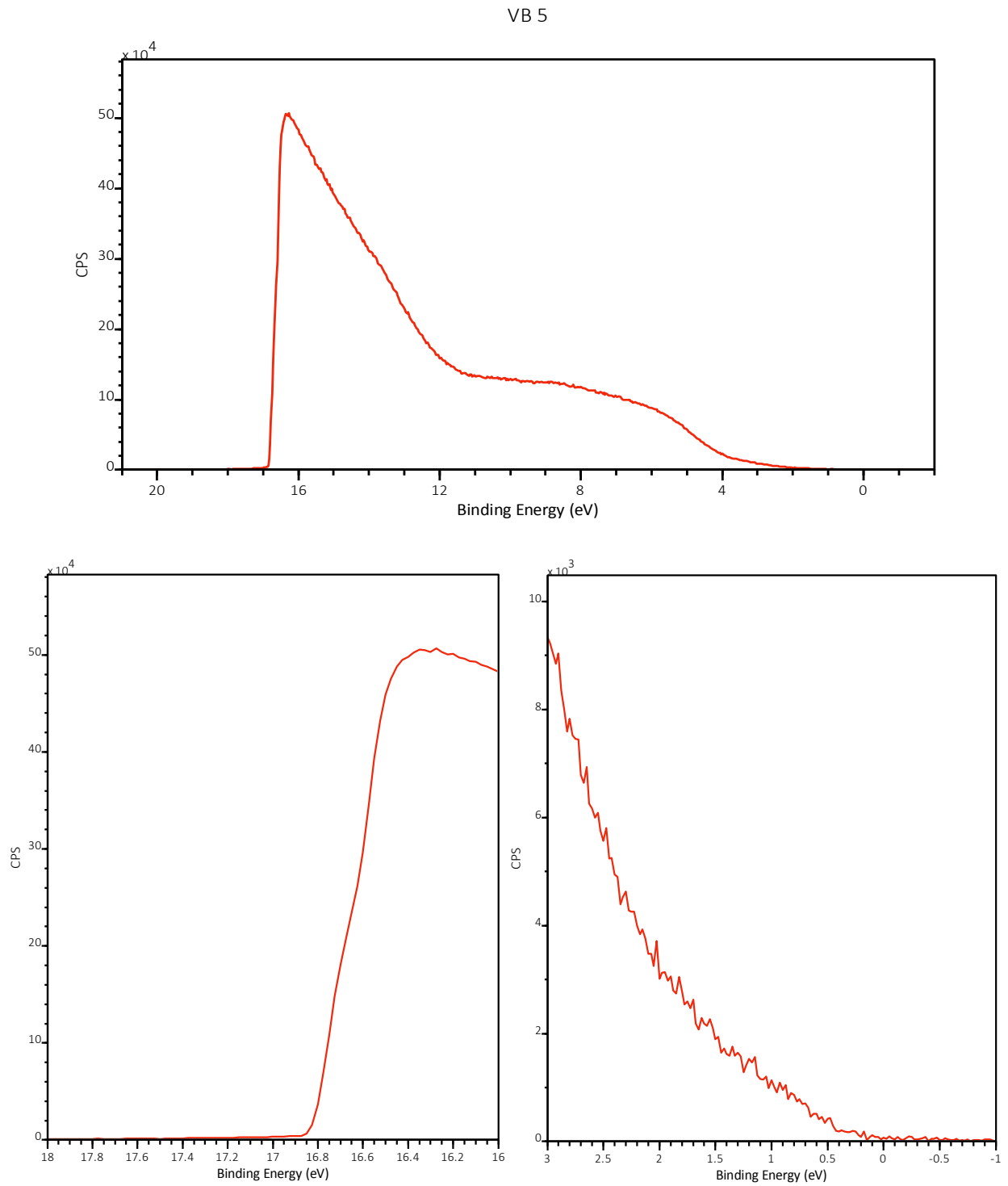


Figure 2- 25- UPS measurement.

From the measurements, it is obtained:

Work function= 4.4 eV

VBM at -4.6 eV versus vacuum

2. 7. 4. Comparison of the rGO deposited sample with bare ITO substrate

Comparison of XPS and UPS spectra with those of the clean ITO substrate. Sample 3 has been chosen for the comparison.

2. 7. 4.1. XPS comparison

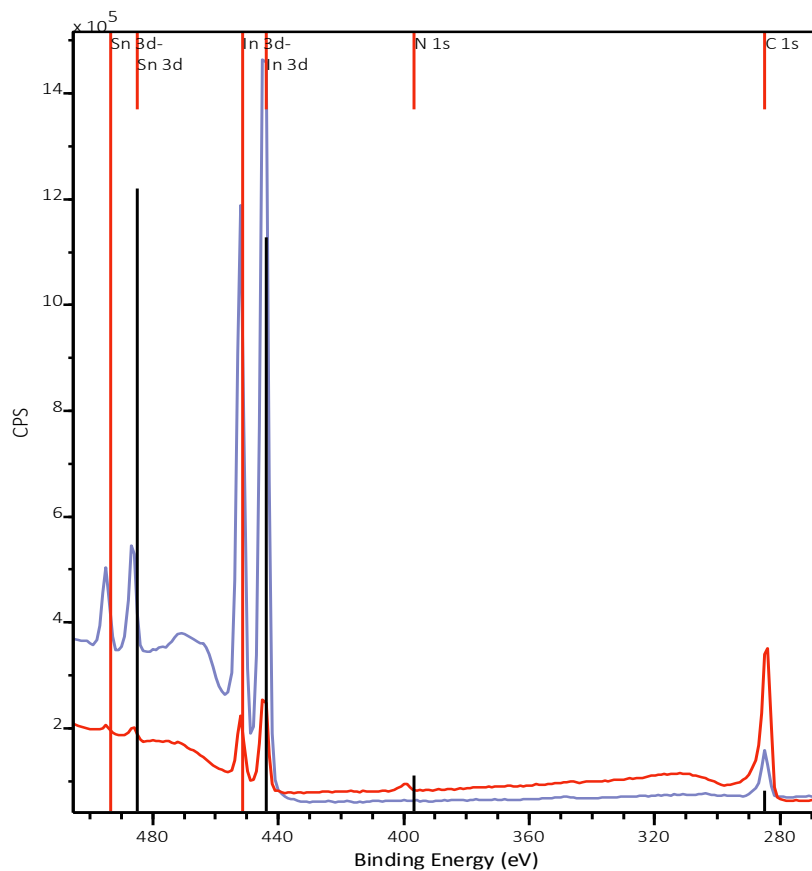


Figure 2- 26- XPS comparison. Sample 3 in red and bare ITO in Violet.

The In and Sn signals are drastically attenuated in the case of sample3 like other samples. By the attenuation of these signals, a thickness value for the rGO layer could be calculated. It is assumed, that is possible to use the attenuation length reported in literature for graphite. According to this estimation, estimated thickness will be 3.5 nm for rGO layer in sample 3.

2. 7. 4. 2. UPS comparison

The UPS spectra are substantially different, also considering the estimated thickness of the rGO layer.

For ITO, the work function is 3.8 eV, quite low with respect to the reported values for ITO. The reason could be the thin over layer on the ITO (probable contamination occurred during transportation and testing), as suggested by the presence of carbon in the XPS spectrum.

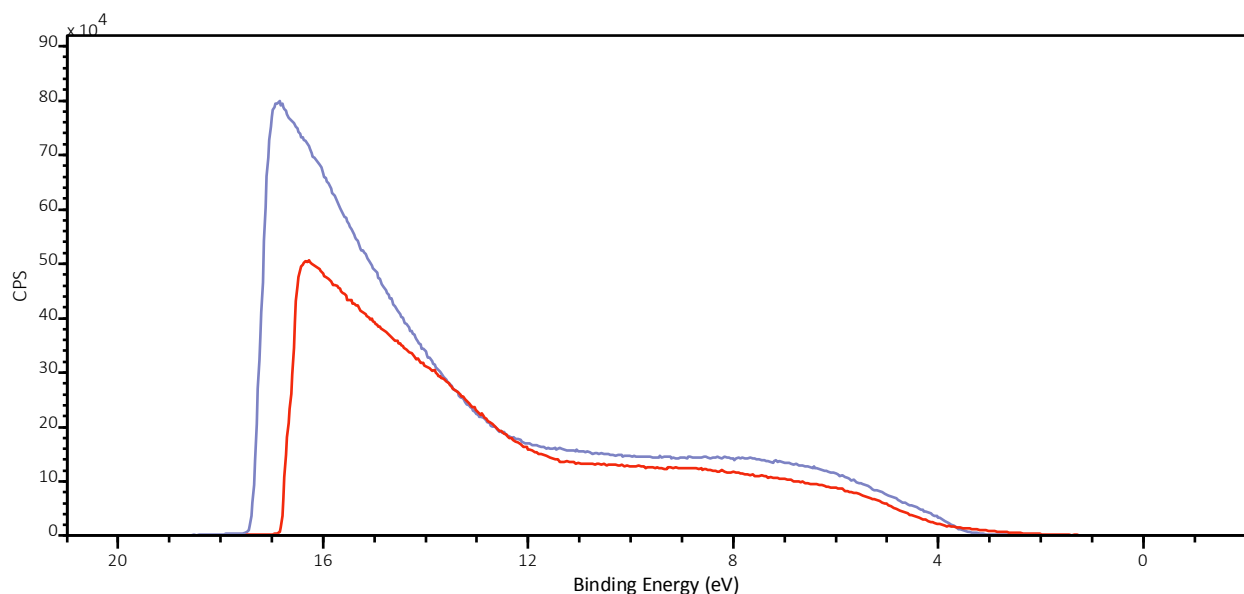


Figure 2- 27- UPS comparison. Sample 3 in red and bare ITO in violet.

It can be inferred from the above measurements that spin coated samples with thermal annealing for the reduction is the best recipe for the preparation of the rGO film. From this moment, spin coating with thermal reduction was used for the cell fabrication.

2. 8. Deciding to Use rGO film as a hole transporting layer or as an electron transporting layer?

To know whether rGO is a hole transporting material or electron transporting material the position of the valence and conduction band of the rGO have to be known. UPS measurements revealed that valence band poisoned at -4.6 eV versus vacuum. For knowing the position of the conduction band, it is possible to use edge of the absorption in the optical absorption measurement. For this purpose and checking also losses of the light in the rGO layer, some optical spectroscopies have been done on the selected samples.

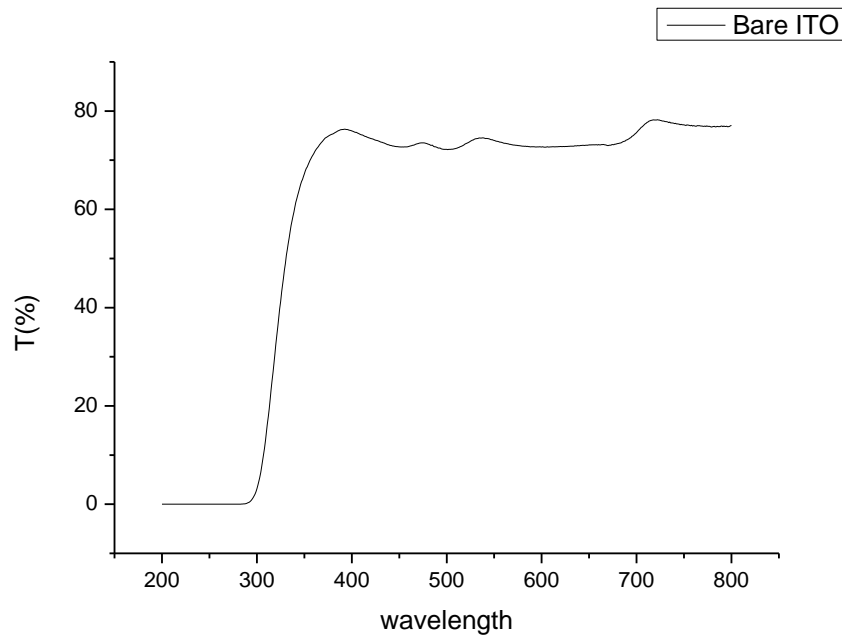


Figure 2- 28- bare ITO Transmission.

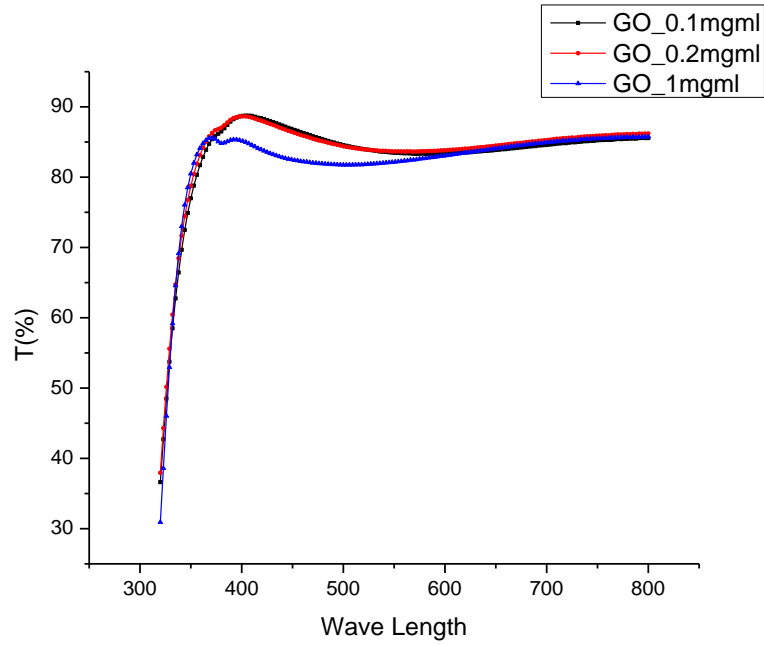


Figure 2- 29- Before Reduction (respect to bare ITO). Transmittance at 550nm wave length, solution with 0.1mg/ml Go = 83.65 (%) (black), solution with 0.2mg/ml Go=83.35 (%) (red), solution with 1mg/ml Go=82.16 (%) (blue)

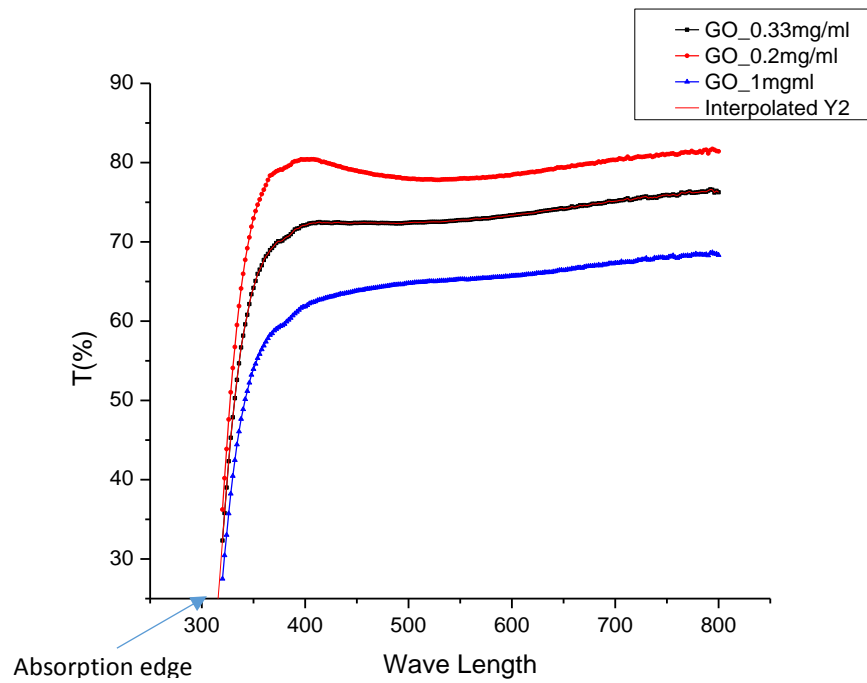


Figure 2- 30- After Reduction: Transmittance (respect to bare ITO) at 550nm wave length, solution with 0.2mg/ml Go= 78 (%) (red), solution with 0.33mg/ml Go=72.75 (%) (black), solution with 1mg/ml Go=65.28 (%) (blue)

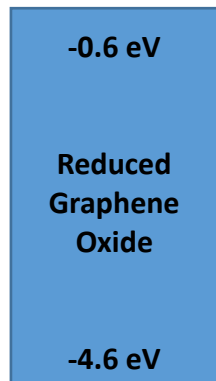
As it is clear from Figure 2- 29 and 30, there was a loss of light with respect to the bare ITO, but this loss was completely reasonable since a layer was added (deposited). Additionally, it is clear that after reduction there was an extra loss due to closing the band gap of the GO.

Other thing which can be obtained from extrapolation of the rGO spectra, is the wavelength in which there is a complete absorption. This point is called edge of the absorption and it is an indication of the value of the band gap of the film. This point is located at 307nm. So, with a very simple calculation, it is possible to get the energy corresponds to this wavelength.

$$eV = 1240/\lambda \cong 4 eV$$

Therefore, by knowing the position of the valence and conduction band of rGO, it is possible to obtain the band diagram of the different layers in the perovskite cell and their relative positions. Below is a carton of the relative position of the different layers.

Conduction Band



Valance Band

Figure 2- 31- position of the Valance and Conduction band of rGO versus Vacuum.

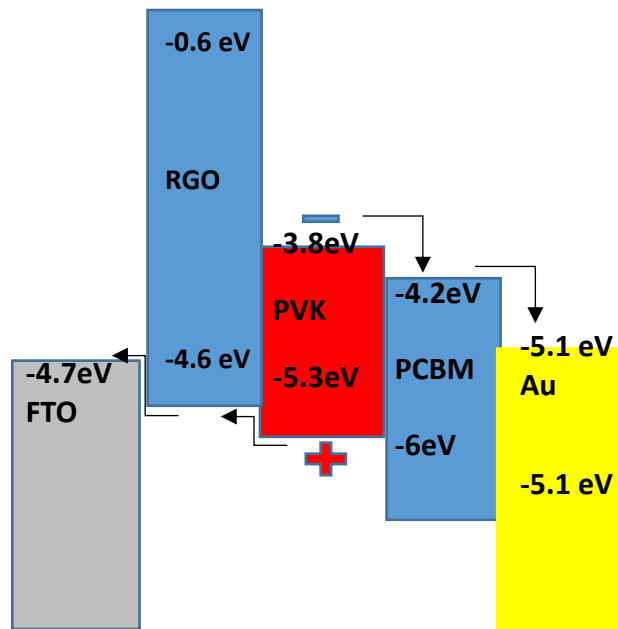


Figure 2- 32- Band diagram alignments. rGO acting as a hole transporting layer.

From the Figure 2- 32 it is possible to reach to the conclusion that, rGO layer can act as a hole transport layer [54, 87]. However, since in the experimental works, it is not possible to rely 100 percent on the measurement data, it is assumed that it is also possible to use rGO also as an electron transporting layer according to some literatures [????]. Additionally, since according to XPS results, rGO annealed in the glove box has some contents of the nitrogen due to the saturated nitrogen atmosphere inside the glove box, so it is not far from imagination to consider it also as an electron transporting layer. Therefore, below configuration also decide to be tested.

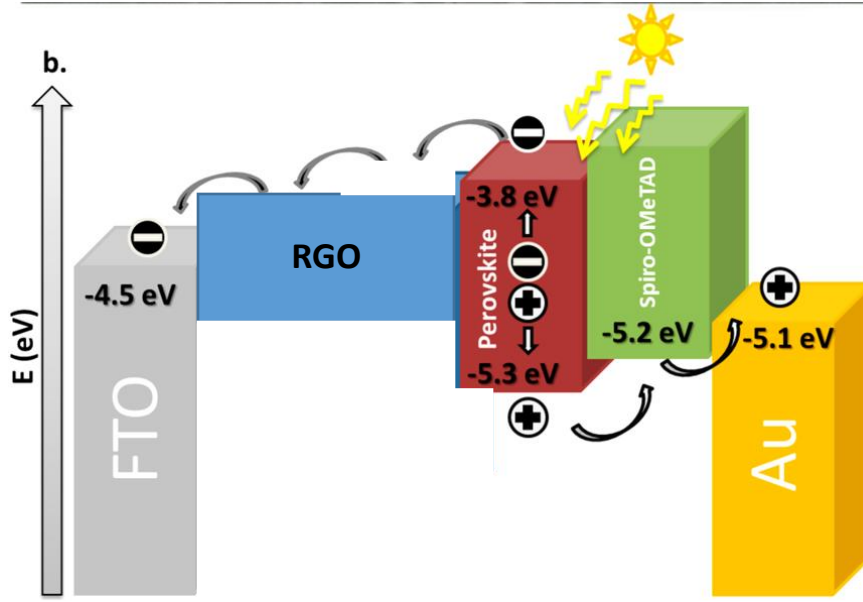




Figure 2- 33- Band diagram alignment. *rGO* acting as an electron transport layer.



Chapter 3

Perovskite layer

Deposition



In this section, there will be a brief summary of some of the experiment and results of the perovskite layer deposition. Due to a huge number of works which have been done, some of them will be omitted to be as direct as possible.

3. 1. Perovskite layer

Generally three different techniques have been adopted to deposit perovskite layer.


1. Two-step deposition
2. Solvent quenching
3. Evaporation of PbI_2

It is worth to mention that, the main problem for the perovskite deposition on rGO film was the low wettability of the rGO film to the DMF solvent which was the solvent of the perovskite solution. So, in the first month of the deposition of the perovskite layer it was trying to increase this wettability in different ways. In the beginning it was thought to change the solvent of the perovskite but after few searches and tries it has been proven, it is not possible to change DMF solvent. The other option which decided to be checked was using vacuum evaporation which is not dependent on the wettability of the target substrate.

In the end, by changing deposition technique of the perovskite. It became possible to deposit a good spin coated perovskite film.

3. 1. 1. Two-step deposition

In this technique, in the first step PbI_2 in DMF solution would be spin coated on the sample. Then, sample should be left to be dried for 15 minutes inside glove box atmosphere, or should be annealed on hot plate at 100 °C for 5 minutes. Then in the second step Methylammonium Iodide (MAI) which is dissolved in IPA has to be spin coated on top. The second step is aimed to convert PbI_2 layer to perovskite, so the



amount of the added MAI has to be chosen according to the right stoichiometry to have a complete conversion.

PbI₂ solution was prepared with 600 mg/ml concentration in DMF solvent. Accordingly, MAI solution was prepared with 70 mg/ml concentration in IPA solvent. PbI₂ solution has been heated up to 80 °C for 30 minutes while stirring, before spin coating. Also, MAI solution has been stirred very well before spin coating.

Spin rotation speed for PbI₂ was set to 5000 rpm for 45 seconds and for MAI, 4000 rpm for 30 seconds.

3. 1. 1. 1. SEM

After preparation of the perovskite layer, crystal grain sizes have been checked to be sure deposited film had a good quality and enough big grain sizes in order to decrease losses due to recombination in grain boundaries. Additionally, big grain size is beneficiary for electron and hole mobility. Moreover, low defect, homogeneity, coverage and presence of the so called pin hole on the film have to be checked to be sure about functionality of the film. Therefore, deposited film was subjected to SEM measurement to realize the quality of the film. Below you can find an example of the deposited perovskite layer on top of the rGO film.

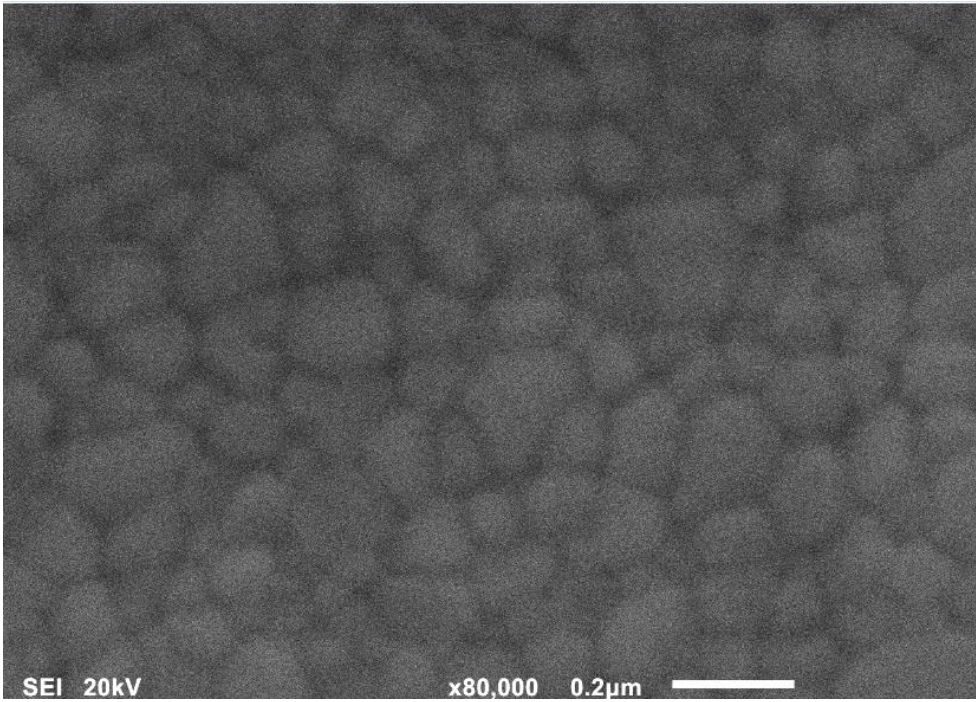


Figure 3- 1- close look on the grain sizes of the as prepared perovskite layer on top of the rGO.

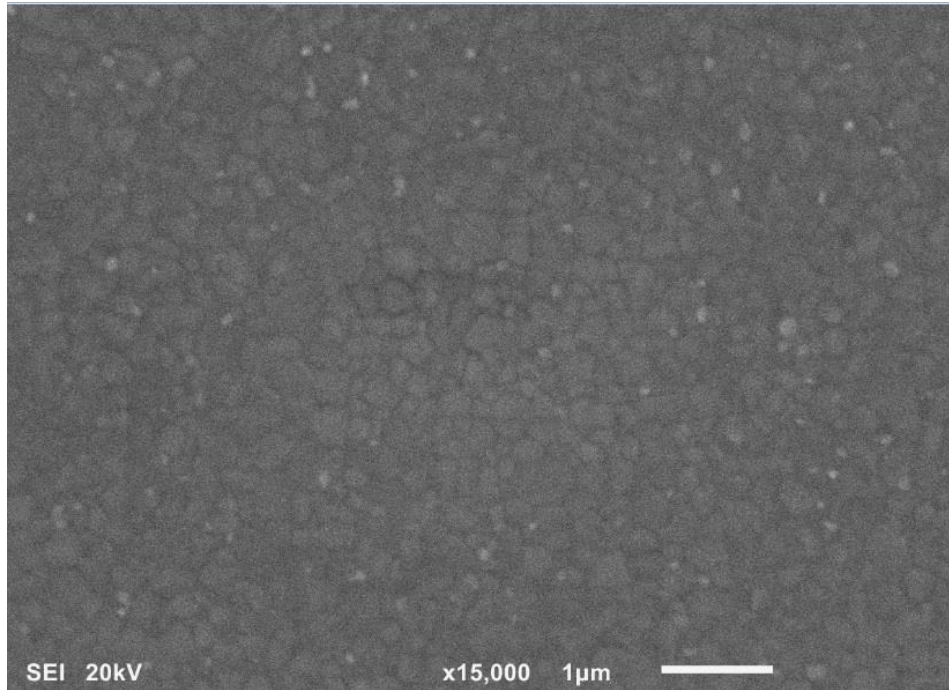


Figure 3- 2- large view of the as deposited perovskite film on top of the rGO.

As it is obvious from the SEM image, grain sizes are enough big to be considered as a good quality film. In average grain sizes around $200 \mu m$ have been reported in the literatures for the good perovskite layer. Here, in average grain sizes are bigger than $350 \mu m$. This is an indication of the high quality of perovskite layer. Also, there was no pin hole and defect visible on the film.

3. 1. 2. Solvent Quenching

In this technique, one solution with all the components of the perovskite layer with right stoichiometry is prepared. Then, during spin coating another solvent which is called quencher will be added to lead to complete conversion.

Solution is a mixture of the PbI_2 , MAI and DMSO with molar ratio 1:1:1, then adding DMF solvent to acquire desired solvent concentration. The best concentration after optimization was obtained equal to 54.2 weight percent.

Spin coating has been done with rotation speed 4000 rpm and for 17 seconds. At 8th second, quencher which was Toluene or Benzene was spread over the sample while it was rotating in the spin coater. Then samples were placed on the hot plate at 150°C for 30 min.

3. 1. 2. 1. SEM

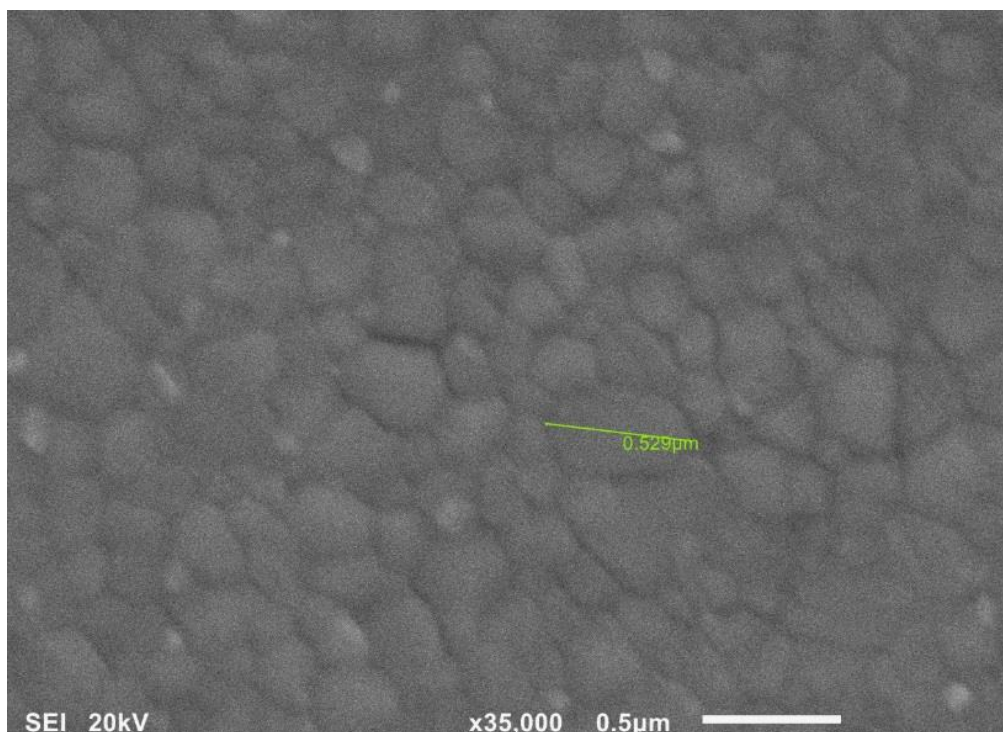



Figure 3- 3- SEM image of the perovskite layer prepared by solvent quenching technique on top of rGO.

On average grain sizes for solvent quenching technique were bigger than previous technique. This means solvent quenching is a better technique respect to two-step one.

3. 1. 3. Evaporation of PbI_2 [108]

In this technique PbI_2 powder was deposited on the sample via vacuum evaporation. 8 small size (24*24mm) samples were placed in the organic evaporator. Subsequently, evaporator set to go to high vacuum ($10\text{e-}7$ Torr). Then power of the crucible which



contained PbI_2 gradually was increased to the value when evaporation of the PbI_2 starts. Evaporation rate was kept very low (0.1 \AA/s) at the beginning and then after deposition of a few nm PbI_2 again power was increased gradually to reach the thickness about 250 nm. For checking the real thickness of the evaporated samples, one of them randomly subjected to thickness measurement with a profilometer. Real evaporation thickness has to be accurate since amount of the MAI which is needed for the conversion of PbI_2 to perovskite have to be selected accordingly. Real measured thickness with profilometer was around 200 nm. For this thickness, MAI concentration have been selected 50 mg/ml in IPA. MAI solution then spin coated on top of samples with spin rotation speed 4000 rpm for 30 seconds.

3. 1. 3. 1. SEM

Unfortunately SEM images was taken after the deposition of the top carrier transporting layer. So, in the images you can see another layer on top of the perovskite layer. However, perovskite crystals are still visible because of the not good coverage of the top layer.

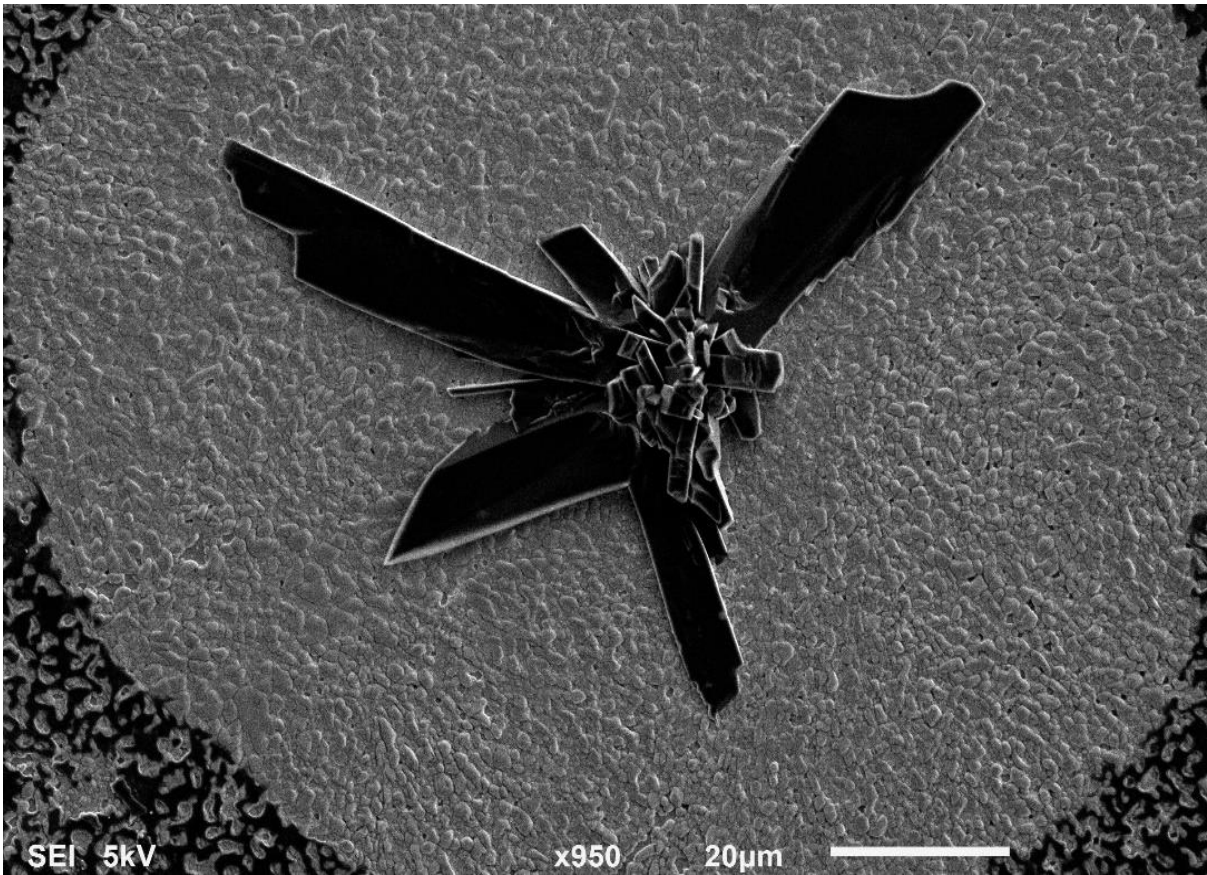


Figure 3- 4- Evaporated perovskite layer underneath of the top carrier transport layer. Notice, gray areas are the perovskite layer without coverage of the top layer. The black areas are top carrier transporting layer (Spiro). Strange Spiro tree in the center.

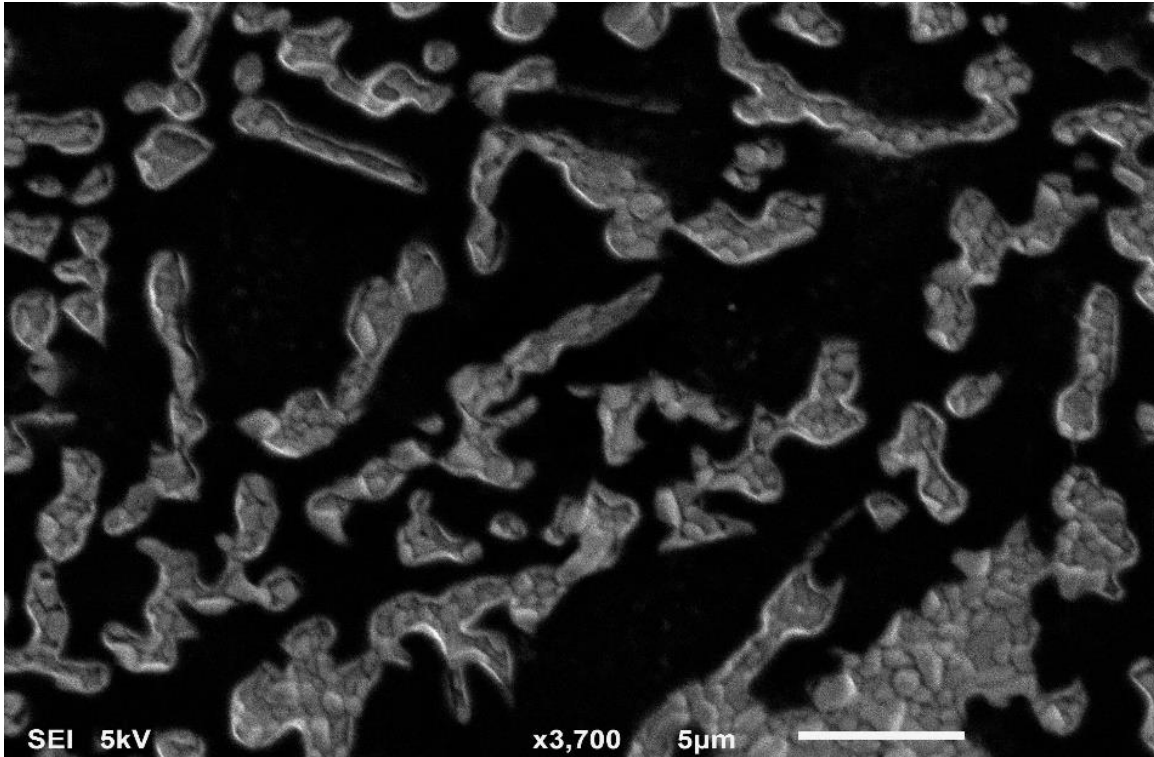



Figure 3- 5- visible grains of the perovskite layer under the top carrier transport layer (Spiro) due to not complete coverage.


Not complete coverage of the top carrier transport layer can be due to high roughness of the perovskite layer. The best cell fabricated with this technique had 1.7% efficiency.

The organic evaporator in the lab did not work properly and every time it gave random thickness and also non uniform film. Therefore, decided to not use this technique anymore. Later just two-step and solvent quenching techniques were used for cell fabrications.



Chapter 4

Results



In this section some of the best results among lots of the experiments have been reported.

Fabrication of the perovskite cells is mainly performed in the glove box with well controlled atmosphere.

During fabrication, cells have not to be in a direct contact with humidity and oxygen. Humidity is a detrimental agent for the cell and have to be avoided in every step.

4. 1. Reference Cell

In the beginning several types of the reference cells have been fabricated. These different types aimed to make easy the comparison between the original cells with the modified ones with rGO.

As mentioned previously, there are two distinct types of the cells which would be modified with rGO. Generally in the perovskite cell field they called standard and inverted structure.

4. 1. 1. Standard structure [25, 43, 62, 63, 65, 88, 94, 107]

This structure is the most used structure. The usual configuration of this cell starts with TiO₂ compact or porous layer as an electron transport layer on top of FTO/ITO substrate. Subsequently, perovskite layer as an active layer, doped Spiro-OMeTAD as a hole transport layer and Gold electrode as a top charge collector. (Figure 4- 1)

4. 1. 2. Inverted Structure [94, 95, 123]

This structure starts with PEDOT: PSS layer as a hole transporting layer on top of ITO/FTO substrate. Subsequently, perovskite layer as an active layer, PCBM as an electron transport layer and Gold or Aluminum electrode as a top charge collector. (Figure 4- 1)

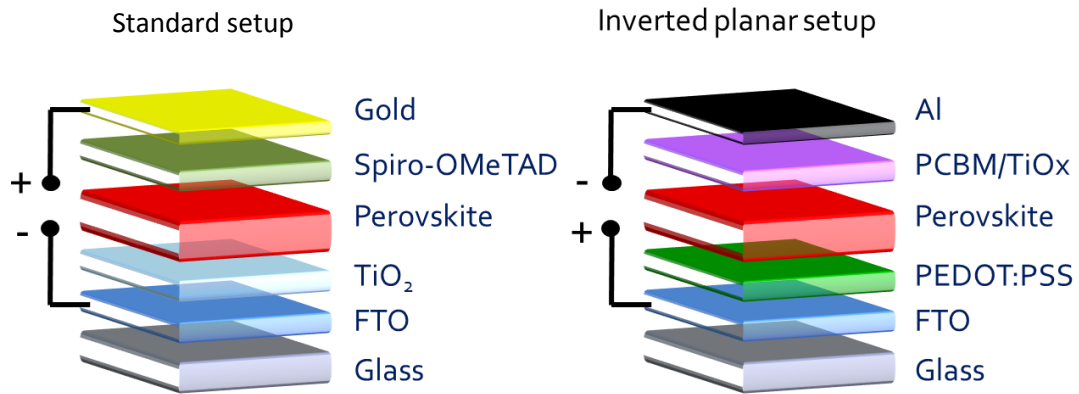


Figure 4- 1- Standard and Inverted Perovskite cell structures

Additional to these two structures, another reference cell without electron transport layer was fabricated. In this type, perovskite layer was fabricated directly on top of the ITO/FTO substrate. (Figure 4- 2)

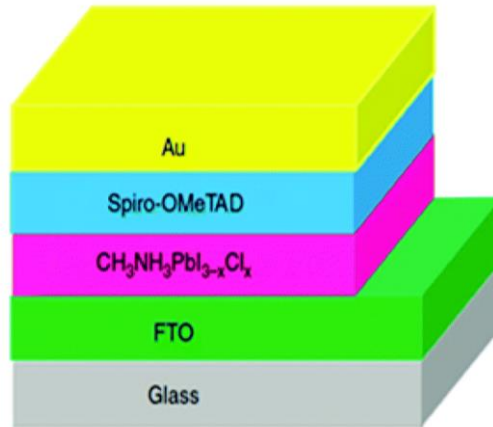


Figure 4- 2- Perovskite cell without electron transport layer.

4. 2. Reference Standard Structure Cell

First step starts with fabrication of the compact TiO₂ layer as an electron transporting layer. To deposit TiO₂ layer, first FTO/ITO patterned substrates were cleaned according to previously mentioned procedure. Then, cleaned FTO/ITO substrates were subjected to plasma treatment to completely remove organic contaminations and absorbed water on the surface. After all these steps, TiO₂ solution was spin coated on top of the substrate. Rotation speed was set to 2000 rpm and duration to 45 seconds.


TiO₂ solution consists of Ti-isopropoxide (Sigma Aldrich), IPA and Hydrochloric acid. Concentration of the Ti-isopropoxide set to 140 µl/ml in IPA solvent. Additionally, 5µl Hydrochloric acid (2M) per each milliliter of the solution was added in order to prevent the oxidation of the solution.

After spin coating of the TiO₂ immediately samples were placed over a hot plate to be annealed at 500 °C for 30 minutes.

After cooling down the samples, they have been moved to glove box for further steps. The first step in the glove box was spin coating of the perovskite layer as reported previously. After deposition of the perovskite layer, it is time to deposit a hole transporting layer. The hole transporting layer is Spiro-OMeTAD. The solution of the Spiro was spin coated on top of the perovskite layer with spin rotation speed equal to 4000 rpm and for 60 seconds.

The Spiro-OMeTAD solution was prepared by dissolving 75 mg of Spiro-OMeTAD in 1 ml of chlorobenzene, in which 29 µl of 4-tert-butyl pyridine (tBP) and 18.25 µl of lithium bis(tri fluoro methanesulfonyl)imide (Li-TFSI) solution (520 mg LI-TSFI in 1 ml acetonitrile, Sigma-Aldrich) were added. [51]

Subsequently, since Spiro layer has to be doped, samples were placed in a desiccator outside the glove box to be doped with oxygen in the air. Samples remained there for more than 8 hours to be effectively doped.



Finally, the last layer was the gold top electrode layer which has been deposited with vacuum evaporator.

For the cell characterization, the IV curves obtained under solar simulator illumination equal to one sun. For all the measurements, range of the scan voltage was set to 0 to 1.4 volts. Additionally, 1.4 volts for 5 seconds was applied as a pre biasing for all the measurements, otherwise it would be mentioned. Scan rate was set to 1 V/s which is moderately fast scan rate. This fast scan rate was applied to have a better insight of the cell performance under fast changes in the cell. Additionally, it would intensify the hysteresis effect in order to study it better.

Moreover, it has to notice all over this chapter rGO layer was fabricated according to the optimized conditions which have been pointed out earlier in Chapter 2.

In Figure 4- 3, IV scan curves and results for a reference with standard structure has been depicted.

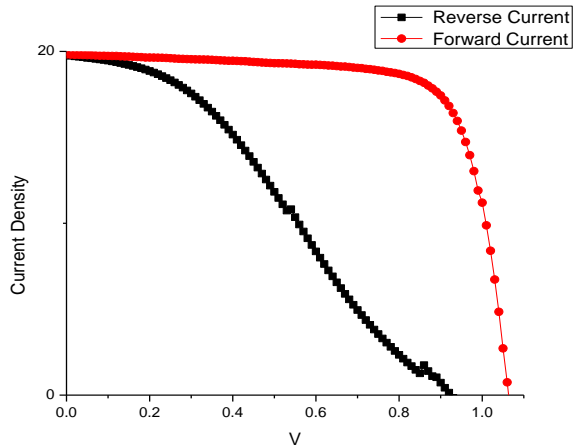


Figure 4- 3- Reference Standard Structure sample, Cell layers sequence: FTO/compact TiO₂/Perovskite/Spiro/Gold electrode

- Reverse Scan:
 - PCE (%) = 15.71
 - Jsc (mA/cm^2)= 19.83 (Jsc stands for Short Circuit Current density)
 - Voc (V) = 1.06 (Voc stands for Open Circuit Voltage)
 - FF = 0.75 (FF stands for Fill Factor)
- Forward Scan:
 - PCE (%)= 6.12
 - Jsc (mA/cm^2)= 19.77
 - Voc (V) = 0.92
 - FF = 0.33

Cell architecture:

FTO/ TiO₂/Perovskite/Spiro/Gold electrode

Perovskite material: CH₃NH₃PbI₃

Perovskite fabrication technique: solvent quenching

In this reference cell as it is clear from the results, cell had a good performance respect to efficiency, but the problem is high hysteresis, which means a large discrepancy between forward and reverse scan. This cell can be a good reference for the modification of the cell with rGO addition.

In Figure 4- 4, another reference cell with the standard structure, but with different perovskite material has been depicted

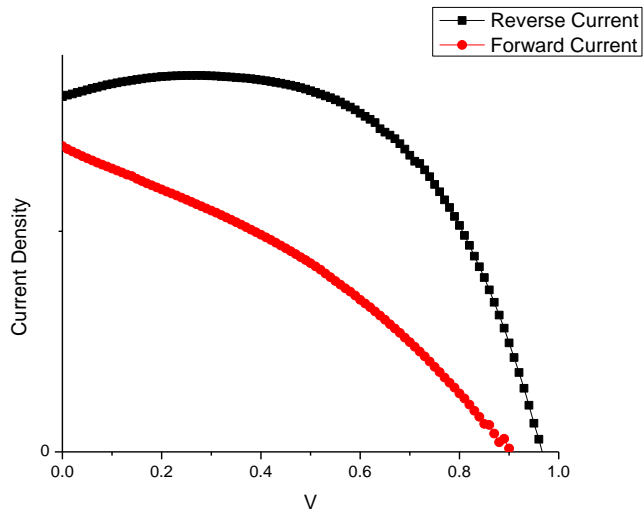


Figure 4- 4- Standard Structure Reference Cell, Cell layers sequence: FTO/Compact TiO₂/Perovskite(Lead Acetate) /Spiro/Gold electrode

- | | |
|---|--|
| <ul style="list-style-type: none"> ➤ Reverse Scan: ➤ PCE (%)= 9.51 ➤ Jsc (mA/cm²)= 16.11 ➤ Voc (V) = 0.97 ➤ FF = 0.61 | <ul style="list-style-type: none"> ➤ Forward Scan: ➤ PCE (%) = 4.3 ➤ Jsc (mA/cm²)= 13.87 ➤ Voc (V) = 0.9 ➤ FF = 0.34 |
|---|--|

Cell architecture:


FTO/ TiO₂/Perovskite/Spiro/Gold electrode

Perovskite material: MAPbI₃ Lead Acetate

Perovskite fabrication technique: solvent quenching

In this reference cell, by keeping the same cell structure, perovskite layer material have been changed. The new material for the perovskite layer is the lead acetate instead of lead iodide. Cell fabrication is exactly the same except the spin speed rotation for the perovskite layer which set to 2000 rpm instead of 4000 rpm.

This reference cell had lower performance respect to efficiency, but respect to hysteresis is slightly better than lead iodide one. However, since it would make it rather complicated



to compare the modification with two distinct reference cells, it has been decided to continue just with lead Iodide one.

4. 3. Modification of the standard structure with rGO replacement

It means using rGO as an electron transport layer in the standard structure instead of TiO₂.

4. 3. 1. Solvent Quenching modified Standard Structure cell with rGO

In Figure 4- 5, a standard cell structure modified by using rGO as an electron transporting layer, has been illustrated.

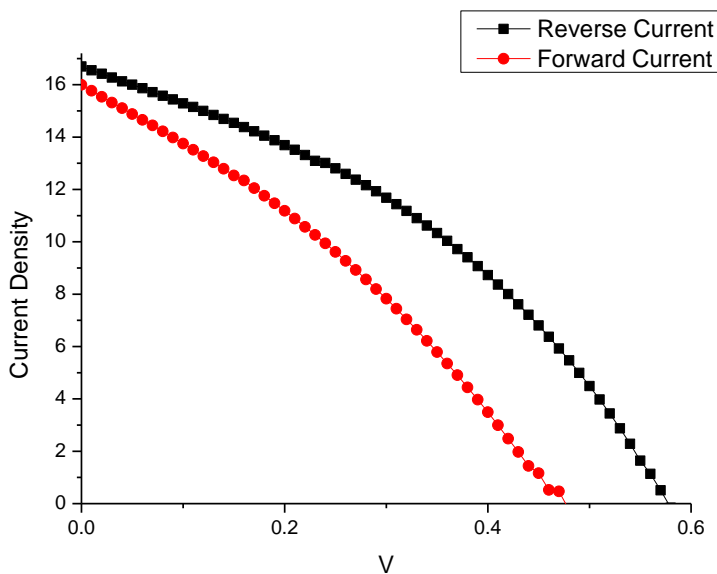


Figure 4- 5- Standard structure modified by using rGO as an electron transport layer instead of compact TiO₂, cell layers sequence: FTO/rGO/Perovskite (Solvent quenching method)/Spiro/Gold electrode

- | | |
|-----------------------------------|---------------------------------|
| ■ Reverse Scan: | ■ Forward Scan: |
| ➤ PCE (%)= 3.6 | ➤ PCE (%)= 2.41 |
| ➤ Jsc (mA/cm ²)= 16.7 | ➤ Jsc (mA/cm ²)= 16 |
| ➤ Voc (V) = 0.58 | ➤ Voc (V) = 0.48 |
| ➤ FF = 0.38 | ➤ FF = 0.32 |

Perovskite material: CH₃NH₃PbI₃

Perovskite fabrication technique: solvent quenching

In this cell as it is obvious from the results, the cell did not work properly In terms of efficiency, but with respect to hysteresis it had better function. Actually, the problem of this cell is low Voc and FF, which can be due to miss alignment of the energy levels of different layers. However, since the only difference was replacing rGO instead of TiO₂, it can be inferred that rGO cannot act very well as an electron transporting layer, as it was suggested before.

4. 3. 2. Two-step deposition modified standard structure cell with rGO

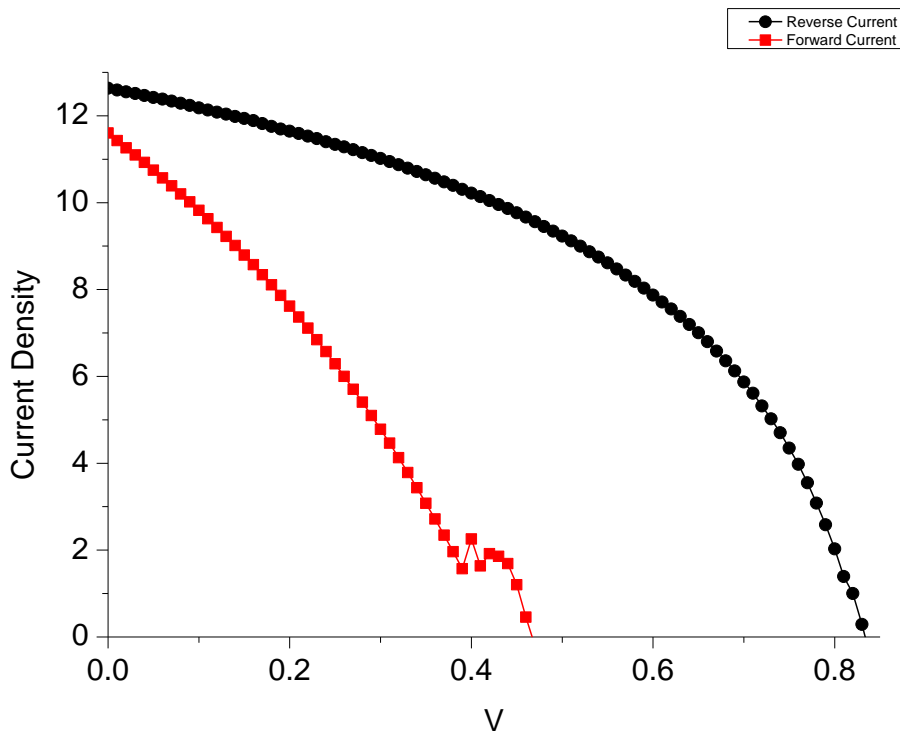



Figure 4- 6- Standard structure modified by using rGO as an electron transport layer instead of compact TiO₂, cell layers sequence: FTO/rGO/Perovskite (Two-step method)/Spiro/Gold electrode

- | | |
|--|--|
| <ul style="list-style-type: none"> ➤ Reverse Scan: ➤ PCE (%)= 4.88 ➤ Jsc (mA/cm^2)= 12.37 ➤ Voc (V) = 0.86 ➤ FF = 0.46 | <ul style="list-style-type: none"> ➤ Forward Scan: ➤ PCE (%)= 1.18 ➤ Jsc (mA/cm^2)= 11.21 ➤ Voc (V) = 0.39 ➤ FF = 0.27 |
|--|--|



Perovskite material: $\text{CH}_3\text{NH}_3\text{PbI}_3$

Perovskite fabrication technique: Two-step Method

Data shows that this cell respect solvent quenching one, had a better performance respect efficiency but worse respect hysteresis. However, generally using the rGO as an electron transport layer was not satisfying. Although it would be possible to improve the performance of this cell further for a few percent in terms of efficiency, the cell has been put aside. Since it had fundamentally problem of low V_{oc} respect to reference cell which it may be aroused from not perfect alignment of different layers.

If the problem would be just very low current respect to the reference cell, then it could be related to the fabrication techniques of the perovskite layer and presence of the defects and small grain size, however it is not.

Following in the Figure 4- 7, dependency of the IV curves to pre biasing condition and scan rate have been investigated.

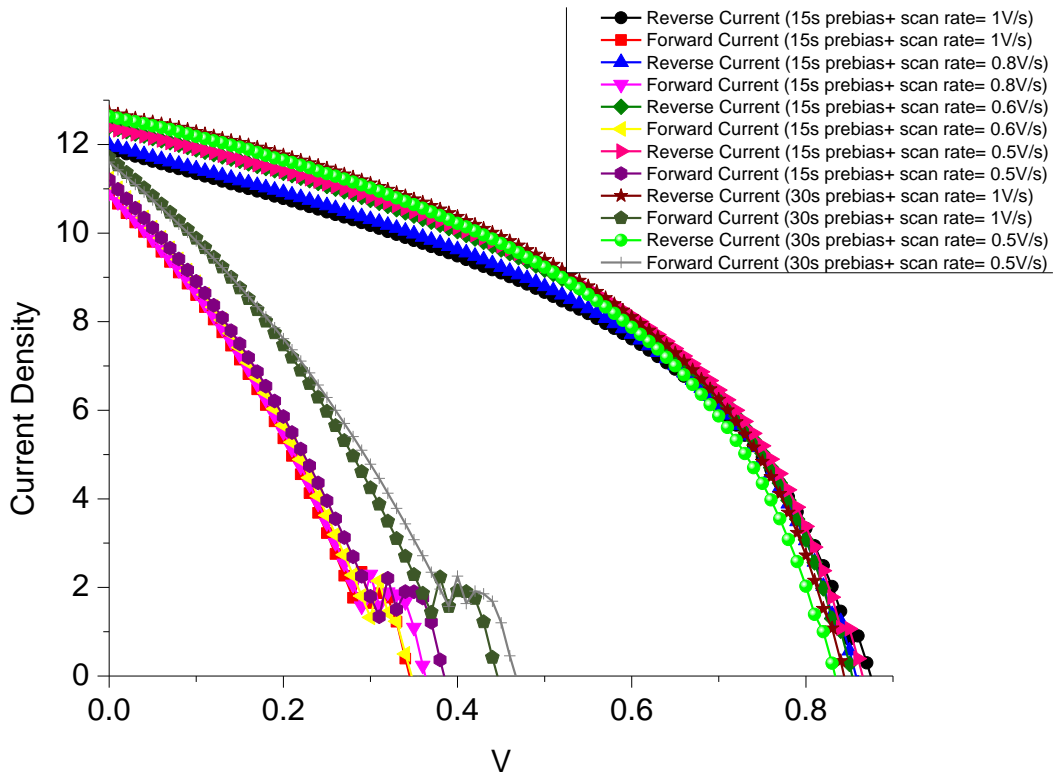


Figure 4- 7- Pre biasing condition and scan rate dependency. cell layers sequence: FTO/rGO/Perovskite (Two-step method)/Spiro/Gold electrode,

It can be realized from the trend in the Figure 4- 7, if scan rate increased in the fix pre biasing, hysteresis goes higher. On the other hand, increasing the pre biasing time, increase the Voc and Isc and in general PCE of the cell.

4. 4. Reference cell without electron transport layer

In this section a reference cell without any electron transport layer has been presented. This reference cell was fabricated in order to understand whether using rGO layer as an electron transporting layer is beneficial for the cell performance or not. For this purpose, electron transporting layer has been ignored completely.

Perovskite layer was fabricated directly on top of the cleaned and plasma treated FTO substrate.

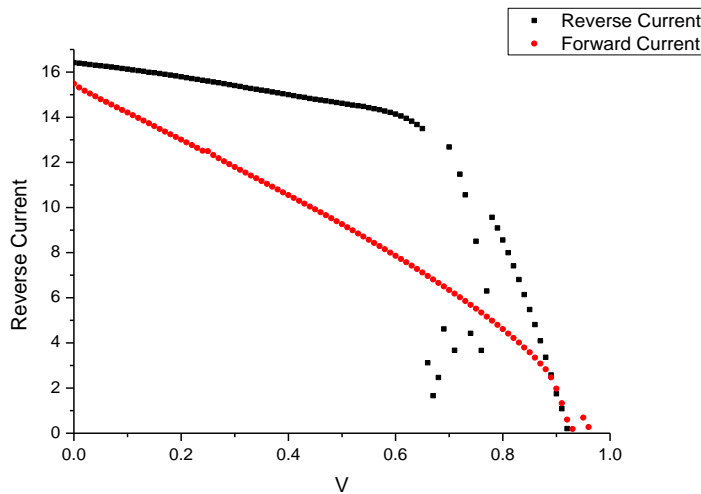


Figure 4- 8- Reference standard structure cell without electron transporting layer, Cell layers sequence: FTO/Perovskite (solvent quenching) /Spiro/Gold electrode, sample1

- | | |
|---|---|
| <ul style="list-style-type: none"> ➤ Reverse Scan: ➤ PCE (%)= 8.88 ➤ $J_{sc} (mA/cm^2)$= 16.42 ➤ Voc (V) =0.93 ➤ FF =0.59 | <ul style="list-style-type: none"> ➤ Forward Scan: ➤ PCE (%)= 4.73 ➤ $J_{sc} (mA/cm^2)$= 15.49 ➤ Voc (V) = 0.97 ➤ FF = 0.32 |
|---|---|

Cell architecture:

FTO/Perovskite/Spiro/Gold electrode

Perovskite material: $CH_3NH_3PbI_3$

Perovskite fabrication technique: solvent quenching

It has been realized that above reference cell respect the one modified with rGO had a better performance both from PCE and Hysteresis points of views.

So, it can be inferred that, rGO layer acting as an electron transporting layer has detrimental effects on the cell performance. So, in contrary to some literature [99,102] which claimed to use rGO as a good electron transporting layer, here it was not possible.

For being sure about the validity of the aforementioned conclusion, another batch of reference cell was fabricated with the exact same procedure.

Below the results for the second batch of reference cell without electron transporting layer, is presented.

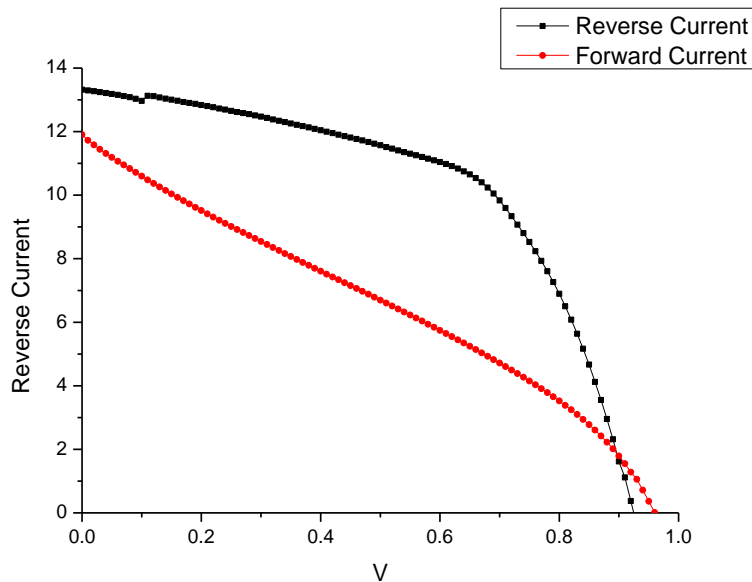


Figure 4- 9- Reference Standar Structure cell without electron transporting layer, Cell layers sequence: FTO/Perovskite (solvent quenching) /Spiro/Gold electrode, sample2

- | | |
|--|---|
| <ul style="list-style-type: none"> ■ Reverse Scan: ➤ PCE (%)= 6.97 ➤ Jsc (mA/cm^2)= 13.32 ➤ Voc (V) = 0.93 ➤ FF = 0.57 | <ul style="list-style-type: none"> ■ Forward Scan: ➤ PCE (%)= 3.45 ➤ Jsc (mA/cm^2)= 11.91 ➤ Voc (V) = 0.96 ➤ FF = 0.3 |
|--|---|

Again approximately same results were obtained. So, it is possible to conclude that it is not an efficient scheme to use our rGO as an electron transporting layer.

4. 5. Reference Inverted Structure cell with PEDOT: PSS and PCBM

In this section, reference cell for the inverted structure is presented. This cell configuration was fabricated to be a reference cell for the case when the rGO layer would be used as a hole transporting layer. Earlier, it was mentioned that rGO expected to perform well when it is used as a hole transporting layer. Here, the results of the measurements have been presented.

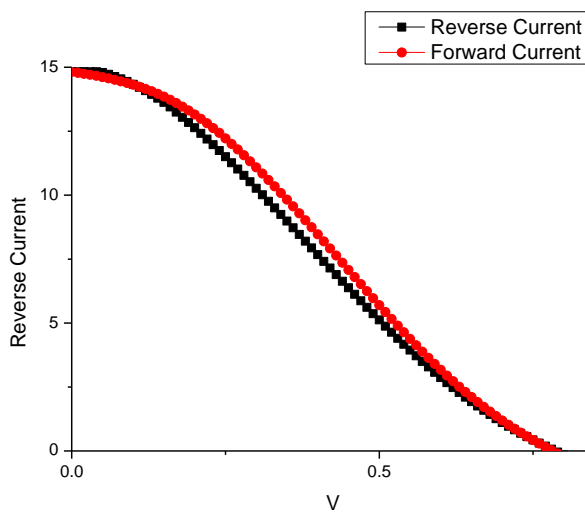


Figure 4- 10- Reference Inverted Structure. Cell layers sequence: FTO/PEDOT : PSS/Perovskite/PCBM/Gold electrode


- | | |
|------------------------------|------------------------------|
| ▶ Reverse Scan: | ▶ Forward Scan: |
| ➤ PCE (%)= 3.16 | ➤ PCE (%)= 3.45 |
| ➤ $J_{sc} (mA/cm^2)$ = 15.11 | ➤ $J_{sc} (mA/cm^2)$ = 14.86 |
| ➤ Voc (V) = 0.78 | ➤ Voc (V) = 0.78 |
| ➤ FF = 0.27 | ➤ FF = 0.3 |

Cell Architecture:

FTO/PEDOT: PSS/Perovskite/PCBM/Gold electrode

Perovskite material: $CH_3NH_3PbI_3$

Perovskite fabrication technique: solvent quenching



In the Figure 4- 10, IV curve for a reference inverted structure is shown. The reference cell itself did not show reasonable performance with respect to efficiency, but in terms of hysteresis, it was well performed. The source of this low efficiency was not clear, but in general inverted structures have lower efficiency respect to standard ones. It can be attributed to low performance of the carrier transporting layer whether PEDOT: PSS or PCBM. Additionally, another problem related to this structure is due to low stability of the cell in the environment which leads to lose the functionality in a few hours outside the glove box. It is suggested to be related to low stability of the PCBM layer on top of the cell.

4. 6. Modification of the inverted structure with rGO replacement

In this section, inverted structure with replacement of the rGO layer instead of PEDOT: PSS layer has been presented. In this configuration rGO layer acts as a hole transporting layer.

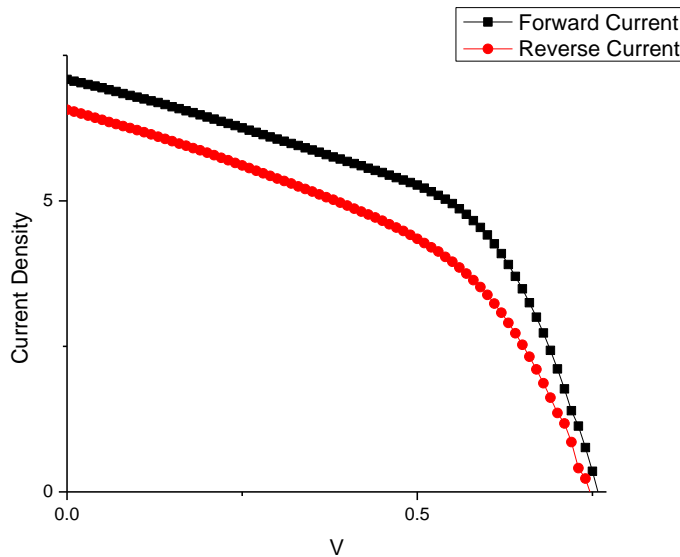


Figure 4- 11- Modified Inverted Structure with rGO. Cell layers sequence: FTO/rGO/Perovskite/PCBM/Gold electrode, (Fast Scan rate)

- | | |
|-----------------------------------|-----------------------------------|
| ➤ Forward Scan: | ➤ Reverse Scan: |
| ➤ PCE (%)= 2.72 | ➤ PCE (%)= 2.19 |
| ➤ Jsc (mA/cm ²)= 7.09 | ➤ Jsc (mA/cm ²)= 6.57 |
| ➤ Voc (V) = 0.76 | ➤ Voc (V) = 0.75 |
| ➤ FF = 0.51 | ➤ FF = 0.45 |

Cell Architecture:

FTO/rGO/Perovskite/PCBM/Gold electrode

Perovskite material: CH₃NH₃PbI₃

Perovskite fabrication technique: solvent quenching

Scan rate: 1 V/s

The Results show that, the cell had a reasonably enough good performance both in efficiency point of view and also in terms of hysteresis. An important point to focus is to

consider low short circuit current respect to the reference cell. This can be mainly due to the perovskite layer quality and suggests presence of the defects and also small grain sizes. So, it is possible to improve cell performance by focusing on the perovskite layer quality.

However, afterward, a few batches have been fabricated to improve perovskite film quality, but it was not effective and cell performance in contrary to get a good perovskite film quality, did not improved. So, the problem could be due to low performance of the PCBM layer. Nevertheless, because of the time limit it was not possible to further investigate this configuration. But, it can be a good starting point for the application of the rGO layer as an efficient hole transporting layer in the future works.

Below, details of the dependency of the IV curve to scan rate has been reported.

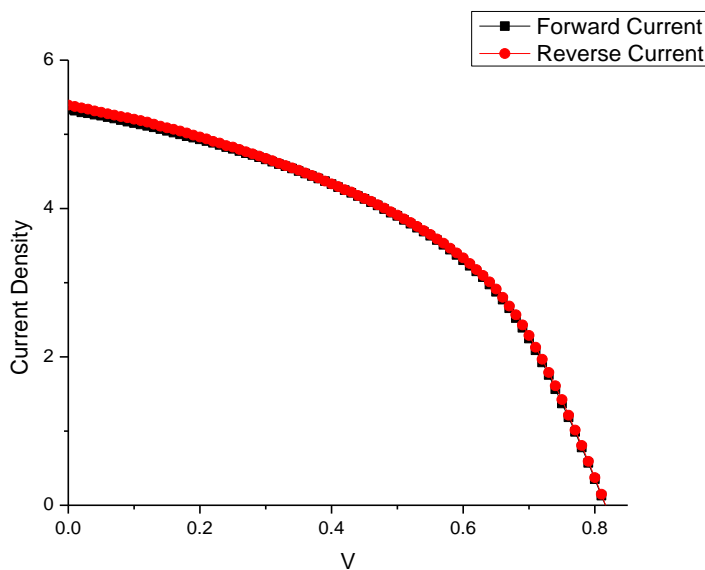



Figure 4- 12- Modified Inverted Structure with rGO. Cell layers sequence: FTO/rGO/Perovskite/PCBM/Gold electrode, (Slow Scan rate)

- | | |
|--|---|
| <ul style="list-style-type: none"> ➤ Forward Scan: ➤ PCE (%)= 2 ➤ J_{sc} (mA/cm^2)= 5.33 ➤ Voc (V) = 0.82 ➤ FF = 0.46 | <ul style="list-style-type: none"> ➤ Reverse Scan: ➤ PCE (%)= 2.01 ➤ J_{sc} (mA/cm^2)= 5.39 ➤ Voc (V) = 0.82 ➤ FF = 0.46 |
|--|---|

Scan rate: 0.5 V/s



As it is shown in Figure 4- 12, by reducing the scan rate to moderately slow scan rate there would not be any hysteresis. This shows that this cell configuration is working near steady state.

In the rest of this chapter, some works will be presented to come up with some new ideas related to integration of the RGO in different ways.

4. 7. Control cell for using reduced Graphene Oxide (rGO) as an interlayer between TiO_2 and Perovskite layer

In this section some other ideas which were proposed by the authors of this study have been checked to see whether it is possible to utilize from rGO in the other ways.

The first Idea was to use rGO as an interlayer between perovskite and TiO_2 layers in the standard structure. Purpose is to modify the interface of the perovskite and TiO_2 layers which is a source of the hysteresis from some researcher's prospective. [116, 17, 106]

Please notice, because of the low reproducibility of the perovskite solar cells in general, for every batch of samples one control cell fabricated with a standard structure to compare the results.

Below, first a control cell with regular standard structure was fabricated. This cell was fabricated for comparison of the regular structure with modified ones with rGO in the same batch of the samples.

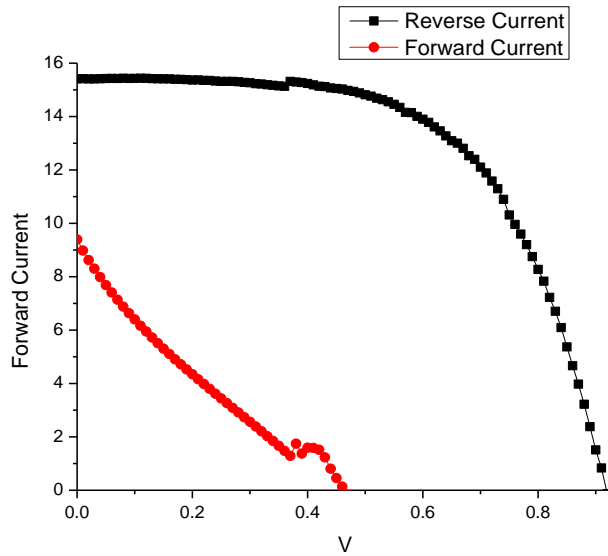


Figure 4- 13- Control Standard Structure Cell, Cell layers sequence: FTO/TiO₂/Perovskite (solvent quenching)/Spiro/Gold electrode.

► Reverse Scan:

- J_{sc} (mA/cm²) = 15.41
- Voc (V) = 0.92
- FF = 0.61
- PCE (%) = 8.58

► Forward Scan:

- J_{sc} (mA/cm²) = 13.55
- Voc (V) = 0.83
- FF = 0.27
- PCE (%) = 3.08

This cell had not very good performance, but because the conditions will be same for all the samples it is good for comparison to distinguish the improvement.

4. 7. 1. Using Reduced Graphene Oxide (rGO) As an Interlayer between TiO₂ and Perovskite layer

In this structure rGO layer was placed in between TiO₂ and Perovskite layer.

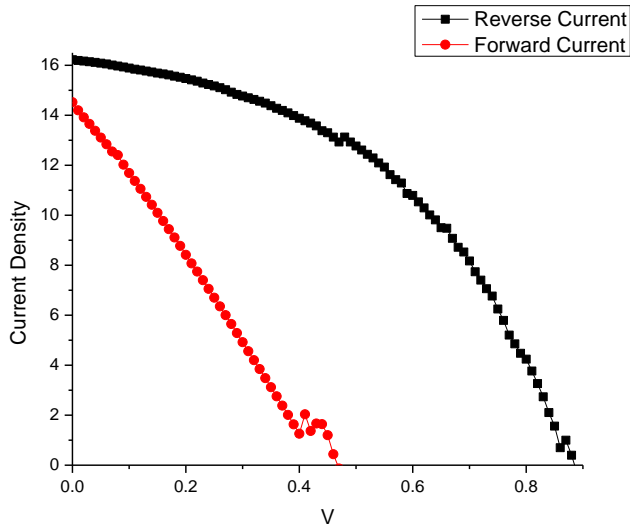


Figure 4- 14- Standard structure cell with rGO interlayer layer. Cell layers sequence: FTO/TiO₂/RGO/Perovskite (Solvent quenching)/Spiro/Gold electrode

- | | |
|--|--|
| <ul style="list-style-type: none"> ➤ Reverse Scan: ➤ J_{sc} (mA/cm²) = 16.22 ➤ Voc (V) = 0.88 ➤ FF = 0.46 ➤ PCE (%) = 6.56 | <ul style="list-style-type: none"> ➤ Forward Scan: ➤ J_{sc} (mA/cm²) = 14.52 ➤ Voc (V) = 0.47 ➤ FF = 0.25 ➤ PCE (%) = 1.70 |
|--|--|

In this cell it seems rGO layer had not beneficial effect.

4. 7. 2. Using Reduced Graphene Oxide (rGO) deposited on top of PDDA layer As an Interlayer between TiO₂ and Perovskite layer

This cell was fabricated exactly the same as the pervious case, but with PDDA pre layer which described in chapter 2 section 5. Here, influence of adding PDDA monolayer which is a polymer material on the cell performance has been investigated.

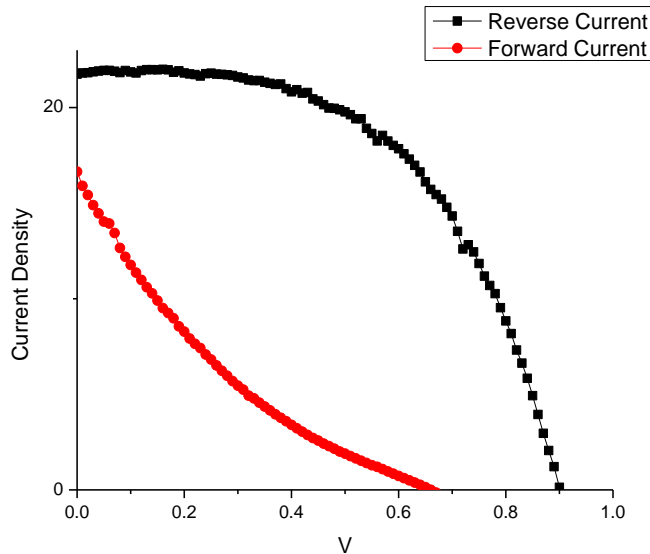


Figure 4- 15- Standard structure cell with rGO-PDDA interlayer layer. Cell layers sequence: FTO/TiO₂/rGO on top of PDDA mono layer/Perovskite layer (Solvent quenching)/Spiro/Gold electrode.

- | | |
|---|--|
| <ul style="list-style-type: none"> ■ Reverse Scan: ➤ J_{sc} (mA/cm²) = 21.75 ➤ Voc (V) = 0.90 ➤ FF = 0.55 ➤ PCE (%) = 10.73 | <ul style="list-style-type: none"> ➤ Forward Scan: ➤ J_{sc} (mA/cm²) = 16.65 ➤ Voc (V) = 0.66 ➤ FF = 0.16 ➤ PCE (%) = 1.71 |
|---|--|

As it is clear cell had better performance in term of PCE but worse in hysteresis point of view. It seems PDDA play a positive role for increasing current density, but it causes charge accumulation at the interface and leads the cell works unsteadily, simultaneously.

4. 8. Using another Perovskite material

Here, a mixture of Formamidinium and Methylammonium lead Iodide with the addition of inorganic Cesium (Cs/MA/FA) was used as a perovskite material. My colleague Dr. Peter Topolovsek has made this solution for this part of the work. He optimized this technique and had a good stabilized efficiency around 15%. However, since he did not publish this work yet, it is not possible to reveal his procedure.

This new perovskite material was expected to be hysteresis free and performs very well in terms of efficiency.

This new perovskite material has been selected to realize the influence of the better perovskite material on the modifications with rGO. Since, in earlier steps, there was always doubts about quality of the fabricated perovskite layer, so, to ignore contributions of the low quality of the perovskite layer, another material with verified stable efficiency have been tested.

Later, some modifications with integration of rGO have been made. The results have been compared with the reference cell.

4. 8. 1. Reference Standard Structure Cell with Cs/MA PbI₂/FA perovskite material

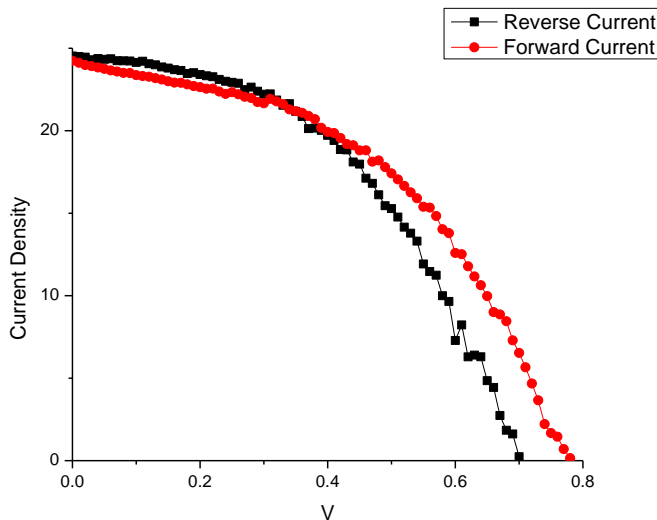


Figure 4- 16- Reference Standard Structure Sample, Cell layers sequence: FTO/compact TiO₂/Perovskite(Solvent quenching)/Spiro/Gold electrode

➤ Reverse Scan:

- Jsc (mA/cm²) = 24.53
- Voc (V) = 0.70
- FF = 0.47
- PCE (%) = 8.1

➤ Forward Scan:

- Jsc (mA/cm²) = 24.24
- Voc (V) = 0.78
- FF = 0.46
- PCE (%) = 8.74

Cell architecture:

FTO/ TiO₂/Perovskite/Spiro/Gold electrode

Perovskite material: Cs/MA Pbl₂/FA

Perovskite fabrication technique: solvent quenching

As it is clear from Figure 4- 16, the cell had a good performance in terms of hysteresis but not efficiency.

In the followings, there are some Ideas which have been tested to see whether it is possible to improve cell performance.

4. 8. 2. Standard Structure Cell with Cs/MA Pbl₂/FA perovskite material and rGO as an interlayer between TiO₂ and perovskite layers

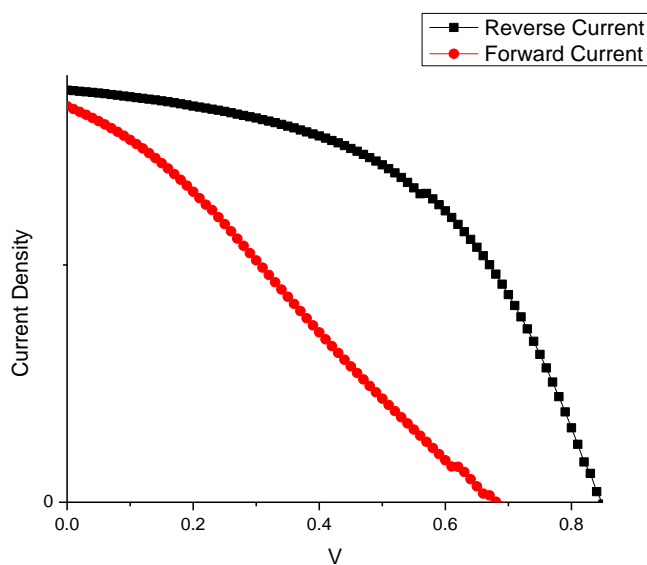


Figure 4- 17- Cell layers sequence: FTO/compact TiO₂/rGO/Perovskite(Solvent quenching)/Spiro/Gold electrode

➤ Reverse Scan:

- J_{sc} (mA/cm²) = 17.37
- Voc (V) = 0.85
- FF = 0.5
- PCE (%) = 7.42

➤ Forward Scan:

- J_{sc} (mA/cm²) = 16.69
- Voc (V) = 0.68
- FF = 0.27
- PCE (%) = 3.07

Perovskite material: Cs/MA Pbl₂/FA

This configuration made the performance of the cell worse than the reference cell.

4. 8. 3. Standard Structure Cell with Cs/MA Pbl₂/FA perovskite material and rGO as an interlayer between TiO₂ and PCBM layers

Another Idea is to use rGO as an interlayer between PCBM and TiO₂. In this structure, it is possible to benefit from high electron mobility of the PCBM and electron blocking property of the TiO₂ at the same time. Besides, rGO role is to make better interface between PCBM and TiO₂.

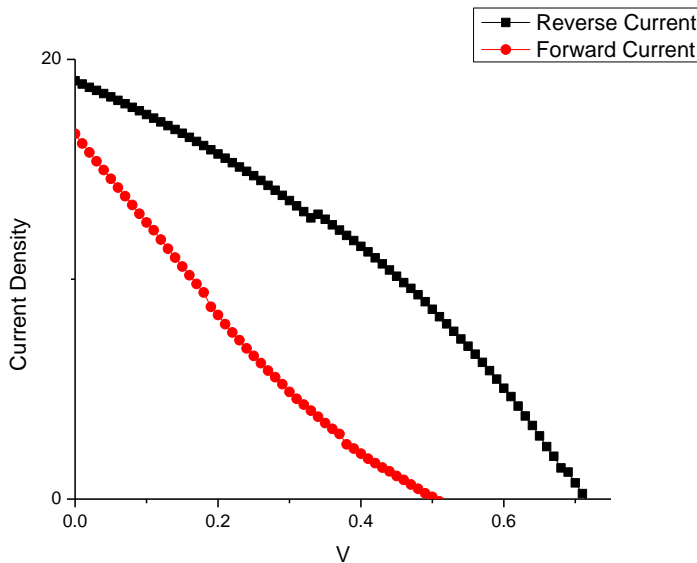


Figure 4- 18- Cell layers sequence: FTO/ TiO₂/rGO/PCBM/Perovskite(Solvent quenching)/Spiro/Gold electrode

➤ Reverse Scan:

- Jsc (mA/cm²) = 19.3
- Voc (V) = 0.72
- FF = 0.34
- PCE (%) = 4.61

➤ Forward Scan:

- Jsc (mA/cm²) = 16.62
- Voc (V) = 0.5
- FF = 0.2
- PCE (%) = 1.7

Perovskite material: Cs/MA Pbl₂/FA

Indeed, this idea also was not successful and cell had worse performance.

4. 8. 4. Reference Standard Structure Cell with Cs/MA PbI₂/FA perovskite material and PCBM as an electron transport layer

Here, a reference cell with PCBM as an electron transporting layer have been presented. This cell was fabricated in order to compare modified structures with rGO.

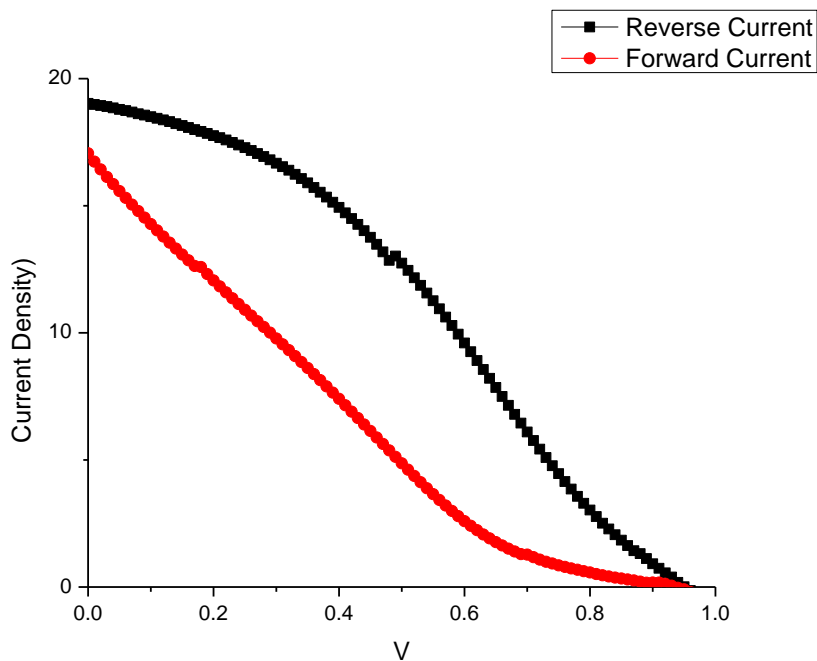


Figure 4- 19- Cell layers sequence: FTO/PCBM/Perovskite(Solvent quenching)/Spiro/Gold electrode

- | | |
|---|---|
| ➤ Reverse Scan: | ➤ Forward Scan: |
| ➤ Jsc (mA/cm^2) = 19.03 | ➤ Jsc (mA/cm^2) = 17.06 |
| ➤ Voc (V) = 0.95 | ➤ Voc (V) = 0.94 |
| ➤ FF = 0.35 | ➤ FF = 0.19 |
| ➤ PCE (%) = 6.38 | ➤ PCE (%) = 3.02 |

Perovskite material: Cs/MA PbI₂/FA

4. 8. 5. Standard Structure Cell with Cs/MA PbI₂/FA perovskite material and rGO+ PCBM as an electron transport layer

Another idea was to add a layer of rGO before the PCBM layer in standard structure.

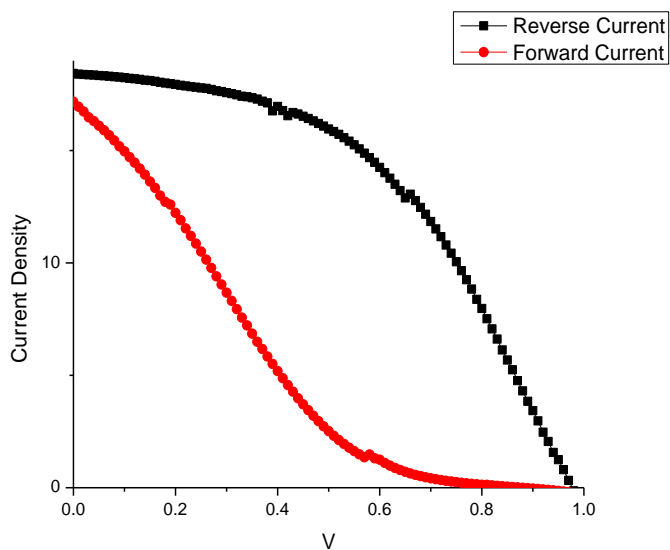



Figure 4- 20- Cell layers sequence: FTO/rGO/PCBM/Perovskite(Solvent quenching)/Spiro/Gold electrode

- | | |
|------------------------------|------------------------------|
| ➤ Reverse Scan: | ➤ Forward Scan: |
| ➤ $J_{sc} (mA/cm^2) = 18.43$ | ➤ $J_{sc} (mA/cm^2) = 17.17$ |
| ➤ $V_{oc} (V) = 0.98$ | ➤ $V_{oc} (V) = 0.88$ |
| ➤ $FF = 0.49$ | ➤ $FF = 0.18$ |
| ➤ $PCE (\%) = 8.62$ | ➤ $PCE (\%) = 2.64$ |

In this configuration, it is observed that adding rGO layer was beneficial for the cell in term of efficiency, but not from hysteresis point of view.



Chapter 5

Conclusion and Future Work

5. Conclusion

In this work, it was tried to investigate ways to improve the perovskite cell performance.

The solution which have been proposed was integration of the reduced Graphene Oxide (rGO) in the perovskite cell. It was suggested because of the interesting properties of the rGO. These properties made it a good candidate for this application. Additionally, it has been proposed by several authors who made the first cells with this material.

According to aforementioned reasons, rGO has been selected to be integrated into the cell.

This integration has been made in different ways:

1. Using rGO as an electron transporting layer instead of TiO_2 in standard structure.
2. Using rGO as a hole transporting layer instead of PEDOT: PSS in the inverted structure.
3. Using rGO as an interlayer between TiO_2 and perovskite layer in the standard structure.
4. Using rGO as an interlayer between PCBM and Perovskite layer in the standard structure.


For the first case integration was not successful and rGO could not act as an electron transport layer.

For the second case rGO integration was successful and cell had better performance in respect the reference cell.

For the third and fourth case also it was not good idea and rGO could not act very well as an interface modifier.

So, in general our reduced Graphene Oxide was a P-type semiconductor. This made it appropriate just for a hole transporting layer.

It was not possible to get high efficiency cell, but the aim which was reducing hysteresis was obtained.



Additionally, without saying, it is well accepted that rGO has a higher environmental stability. So, also from stability point of view, there was a good achievement.

Unfortunately, no stability test performed on the rGO modified samples, but as some authors [87, 99] suggested it would improve the stability of the cell during shelf life cycle.

Reference

1. *Krystallbau und chemische Zusammensetzung*, Ber. **Goldschmidt, V.M.** 1927, Ber. Dtsch. Chem. Ges.
2. *Crystal Structure Formation of CH₃NH₃PbI_{3-x}Cl_x Perovskite*. **Daoud, Shiqiang Luo and Walid A.** 2016, Materials.
3. *Prediction of lattice constant in cubic perovskites*. **Jiang, L. Q., Guo, J. K., Liu, H. B., Zhu, M., Zhou, X., Wu, P., Li, C. H.** 2006, Physics and Chemistry of Solids.
5. *First-Principles Modeling of Mixed Halide Organometal Perovskites for Photovoltaic Applications*. **Edoardo Mosconi, Anna Amat, Md. K. Nazeeruddin, Michael Grätzel, and Filippo De Angelis.** sl : Phys. Chem. C, 2013, Vol. 117.
6. *Semiconducting tin and lead iodide perovskites with organic cations: phase transitions, high mobilities, and near-infrared photoluminescent properties*. **Stoumpos CC, Malliakas CD, Kanatzidis MG.** sl : Inorganic Chemistry, 2013, Vol. 52.
7. *Synthesis, structure, and photovoltaic property of a nanocrystalline 2H perovskite-type novel sensitizer (CH₃CH₂NH₃)PbI₃*. **Im JH, Chung J, Kim SJ, Park NG.** sl : Nanoscale Res Lett, 2012, Vol. 7.
8. **G. C. Papavassiliou, G. A. Mousdis and I. B. Koutselas.** sl : Adv. Mater. Opt. Electron., 1999, Vol. 9.
9. *Comparative study on the excitons in lead-halide-based perovskite-type crystals CH₃NH₃PbBr₃ CH₃NH₃PbI₃*. **Tanaka, Kenichiro, et al.** sl : Solid State Communications, 2003, Vol. 127.
10. **Papavassiliou, G. C.** sl : Prog. Solid State. Chem., 1997, Vol. 25.
11. **G. A. Mousdis, V. Gionis, G. C. Papavassiliou, C. P. Raptopoulou and A. Terzis.** sl : Mater. Chem., 1998, Vol. 8.
12. *Synthesis, structural and optical properties of a novel bilayered organic-inorganic perovskite C₅Pb₂I₅*. **S. Elleuch, T. Dammak, Y. Abid, A. Mlayah and H. Boughzala.** sl : Journal of Luminescence, 2010, Vol. 130.
13. *Electron-hole diffusion lengths exceeding 1 micrometer in an organometal trihalide perovskite absorber*. **Stranks SD, Eperon GE, Grancini G, Menelaou C, Alcocer MJ, Leijtens T, Herz LM, Petrozza A, Snaith HJ.** 2013, Vol. 342.
14. *Lead iodide perovskite sensitized all-solid-state submicron thin film mesoscopic solar cell with efficiency exceeding 9%*. **Kim HS, Lee CR, Im JH, Lee KB, Moehl T, Marchioro A, Moon SJ, Humphry-Baker R, Yum JH, Moser JE, Grätzel M, Park NG.** sl : Scientific Report, 2012, Vol. 2.
15. *Efficient hybrid solar cells based on meso-superstructured organometal halide perovskites*. **Lee MM, Teuscher J, Miyasaka T, Murakami TN, Snaith HJ.** sl : Science, 2012, Vol. 2.
16. *Perovskites: Solar cells & engineering applications – materials and device developments*. **Milos Petrovic, Vijila Chellappan, Seeram Ramakrishna.** sl : Solar Energy, 2015, Vol. 122.

17. Interface engineering of highly efficient perovskite solar cells. **Zhou, H., et al.** *sl* : Science, 2014, Vol. 345.
18. Carbon Nanotube/Polymer Composites as a Highly Stable Hole Extraction Layer in Perovskite Solar Cells. **Habisreutinger, Severin N., et al.** *sl* : Nano Letters, 2014.
19. Cheap solar cells tempt businesses. **Van Noorden, Richard.** *sl* : Nature News, 2014.
20. Device modeling of perovskite solar cells based on structural similarity with thin film inorganic semiconductor solar cells. **Minemoto, Takashi en Murata, Masashi.** *sl* : Applied Physics, 2014, Vol. 116.
21. Overcoming ultraviolet light instability of sensitized TiO₂ with meso-superstructured organometal tri-halide perovskite solar cells. **Tomas Leijtens, Giles E. Eperon, Sandeep Pathak, Antonio Abate, Michael M. Lee & Henry J. Snaith.** *sl* : Nature Communications, 2013, Vol. 4.
22. Ultra-Low Thermal Conductivity in Organic–Inorganic Hybrid Perovskite CH₃NH₃PbI₃. **Pisoni, Andrea, et al.** *sl* : Physical Chemistry Letters, 2014, Vol. 5.
23. CH₃NH₃PbI₃ perovskite / silicon tandem solar cells: characterization based optical simulations. **Filipič, Miha, et al.** *sl* : Optics Express, 2015, Vol. 23.
24. Bifacial Si heterojunction-perovskite organic-inorganic tandem to produce highly efficient ($\eta T^* \sim 33\%$) solar cell. **Asadpour, Reza, et al.** *sl* : Applied Physics Letters, 2015, Vol. 106.
25. High-Performance and Environmentally Stable Planar Heterojunction Perovskite Solar Cells Based on a Solution-Processed Copper-Doped Nickel Oxide Hole-Transporting Layer. **Jong H. Kim, Po-Wei Liang, pencer T. Williams, Namchul Cho, Chu-Chen Chueh, Micah S. Glaz, David S. Ginger, Alex K.-Y. Jen.** *sl* : Advanced Materials, 2015, Vol. 27.
26. Anomalous Hysteresis in Perovskite Solar Cells. **Snaith, Henry J., et al.** *sl* : Physical Chemistry Letters, 2014, Vol. 5.
27. Hysteresis and transient behavior in current-voltage measurements of hybrid-perovskite absorber solar cells. **Unger, Eva L., et al.** *sl* : Energy & Environmental Science, 2014, Vol. 7.
28. Enhanced Photoluminescence and Solar Cell Performance via Lewis Base Passivation of Organic–Inorganic Lead Halide Perovskites. **Noel, Nakita K, et al.** *sl* : ACS Nano, 2014, Vol. 8.
29. Supramolecular Halogen Bond Passivation of Organic–Inorganic Halide Perovskite Solar Cells. **Abate, Antonio, et al.** *sl* : Nano Letters, 2014, Vol. 14.
30. Efficient, High Yield Perovskite Photovoltaic Devices Grown by Interdiffusion of Solution-Processed Precursor Stacking Layers. **Xiao, Zhengguo, et al.** *sl* : Energy & Environmental Science, 2014, Vol. 7.
31. **PARK, NAM-GYU.** Perovskite Solar Cells. 2014.
32. **Helen, M.** *sl* : Nature, 1945, Vol. 155.
33. **Wul, B.** *sl* : Nature, 1946, Vol. 157.
34. **Cohen, R.** *sl* : Nature, 1992, Vol. 358.

35. **C. N. R. Rao, P. Ganguly, A. K. Raychaudhuri, R. A. Mohan Ram and K. Sreedhar.** *sl : Nature*, 1987, Vol. 326.
36. **A. Schilling, M. Cantoni, J. D. Guo and H. R. Ott.** *sl : Nature*, 1993, Vol. 363.
37. **D. B. Mitzi, C. A. Feild, W. T. A. Harrison and A. M. Guloy.** *sl : Nature*, 1994, Vol. 369.
38. **R. E. Wasylshen, O. Knop and J. B. Macdonald.** *sl : Solid State Commun.*, 1985, Vol. 56.
39. **Weber, A. Poglitsch and D.** *sl : Chem. Phys.*, 1987, Vol. 87.
40. *Organometal Halide Perovskites as Visible-Light Sensitizers for Photovoltaic Cells.* **Akihiro Kojima, Kenjiro Teshima, Yasuo Shirai and Tsutomu Miyasaka.** *sl : Am. Chem. Soc.*, 2009, Vol. 131.
41. *6.5% efficient perovskite quantum-dot-sensitized solar cell.* **Im JH, Lee CR, Lee JW, Park SW, Park NG.** *sl : Nanoscale*, 2011, Vol. 3.
42. *Sequential deposition as a route to high-performance perovskite-sensitized solar cells.* **Burschka J, Pellet N, Moon SJ, Humphry-Baker R, Gao P, Nazeeruddin MK, Grätzel M.** *sl : Nature*, 2013, Vol. 499.
43. *Efficient planar heterojunction perovskite solar cells by vapour deposition.* **Mingzhen Liu, Michael B. Johnston & Henry J. Snaith.** *sl : Nature*, 2013, Vol. 501.
44. *Synthesis and Characterization of Organic-Inorganic Perovskite Thin Films Prepared Using a Versatile Two-Step Dipping Technique.* **Kangning Liang, David B. Mitzi and Michael T. Prikas.** *sl : Chem. Mater.*, 1998, Vol. 10.
45. *Perovskite Solar Cells: From Materials to Devices.* **Hyun Suk Jung, Nam-Gyu Park.** *sl : Materials Views*, 2014, Vol. 11.
46. *Graphene oxide-based transparent conductive film.* **Qingbin Zheng, Zhigang Li, Junhe Yang and Jang-Kyo Kim.** 2014, *Progress in Materials Science*, pp. 200-247.
47. *Direct reduction of graphene oxide films into highly conductive and flexible graphene films by hydrohalic acids.* **Songfeng Pei, Jinping Zhao, Jinhong Du, Wencai Ren, Hui-Ming Cheng.** 2010, *Carbon*, pp. 4466-4474.
48. *Effect of the Exposure Time of Hydrazine Vapor on the Reduction of Graphene Oxide Films.* **Sang Cheon Youn, Jianxin Geng, Baek Sik Son, Seung Bo Yang, Dae Woo Kim, Hye Mi Cho, and Hee-Tae Jung.** *sl : Journal of Nanoscience and Nanotechnology*, 2011, Vol. 11, 5959–5964.
49. *Graphene production via electrochemical reduction of graphene oxide: Synthesis and characterisation.* **Shaw Yong Toh, Kee Shyuan Loh, Siti Kartom Kamarudin, Wan Ramli Wan Daud.** *sl : Chemical Engineering Journal*, 2014, Vol. 251, 422–434.
50. *Electrochemically Reduced Graphene Oxide Multilayer Films as Efficient Counter Electrode for Dye-Sensitized Solar Cells.* **Xiaobao Xu, Dekang Huang, Kun Cao, Mingkui Wang, Shaik M. Zakeeruddin & Michael Graätzel.** *sl : nature research journal*, 2013.

51. Growth of $\text{CH}_3\text{NH}_3\text{PbI}_3$ cuboids with controlled size for high-efficiency perovskite solar cells. **Jeong-Hyeok Im, In-Hyuk Jang, Norman Pellet, Michael Grätzel and Nam-Gyu Park.** *sl : NATURE NANOTECHNOLOGY*, 2014, Vol. 9.
52. Highly efficient and stable planar perovskite solar cells with reduced graphene oxide nanosheets as electrode interlayer. **Jun-Seok Yeo, Rira Kang, Sehyun Lee, Ye-Jin Jeon, NoSung Myoung, Chang-Lyoul Lee, Dong-Yu Kim, Jin-Mun Yun, You-Hyun Seo, Seok-Soon Kim, Seok-In Na.** *sl : Elsevier, Nano Energy*, 2015, Vol. 12.
53. Graphene oxide hole injection layer for high-efficiency polymer light-emitting diodes by using electrophoretic deposition and electrical reduction. **Jungyoon Kim, Shraddha Ganorkar, Young-Hwan Kim, Seong-Il Kim.** *sl : Carbon*, 2015, Vol. 94.
54. Graphene oxide/PEDOT:PSS composite hole transport layer for efficient and stable planar heterojunction perovskite solar cells. **Da-Young Lee, Seok-In Na, Seok-Soon Kim.** *sl : Nanoscale*, 2015.
55. Reduction of graphene oxide films on Al foil for hybrid transparent conductive film applications. **Sergio H. Domingues, Iskandar N. Kholmanov, TaeYoung Kim, JinYoung Kim, Cheng Tan, Harry Chou, Zeineb A. Alieva, Richard Piner, Aldo J.G. Zarbin, Rodney S. Ruoff.** *sl : Carbon*, 2013, Vol. 63.
56. Cupric bromide hybrid perovskite heterojunction solar cells. **Xue-Ping Cui, Ke-Jian Jiang, Jin-Hua Huang, Qian-Qian Zhang, Mei-Ju Su, Lian-Ming Yang, Yan-Lin Song, Xue-Qin Zhou.** *sl : Synthetic Metals*, 2015, Vol. 209.
57. Nanocarbons for mesoscopic perovskite solar cells. **Munkhbayar Batmunkh, Cameron J. Shearer, Mark J. Biggs and Joseph G. Shapter.** *sl : Materials Chemistry A*, 2015, Vol. 3.
58. Nitrogen-doped perovskite-type $\text{La}_2\text{Ti}_2\text{O}_7$ decorated on graphene composites exhibiting efficient photocatalytic activity toward bisphenol A in water. **Zulin Hua, Xiaoyuan Zhang, Xue Bai, Lingling Lv, Zhengfang Ye, Xin Huang.** *sl : Colloid and Interface Science*, 2015, Vol. 450.
59. Simple approach for large-scale production of reduced graphene oxide films. **Ming Zhang, Bin Gao, Diana C. Vanegas, Eric S. McLamore, June Fang, Lin Liu, Lei Wu, Hao Chen.** *sl : Chemical Engineering*, 2014, Vol. 243.
60. A simple and flexible route to large-area conductive transparent graphene thin-films. **Kirill Arapov, Andrey Goryachev, Gijsbertus de With, Heiner Friedrich.** *sl : Synthetic Metals*, 2015, Vol. 201.
61. Langmuir-Blodgett assembly of ultra-large graphene oxide films for transparent electrodes. **ZHENG Qing-bin, SHI Li-fang, YANG Jun-he.** *sl : Trans. Nonferrous Met. Soc. China*, 2012, Vol. 22.
62. Fast-growing procedure for perovskite films in planar heterojunction perovskite solar cells. **Tang-Hao Liu, Ke Chen, Qin Hu, Jiang Wu, De-Ying Luo, Shuang Jia, Rui Zhu, Qi-Huang Gong.** *sl : Chinese Chemical Letters*, 2015.
63. TCO-free flexible organo metal trihalide perovskite planar-heterojunction solar cells. **M. Dianetti, F.DiGiacomo, G.Polino, C.Ciceroni, A.Liscio, A.D'Epifanio, S.Licocci, T.M.Brown, A.DiCarlo, F.Brunetti.** *sl : Solar Energy Materials & Solar Cells*, 2015, Vol. 140.

64. An efficient polymer solar cell using graphene oxide interface assembled via layer-by-layer deposition. **Lingyu Zhou, Dong Yang, Wei Yu, Jian Zhang, Can Li.** *sl : Organic Electronics*, 2015, Vol. 23.
65. Efficient electron-blocking layer-free planar heterojunction perovskite solar cells with a high open-circuit voltage. **Runsheng Wu, Junliang Yang, Jian Xiong, Peng Liu, Conghua Zhou, Han Huang, Yongli Gao, Bingchu Yang.** *sl : Organic Electronics*, 2015, Vol. 26.
66. Graphene and Its Synthesis. **Y Hernandez, S Pang, X Feng, and K Müllen.** *sl : Elsevier, Polymer Science*, 2012, Vol. 8.
67. Review Graphene oxide: the new membrane material. **R.K. Joshi, S. Alwarappan, M. Yoshimura, V. Sahajwalla, Y. Nishina,.** *sl : Applied Materials Today*, 2015, Vol. 1.
68. Graphene and Graphene Oxide: Synthesis, Properties, and Applications. **Yanwu Zhu, Shanthi Murali , Weiwei Cai , Xuesong Li , Ji Won Suk , Jeffrey R. Potts and Rodney S. Ruoff.** *sl : Advanced Materials*, 2010, Vol. 22.
69. Large-area ultrathin films of reduced graphene oxide as a transparent and flexible electronic material. **GOKI EDA, GIOVANNI FANCHINI AND MANISH CHHOWALLA.** *sl : Nature Nanotechnology*, 2008, Vol. 3.
70. Preparation of Graphitic Oxide. **WILLIAM S. HUMMERS, JR., AND RICHARD E. OFFEMAN.** *sl : NATIONAL LEAD COMPANY*, 1958.
71. High-performance photovoltaic perovskite layers fabricated through intramolecular exchange. **Woon Seok Yang, Jun Hong Noh, Nam Joong Jeon, Young Chan Kim, Seungchan Ryu, Jangwon Seo, Sang Il Seok.** *sl : Materials and Methods*, 2015, Vol. 348.
72. Solvent engineering for high-performance inorganic–organic hybrid perovskite solar cells. **Nam Joong Jeon, Jun Hong Noh, Young Chan Kim, Woon Seok Yang, Seungchan Ryu and Sang Il Seok.** *sl : NATURE MATERIALS*, 2014, Vol. 13.
73. Multi-layer graphene treated by O₂ plasma for transparent conductive electrode applications. **Tingting Feng, Dan Xie, He Tian, Pinggang Peng, Di Zhang, Di Fu, Tianling Ren, Xinming Li, Hongwei Zhu, Yupeng Jing.** *sl : Materials Letters*, 2012, Vol. 73.
74. Multilayer graphene films as transparent electrodes for organic photovoltaic devices. **Yoon-Young Choi, Seong Jun Kang, Han-Ki Kim, Won Mook Choi, Seok-In Na.** *sl : Solar Energy Materials & Solar Cells*, 2012, Vol. 96.
75. Transparent, Conductive Graphene Electrodes for Dye-Sensitized Solar Cells. **Xuan Wang, Linjie Zhi, and Klaus Mullen.** *sl : NANO LETTERS*, 2008, Vol. 8.
76. Transparent conductive thin film of ultra large reduced graphene oxide monolayers. **A. Nekahi, P.H. Marashi, D. Haghshenas.** *sl : Applied Surface Science*, 2014, Vol. 295.
77. Stable dispersions of graphene and highly conducting graphene films: a new approach to creating colloids of graphene monolayers. **Yao Chen, Xiong Zhang, Peng Yu and Yanwei Ma.** *sl : CHEMICAL COMMUNICATIONS*, 2009.

78. Minimizing energy losses in perovskite solar cells using plasma-treated transparent conducting layers. **Van-Duong Dao, Liudmila L. Larina, Ho-Suk Choi.** *sl : Thin Solid Films*, 2015, Vol. 593.
79. LANGMUIR-BLODGETT ASSEMBLY OF GRAPHENE OXIDE SHEETS. **Laura Cote, Franklin Kim, Jiaying Huang.** *sl : Carbon*, 2010.
80. Graphene oxide-based transparent conductive films. **Qingbin Zheng, Zhigang Li, Junhe Yang, Jang-Kyo Kim.** *sl : Progress in Materials Science*, 2014, Vol. 64.
81. **Casari, Carlo.** Raman spectroscopy of carbon.
82. —. Raman spectroscopy of nanostructures.
83. —. Graphene.
84. A Raman spectroscopic investigation of graphite oxide derived graphene. **Ramaprabhu, Adarsh Kaniyoor and Sundara.** *sl : AIP ADVANCES*, 2012, Vol. 2.
85. **Casari, Carlo.** Carbon nanostructures - Graphene.
86. Synthesis and electrochemical properties of reduced graphene oxide via chemical reduction using thiourea as a reducing agent. **Kaveri Satheesh, Ramasamy Jayavel.** *sl : Materials Letters*, 2013, Vol. 13.
87. Solution-Processable Reduced Graphene Oxide as a Novel Alternative to PEDOT:PSS Hole Transport Layers for Highly Efficient and Stable Polymer Solar Cells. **Jin-Mun Yun, Jun-Seok Yeo , Juhwan Kim , Hyung-Gu Jeong , Dong-Yu Kim , Yong-Jin Noh , Seok-Soon Kim , Bon-Cheol Ku and Seok-In Na.** *sl : Advanced Materials*, 2011, Vol. 23.
88. Efficient planar perovskite solar cells with large fill factor and excellent stability. **Xichang Bao, Yujin Wang, Qianqian Zhu, Ning Wang, Dangqiang Zhu, Junyi Wang, Ailing Yang, Renqiang Yang.** *sl : Power Sources*, 2015, Vol. 297.
89. Moderately reduced graphene oxide as transparent counter electrodes for dye-sensitized solar cells. **Hye-Su Jang, Jin-Mun Yun, Dong-Yu Kim, Dong-Won Park, Seok-In Na, Seok-Soon Kim.** *sl : Electrochimica Acta*, 2012, Vol. 81.
90. Morphological, optical, and electrical investigations of solution-processed reduced graphene oxide and its application to transparent electrodes in organic solar cells. **Jin-Mun Yun, Chan-Hee Jung, Yong-Jin Noh, Ye-Jin Jeon, Seok-Soon Kim, Dong-Yu Kim, Seok-In Na.** *sl : Industrial and Engineering Chemistry*, 2015, Vol. 21.
91. Reduced graphene oxide films as transparent counter-electrodes for dye-sensitized solar cells. **Rui Cruz, David Alfredo Pacheco Tanaka, Adelio Mendes.** *sl : Solar Energy*, 2012, Vol. 86.
92. Plasma-assisted simultaneous reduction and nitrogen doping of graphene oxide nanosheets. **Nanjundan Ashok Kumar, Hugo Nolan, Niall McEvoy, Ehsan Rezvani, Richard L. Doyle, Michael E. G. Lyons and Georg S. Duesberg.** *sl : Materials Chemistry A*, 2013, Vol. 1.
93. Recent progress and perspective in solutionprocessed Interfacial materials for efficient and stable polymer and organometal perovskite solar cells. **Chu-Chen Chueh, Chang-Zhi Li and Alex K.-Y. Jen.** *sl : Energy & Environmental Science*, 2015, Vol. 8.

94. Hysteresis-less inverted $\text{CH}_3\text{NH}_3\text{PbI}_3$ planar perovskite hybrid solar cells with 18.1% power conversion efficiency. **Jin Hyuck Heo, Hye Ji Han, Dasom Kim, Tae Kyu Ahn and Sang Hyuk Im.** *sl : Energy & Environmental Science, 2015, Vol. 8.*
95. High efficiency stable inverted perovskite solar cells without current hysteresis. **Chun-Guey Wu, Chien-Hung Chiang, Zong-Liang Tseng, Md. K. Nazeeruddin, Anders Hagfeldt and Michael Gratzel.** *sl : Energy & Environmental Science, 2015, Vol. 8.*
96. Understanding the rate-dependent J–V hysteresis, slow time component, and aging in $\text{CH}_3\text{NH}_3\text{PbI}_3$ perovskite solar cells: the role of a compensate dielectric field. **W. Tress, N. Marinova, T. Moehl, S. M. Zakeeruddin, Mohammad Khaja Nazeeruddin and M. Gratzel.** *sl : Energy & Environmental Science, 2015, Vol. 8.*
97. Evaluation of Solution-Processed Reduced Graphene Oxide Films as Transparent Conductors. **Héctor A. Becerril, Jie Mao, Zunfeng Liu, Randall M. Stoltenberg, Zhenan Bao, and Yongsheng Chen.** *sl : ACS Nano, 2008, Vol. 2.*
98. The Efficiency Limit of $\text{CH}_3\text{NH}_3\text{PbI}_3$ Perovskite Solar Cells. **Wei E.I. Sha, Xingang Ren, Luzhou Chen and Wallace C.H. Choy.** *sl : Applied Physics Letters, 2015.*
99. Efficiency and Stability Enhancement in Perovskite Solar Cells by Inserting Lithium-Neutralized Graphene Oxide as Electron Transporting Layer. **Antonio Agresti, Sara Pescetelli, Lucio Cinà, Dimitrios Konios, George Kakavelakis, Emmanuel Kymakis and Aldo Di Carlo.** *sl : Advanced Functional Materials, 2016.*
100. Optoelectrochemical Biorecognition by Optically Transparent Highly Conductive Graphene-Modified Fluorine-Doped Tin Oxide Substrates. **F. Lamberti, L. Brigo, M. Favaro, C. Luni, A. Zoso, M. Cattelan, S. Agnoli, G. Brusatin, G. Granozzi, M. Giomo and N. Elvassore.** *sl : ACS Applied Materials & Interfaces, 2014, Vol. 6.*
101. Synthesis of Flexible Graphene Transparent Conductive Films by Using Plasma Technique. **Masataka Hasegawa, Ryuichi Kato, Yuki Okigawa, Satoshi Minami, Masatou Ishihara, Takatoshi Yamada.** *sl : AM-FPD, 2015.*
102. Beneficial Role of Reduced Graphene Oxide for Electron Extraction in Highly Efficient Perovskite Solar Cells. **Kyung Taek Cho, Giulia Grancini, Yonghui Lee, Dimitrios Konios, Sanghyun Paek, Emmanuel Kymakis and Mohammad Khaja Nazeeruddin.** *sl : ChemSusChem, 2016, Vol. 9.*
103. The reduction of graphene oxide. **Songfeng Pei, Hui-Ming Cheng.** *sl : CARBON, 2011.*
104. The benefits of graphene for hybrid perovskite solar cells. **Johann Bouclé, Nathalie Herlin-Boime.** *sl : Synthetic Metals, 2016.*
105. In situ graphene doping as a route toward efficient perovskite tandem solar cells. **Felix Lang, Marc A. Gluba, Steve Albrecht, Oleksandra Shargaieva, Jorg Rappich, Lars Korte, Bernd Rech and Norbert H. Nickel.** *sl : Phys. Status Solidi A, 2016.*

106. *Effects of interfacial chemical states on the performance of perovskite solar cells.* **Teng Ma, Daisuke Tadaki, Masao Sakuraba, Shigeo Sato, Ayumi Hirano-Iwata and Michio Niwano.** *sl : Materials Chemistry A*, 2016, Vol. 4.
107. *Highly efficient planar perovskite solar cells through band alignment engineering.* **Juan Pablo Correa Baena, Ludmilla Steier, Wolfgang Tress, Michael Saliba, Stefanie Neutzner, Taisuke Matsui, Fabrizio Giordano, T. Jesper Jacobsson, Ajay Ram Srimath Kandada, Shaik M. Zakeeruddin, Annamaria Petrozza, Antonio Abate, Mohammad Khaja Nazeerud.** *sl : Energy & Environmental Science*, 2015, Vol. 8.
108. *17.6% stabilized efficiency in low-temperature processed planar perovskite solar cells.* **Chen Tao, Stefanie Neutzner, Letizia Colella, Sergio Marras, Ajay Ram Srimath Kandada, Marina Gandini, Michele De Bastiani, Giuseppina Pace, Liberato Manna, Mario Caironi, Chiara Bertarelli and Annamaria Petrozza.** *sl : Energy & Environmental Science*, 2015, Vol. 8.
109. *Plasma-Assisted Reduction of Graphene Oxide at Low Temperature and Atmospheric Pressure for Flexible Conductor Applications.* **Seung Whan Lee, Cecilia Mattevi, Manish Chhowalla and R. Mohan Sankaran.** *sl : Phys. Chem. Lett*, 2012, Vol. 3.
110. *Shunt-Blocking Layers for Semitransparent Perovskite Solar Cells.* **Maximilian T. Hörantner, Pabitra K. Nayak, Sabyasachi Mukhopadhyay, Konrad Wojciechowski, Clara Beck, David McMeekin, Brett Kamino, Giles E. Eperon and Henry J. Snaith.** *sl : Adv. Mater. Interfaces*, 2016.
111. *Efficient and stable large-area perovskite solar cells with inorganic charge extraction layers.* **Wei Chen, Yongzhen Wu, Youfeng Yue, Jian Liu, Wenjun Zhang, Xudong Yang, Han Chen, Enbing Bi, Islam Ashraf, Michael Grätzel, Liyuan Han.** *sl : Scienceexpress*, 2015.
112. *Nitrogen-doped graphene and its electrochemical applications.* **Yuyan Shao, Sheng Zhang, Mark H. Engelhard, Guosheng Li, Guocheng Shao, Yong Wang, Jun Liu, Ilhan A. Aksay and Yuehe Lin.** *sl : Materials Chemistry*, 2010.
113. *Bulk heterojunction perovskite–PCBM solar cells with high fill factor.* **Wu, Chien-Hung Chiang and Chun-Guey.** *sl : NATURE PHOTONICS*, 2016.
114. *Structural and optical properties of methylammoniumlead iodide across the tetragonal to cubic phase transition: implications for perovskite solar cells.* **Claudio Quarti, Edoardo Mosconi, James M. Ball, Valerio D’Innocenzo, Chen Tao, Sandeep Pathak, Henry J. Snaith, Annamaria Petrozza and Filippo De Angelis.** *sl : Energy & Environmental Science*, 2015.
115. *A low-temperature method to produce highly reduced graphene oxide.* **Hongbin Feng, Rui Cheng, Xin Zhao, Xiangfeng Duan & Jinghong Li.** *sl : NATURE COMMUNICATIONS*, 2013.
116. *Enhanced optoelectronic quality of perovskite thin films with hypophosphorous acid for planar heterojunction solar cells.* **Wei Zhang, Sandeep Pathak, Nobuya Sakai, Thomas Stergiopoulos, Pabitra K. Nayak, Nakita K. Noel, Amir A. Haghighirad, Victor M. Burlakov, Dane W. deQuilettes, Aditya Sadhanala, Wenzhe Li, Liduo Wang, David S. Ginger, Richard H. Friend & Henry J. Snaith.** *sl : NATURE COMMUNICATIONS*, 2015, Vol. 6.

117. *Reversible Hydrophobic to Hydrophilic Transition in Graphene via Water Splitting Induced by UV Irradiation.* **Zhemi Xu, Zhimin Ao, Dewei Chu, Adnan Younis, Chang Ming Li & Sean Li.** *sl : SCIENTIFIC REPORTS, 2014, Vol. 4.*
118. *Low-Temperature Processed Electron Collection Layers of Graphene/TiO₂ Nanocomposites in Thin Film Perovskite Solar Cells.* **Jacob Tse-Wei Wang, James M. Ball, Eva M. Barea, Antonio Abate, Jack A. Alexander-Webber, Jian Huang, Michael Saliba, Iván Mora-Sero, Juan Bisquert, Henry J. Snaith, and Robin J. Nicholas.** *sl : Nano Letter, 2014, Vol. 14.*
119. *Metal-halide perovskites for photovoltaic and light-emitting devices.* **Snaith, Samuel D. Stranks and Henry J.** *sl : NATURE NANOTECHNOLOGY, 2015, Vol. 10.*
120. **Zhijia Xu, Kevin Weeks, Taryn De Rosia.** *Perovskite solar cells.*
121. *PEROVSKITE SOLAR CELLS.* **Benli, Ahmet Deniz.** *sl : MATTER, Vol. 2.*
122. *Perovskite solar cells: an emerging photovoltaic technology.* **Park, Nam-Gyu.** *sl : Materials Today, 2015, Vol. 18.*
123. *Recent Advances in the Inverted Planar Structure of Perovskite Solar Cells.* **Lei Meng, Jingbi You, Tzung-Fang Guo and Yang Yang.** *sl : American Chemical Society, 2016, Vol. 49.*
124. *General Working Principles of CH₃NH₃PbX₃ Perovskite Solar Cells.* **Victoria Gonzalez-Pedro, Emilio J. Juarez-Perez, Waode-Sukmawati Arsyad, Eva M. Barea, Francisco Fabregat-Santiago, Ivan Mora-Sero and Juan Bisquert.** *sl : Nano Letters, 2014, Vol. 14.*
125. *Perovskite Solar Cells.* **Users.** *sl : Wikipedia, 2016.*